Intelligent Power Management for Unmanned Air Vehicles

by

James Graham

A Doctoral Thesis Submitted in partial fulfilment of the requirements for the award of Doctor of Philosophy of Loughborough University

January 2015

Abstract

Unmanned Air Vehicles (UAVs) are becoming more widely used in both military and civilian applications. Some of the largest UAVs have power systems equivalent to that of a military strike jet making power management an important aspect of their design. As they have developed, the amount of power needed for loads has increased. This has placed increase strain on the on-board generators and a need for higher reliability. In normal operation these generators are sized to be able to power all on-board systems with out overheating. Under abnormal operating conditions these generators may start to overheat, causing the loss of the generator's power output.

The research presented here aims to answer two main questions: 1) Is it possible to predict when an overheat fault will occur based on the expected power usage defined by mission profiles? 2) Can an overheat fault be prevented while still allowing power to be distributed to necessary loads to allow mission completion?

This is achieved by a load management algorithm, which adjusts the load profile for a mission, by either displacing the load to spare generators, or resting the generator to cool it down. The result is that for non-catastrophic faults the faulty generator does not need to be fully shut down and missions can continue rather than having to be aborted. This thesis presents the development of the load management system including the algorithm, prediction method and the models used for prediction. Ultimately, the algorithms developed are tested on a generator test rig.

The main contribution of this work is the design of a prognostic load management algorithm. Secondary contributions are the use of a lumped parameter thermal model within a condition monitoring application, and the creation of a system identification model to describe the thermal dynamics of a generator.

Acknowledgements

First and foremost I would like to thank my supervisors Roger Dixon and Pete Hubbard for their support, guidance and encouragement, without their constant challenge of my work it would be much less than it currently is.

I would also like to give a large thank you to Ian Harrington from BAE Systems who acted as my industrial supervisor, the alternate, non-academic view of my work has been invaluable.

I would also like to acknowledge the Engineering and Physical Sciences Research Council (EPSRC) and BAE Systems for providing the funding for this PhD research project.

I would also like to thank colleagues past and present in the Control Systems Group within the Electronic, Electrical and Systems School at Loughborough University, for providing advice, support during my research and putting up with me on a daily basis throughout. I wish them all the best in their own research.

Finally I would like to thank my family and friends for their love and support and for creating an environment where I could relax when the day was done.

Contents

List of Figures

List of Tables

Chapter 1

Introduction

1.1 Background

The use of Unmanned Air Vehicles (UAVs) in both civilian and military use is becoming more widespread. These UAVs range in size from small airframes less than a metre long up to the size of military strike jets [3]. The work presented here focusses upon larger UAVs primarily for military use but is also applicable to civilian vehicles of similar size and manned aircraft.

These UAVs have power systems with similar levels of complexity to manned conventional aircraft of similar size. In both cases, the power systems need to be designed to reliably supply the electrical loads in the aircraft. At the same time there is a general push in aircraft to power as many systems with electrical power as possible, reducing the use of pneumatic and hydraulic systems [2]. This is to increase fuel efficiency and improve reliability. This creates extra level of criticality upon electrical power generation sources which need to be supply the loads on-board the aircraft reliably at all times for mission success.

In normal operation these generators are sized to be able to supply the required amount of power to the loads during each phase of flight. There are a number of scenarios which can occur individually or in combination to cause higher than expected heat loads on the generator which can lead to overheating issues. These include reduced cooling capacity in the system or faults in the windings. When an overheat fault is detected load management strategies have be applied and loads are shed to keep the aircraft in flight using remaining power capacity. This tends to result in mission failure as aircraft are returned to base (if possible) or lost.

The aim of this research is to study new load management strategies that would allow some of a generator's capacity to be maintained during conditions which would normally cause an overheat fault and cause the generator to be shut down.

1.2 Aircraft Load Management

The load management systems available in current aircraft are simplistic. The system waits till an overheat is detected, shuts the generator down and cuts all non-essential loads to maintain flight. This is carried out either by a pilot using a list or a simple algorithm also using a list. The current systems are entirely reactive [4].

There are several faults within generators which do not cause an instant overheat and catastrophic failure/shut down, but instead cause an increased heat load on the generator which causes a gradual overheating. These include reductions in coolant flow through the generator and winding short circuits. With these types of fault it is possible that if loads upon the generator can be reduced when they occur these faults can be prevented from causing an overheat/failure. These faults in reality cause a reduction in the power generation capacity of the generator, but if untreated lead to a catastrophic failure in the future.

Another consideration is the power supply requirements of the aircraft over time. It is common for military aircraft to have components updated over the life cycle of the aircraft this tends to include new radar and weapon systems each of which often come with an additional power requirement. This means that over time the generators are required to supply larger amounts of power for greater amounts of time which can lead to more potential overheat problems.

1.3 Thesis Motivation

The research presented in this thesis is an industrial case award from the EPSRC and BAE Systems. The questions to be answered were derived from an initial area of research given by BAE Systems which was to investigate power management on-board UAVs. From this initial area, management of the generators to allow them to reliably output the power required to keep the aircraft in flight was identified as an area of research that could benefit UAVs.

The basis of this research is a shift in how the total power capacity of a generator is defined. Currently the rating of the generator is used to define total capacity and the temperature is measured to detect faults. In this research the temperature of the generator will be used to define its capacity in terms of how much extra power can be drawn before an overheat occurs. When combined with an accurate temperature predict this allows the system to account for a fault by reducing the capacity of the generator according to its severity.

This leads to two major questions that are to be answered by this research, these are:

1. Is it possible to predict when an overheat fault will occur based on the expected power usage defined by mission profiles?

2. Can an overheat fault be prevented while still allowing power to be distributed to necessary loads to allow mission completion?

To answer question 1 an investigation of techniques to model the thermal dynamics of the aircraft will be undertaken. The aim will be to create a model which can predict the future temperature of an aircraft generator based on a known load profile with a good degree of accuracy so that decisions can be made based upon the output.

Question 2 will focus on methods for adjusting the load profile of a generator to allow the required actions of a mission to be completed without causing an overheat fault on a generator. The aim will be to create an algorithm which optimises the load profile based upon the predictions made to prevent overheat faults while minimising the total mission length.

1.4 Research Method

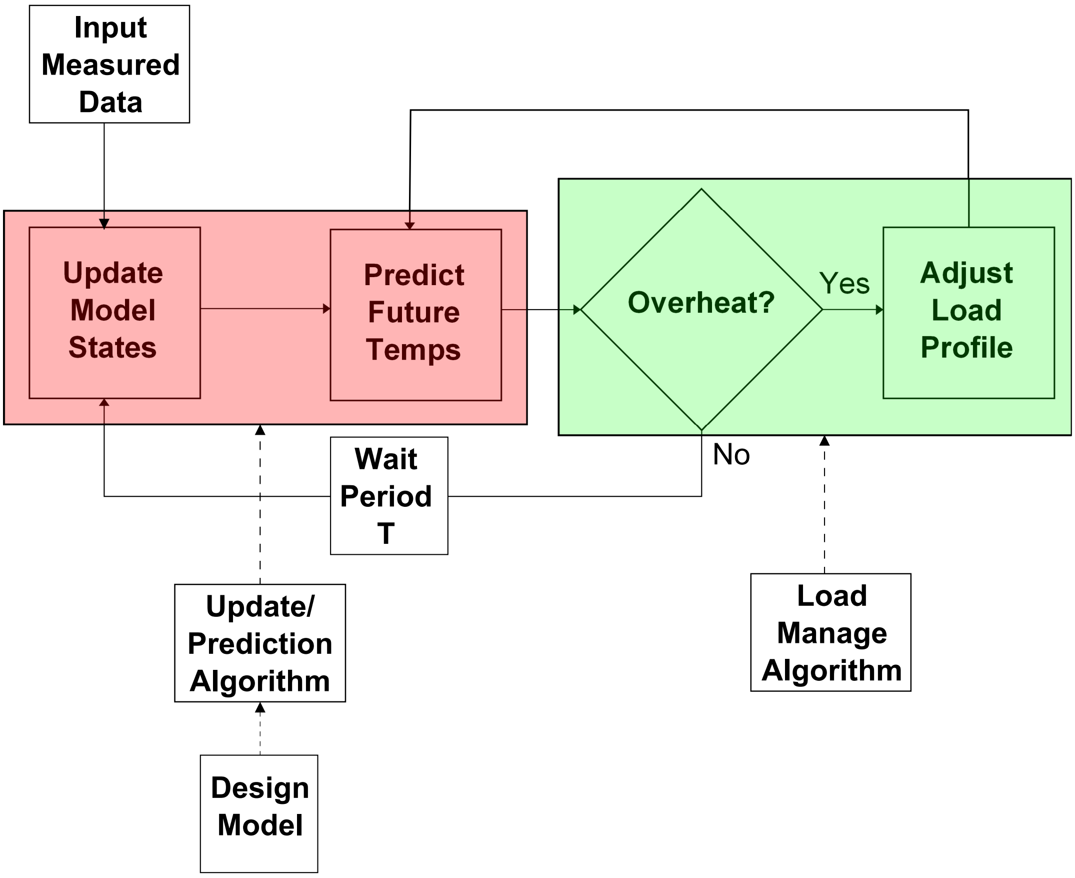

Figure 1.1: Diagram showing method used in research.

Figure 1.1 shows a diagram giving an overview of the method used to address the questions proposed in the previous section. The diagram shows the various parts of the final algorithm that will be present, these are:

1. State Update
2. Prediction of Future States
3. Check for Overheat Fault
4. Adjust Load Profiles

The state update uses measured data from the generator to update the initial states of the system model before any predictions are made to ensure maximum accuracy. The model is then used to predict the future temperatures in the second phase. These predictions are then used to check for any overheat faults, and if any are detected a load management algorithm will be applied to adjust the load profile preventing any overheat faults. This will the repeat periodically to both accommodate new faults and/or check previous outcomes.

1.5 Thesis Objectives and Scope

The objectives of this thesis are:

1. To commission an experimental generator rig. This will be used to validate any models and provide measured data during final system validation tests.
2. To create validated thermal models to represent both the actual generator in simulation and a design model to be used as part of the prediction system.
3. To design a system to predict the future temperature state of a generator based on a known mission profile. This is shown by the red box in figure 1.1 and uses the design model described in the previous objective.

4. To develop a load management system able to correct overheat faults when detected before they caused catastrophic failure of a generator. This is shown by the green box in figure 1.1.

Figure 1.2 shows in which thesis chapters the research relating to each objective is described.

1.6 Thesis Overview

The objectives described in section 1.5 are described in the following chapters an overview of which is presented below.

1.6.1 Literature Review

First, the background information and a survey of current work relating to aircraft load management, prognostics and health management (PHM) and generator thermal modelling is presented. Discussed within this chapter is current load management and PHM and how the work proposed here differs. Also presented is a survey of research showing why decisions for modelling, prediction and load management were made.

1.6.2 Experimental Set-up

This chapter presents a description of the generator rig that was commissioned to record data to allow validation of models of the generator's thermal dynamics. It describes the components of the rig and the sensors present.

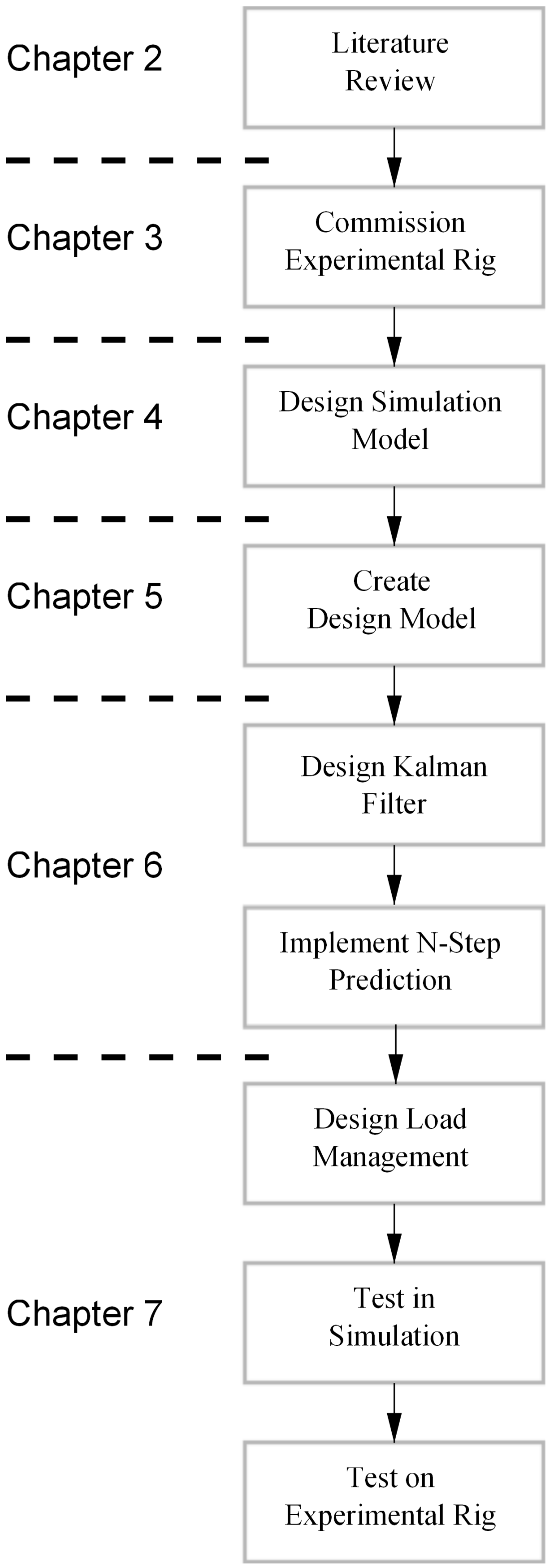

Figure 1.2: Work-flow diagram for thesis objectives.

1.6.3 Derivation of a Thermal Network Model for a Generator

This chapter describes the creation of a lumped parameter thermal network model of the thermal dynamics of a generator. This model is non-linear and is designed to be used in place of the generator rig during simulation tests to prevent the actual generator being damaged.

The model is created from first principles and is validated against data recorded from the experimental rig in chapter 3.

1.6.4 Description and Comparison of Design Models

The first major contributions of this thesis are presented in chapter 5. In this chapter two design models to be used later within the prediction system are defined. These are a linear version of the physics-based model presented in chapter 4 and a system identification model.

The linear version of the physics-based model leads to contribution as the first occurrence of this type of lumped parameter thermal model where a linear representation of winding losses is used. This is also the first time this type of model has been using within a condition monitoring application. Results are also presented to analyse what effect the non-linear representation of winding losses and accounting for winding resistance changing with temperature has on model accuracy.

Within this thesis is the first time a system identification model of the thermal dynamics of a generator has been presented and validated.

The final section of the chapter compares the two models and chooses one for use within the final system.

1.6.5 Kalman Filter Based Prediction

The chapter describes the creation of a Kalman Filter using the design model chosen in chapter 5. Results are presented to show how the well the Kalman Filter based method performs both at correcting model errors and at predicting the future temperature states.

The creation of this prediction system is the first time a Kalman Filter has been used to predict the future thermal states of a generator.

1.6.6 Description of the Load Management System

The final results chapter describes the load management system. This includes showing how the prediction system containing the design model is integrated into it, as well as presenting the algorithm for preventing overheat faults.

To prevent overheats two methods are used: Generator resting and load displacement. Generator resting is a method of placing the generator in a minimum power mode to cool it down before undertaking an action. Load displacement is a method of using spare generation capacity of other power sources to lower the load on a faulty generator.

Finally results are presented to show that the system is able to maintain a faulty generator below a set temperature threshold preventing overheat and allowing mission completion. These tests were performed entirely in a simulation environment and using the experimental rig.

1.6.7 Conclusions

Finally in chapter 8 conclusions are draw and any extensions are suggested.

1.7 Contributions

The research to be presented within this thesis will make contributions in two main areas, these are:

1.7.1 Modelling Contributions

As stated earlier there several contributions made by the models presented here. First the uses of lumped parameter thermal models for a condition monitoring application is a contribution to knowledge. In chapter 2 it is shown that this type of model has only previously been used as a generator design tool.

Another contribution is the creation and validation of a linear form of this model, described in chapter 5, as well as the analysis of the effect of a non-linear winding loss representation and temperature dependent winding resistance upon long term model performance.

The creation and validation of a system identification model of the thermal dynamics of a generator described in chapter 5 also represents a major contribution to knowledge.

The final modelling contribution is the comparison of the physics-based and system identification methods of modelling the thermal dynamics of a generator.

1.7.2 Generator Health Management Contributions

In this area, the main contribution of this thesis is the creation of a prognostic based load management algorithm for an aircraft generator described in chapter 7. Prior work in this area has used only real-time intervention based on the current state of the generator. By introducing a prediction of the future temperature state of the generator action can be taken in advance allow some generator capacity to be maintained after non-fatal faults.

Within the load management system the use of a Kalman Filter using an n-step ahead prediction described in chapter 6 is novel in relation to aircraft generators.

1.7.3 Publications

1. James Graham, Roger Dixon, Keith Gregory, and John Pearson. "Thermal modelling of an alternator for use in a prediction system." In Control (CONTROL), 2012 UKACC International Conference on, pp. 455-460. IEEE, 2012.

2. James Graham, Roger Dixon, and Keith Gregory. "Predicting the Thermal State of Generators On-Board UAVs." No. 2013-01-2251. SAE Technical Paper, 2013.

3. James Graham, Roger Dixon, Peter Hubbard, and Ian Harrington. "Managing Loads on Aircraft Generators to Prevent Overheat In-Flight." No. 2014-01-2195. SAE Technical Paper, 2014.

Chapter 2

Literature Review

2.1 Introduction

As mentioned in the previous chapter the aim for the load management system being developed is to use prognostic condition monitoring techniques to derive and predict the thermal state of generators on-board Unmanned Air Vehicles (UAVs). This health state is then used to define current and future capabilities, adjusting usage during flight to avoid catastrophic breakdown. This review presents a study of the literature in the area of aircraft power systems and prognostics and health management (PHM).

This literature review is structured as follows. The first section reviews load management systems currently in use in aircraft, followed by an analysis of current trends found within the literature. A review of current trends in aircraft PHM is then presented, focussing particularly on aircraft generators.

The final section focusses upon the modelling, prediction and optimisation techniques used within the load management system. The review of thermal model types shows the process of selecting appropriate techniques for both the simulation model and design models. Methods of predicting future thermal states using the thermal models are then reviewed. Finally research focussing on reconfiguration is discussed.

2.2 Description of Current Aircraft Power Systems

This section first reviews typical power systems on-board aircraft currently in operation, summarising how they are constructed and discussing load management systems. This is followed by a discussion of literature that has been published on advanced aircraft power distribution and load management systems.

Moir and Seabridge [5] define a generic aircraft AC power system shown in figure 2.1 compromising:

- Power generation
- Primary power distribution
- Power conversion and energy storage
- Secondary power distribution

While the number of power sources and the size of distribution networks can change all large aircraft power systems can be divided in this way.

Typically in this set-up the primary power distribution delivers AC power to the most important consumers on-board the aircraft. The secondary power distribution consists of a number of different busses to serve any DC loads or lower voltage/current loads.

The Boeing 767 aircraft is a typical example of this, the aircraft has two main generators with a number of backups, two primary buses that can be linked in emergencies and numerous DC and low power AC buses. A similar set-up can be seen for the Boeing 777 [6]. In both cases each generator is able to supply the

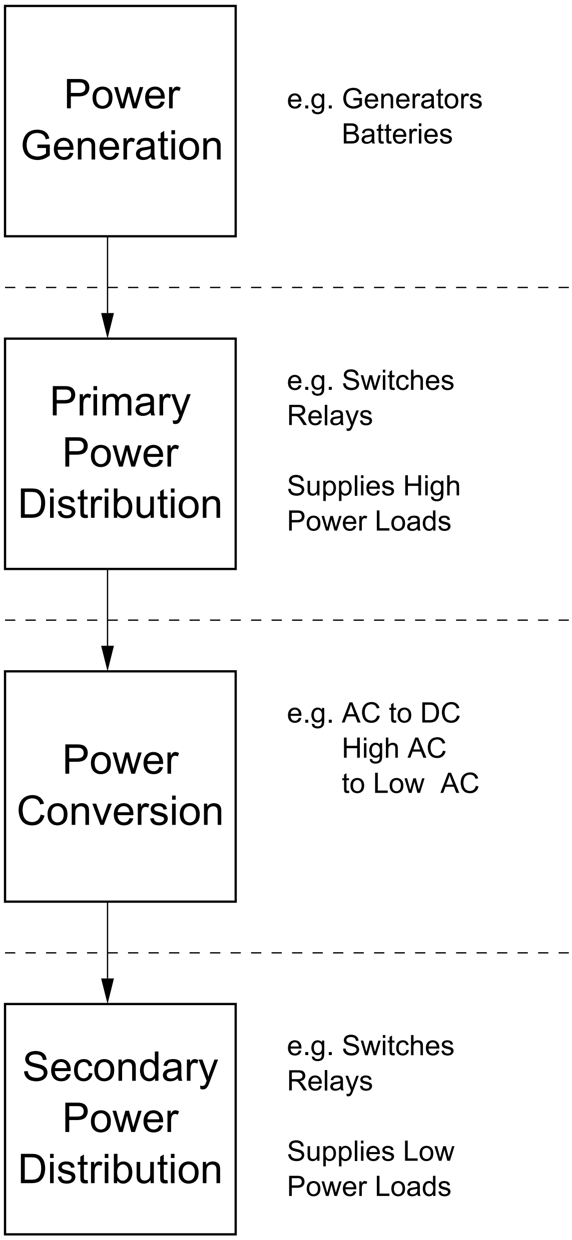

Figure 2.1: Generic aircraft AC electrical system

full power requirement of the aircraft in emergencies by linking the two primary distribution buses, other power sources are available for extreme emergencies.

The power system configuration in 767 is similar to what is present in most aircraft, the loads are all connected to a set bus and emergency power can be sourced if necessary. Research has been undertaken which analyses the use of a more flexible architecture, where power for a load can be taken from other generation sources more easily.

Haak and Lawrence [7] present research focussing on load management centres which are able to distribute power to loads from multiple sources. The advantage of this system is to increase flexibility and reliability by allowing a bank of loads to be powered from multiple different sources, this however would come with an increased wiring requirement.

AbdElhafez and Forsyth [8] review possible power distribution architectures for more-electric aircraft. In this paper two methods are of particular interest; the fault tolerant electrical power distribution system by Glennon [9] and the advanced electrical system (AES) by Worth et. al. [10]. Both papers examine approaches to creating more flexible and reliable power distribution systems. While both authors present plausible solutions both of these are theoretical concepts and no examples showing their implementation are evident.

Looking at the literature it shows that current power systems design will limit the actions, however there is work that in the future will lead to more flexible power distribution systems. This will allow more options for managing loads on a generator. For this research an algorithm will be created which assumes flexibly transferring loads between generators, however as the system is further developed algorithms will have to be extended to manage the loads in discrete blocks even where flexible architectures are available.

2.2.1 Load Management

The term 'power management' is defined as a function that ensures that power generated at an instant in time within a system matches the power consumed. However as noted by Schlabe and Lienig [4] generally on aircraft the term load management is used to describe a function able to control just the loads, not the generators.

Sclabe and Lienig [4] also describe advancements in load management technology. The initial form of load management was a list of loads that a pilot could shed in emergency situations by tripping a circuit breaker; this action could not be undone during flight. The same was true for the first automatic load shedding systems which would do what was previously done by a pilot. This type of system existed in the Boeing 777 [6].

Improvements were made to this by giving crew the ability to switch loads back on after they were automatically shed when power was available, as seen in the US patent by Sodoski et. al. [11]. Hambly et. al. [12] however proposed a system which fully automated the shedding and re-connecting of loads by measuring the power available from all sources then switching on loads up to the maximum power available, prioritising critical loads.

The most advanced load management system was found in a paper by Ding et. al. [13], which is focussed on military ships but the algorithms would be similar to those on an aircraft. A system where loads can be shed and re-connected is proposed. This work improves on previous work by defining an algorithm that adapts the list of load priorities in real time rather than having a set list of loads to shed. This adaptive priority list is an improvement on previous work as it acknowledges that the priority of loads changes with time. What differs it from the work presented in this thesis is that like other load management systems before it the algorithm has no prognostic element to predict future load requirements.

While there are other examples of load management algorithms (e.g. [14, 15]), the author can find no research where future power availability is predicted to assist the load management algorithms. Also discussed in this section is load prioritisation and while this is beyond the scope of this research any future work moving towards a final implementation would have to interact with a load prioritisation algorithm. This would act as a constraint upon what action could be taken.

2.3 Prognostics and Health Management

An important part of the research presented in this thesis is the inclusion of a prognostic element to the final load management algorithm. This section discusses the literature relating to prognostics and health management PHM, focussing mainly on the aircraft industry. Kalgren et al. [16] describes PHM as an approach utilising measurements, models and software to perform incipient fault detection, condition assessment, and failure progression prediction. The aim of this process is to provide improved life-cycle support for the monitored system. Kalgren et al. goes on to define that PHM provides the necessary decision support for these life-cycle improvements. Saxena et al. [17] proposes a similar definition.

The goal of providing decision support is achieved through condition monitoring, with Kalgren et al. [16] defining this as the application of appropriate sensors (data), analysis (knowledge), and reasoning (context).

The aerospace sector is currently one of the leading areas for the application of PHM; the three main motivators for this are:

- Reduced life-cycle costs
- Availability
- Safety

Hess and Fila [18] describe the importance of these factors in allowing both increased operational effectiveness and safety in a time of shrinking budgets. To fulfil these motivators Iyer et. al. [19] describe two types of PHM system; these are long-term off-board PHM (OBPHM), and short-term in-flight prognostics (on-board PHM).

While both OBPHM and on-board PHM use the fundamental principle of producing future condition estimates which are used to influence the systems operation, the difference between the two is in the purpose they are used for. OBPHM uses the condition assessments to schedule optimal maintenance procedures, while on-board PHM focusses on increasing mission success.

Current trends in aircraft PHM are focussed towards OBPHM with Iyer et. al. [19] and Hernandez et al. [20] suggesting frameworks for creating OBPHM systems. An example of this in practice is the automatic logistics system that is being created for the F-35 JSF programme described by Hess et. al. [21]. All of these methods are concerned with generating data about the health condition not just for individual aircraft but fleets of aircraft.

This thesis however focusses on on-board PHM. When researching on-board PHM most of the published material tends to look towards individual sub-systems, Smeulers et al. [22] present a framework for creating PHM systems for any sub-system, the PROMIS (<u>PRO</u>gnostics by <u>M</u>odel-based <u>I</u>nterpretation of <u>S</u>ignals) methodology. This methodology could be applied to any PHM system, however the paper is still focussed on OBPHM.

Rouet et al. [23] have looked at real-time prognostics performed while the aircraft is in flight. This paper particularly addresses the hardware side of the problem, but little information is given regarding the PHM process itself. Again the focus of the work is to inform maintenance, although the output could be re-tasked as part of a decision system for in flight support. Tang et al, [24] do look at on board support, and in-flight reconfiguration. The paper focuses on a jet engine, with a PHM system capable of adapting some engine controls in various fault situations to maintain maximum performance. This shows good initial results, and the authors are working to extend the system to cover the whole engine.

Of the research found that studies on-board PHM none can be found that focusses upon aircraft generators. The research found that studies aircraft generators is still focused upon informing maintenance, examples include Watson et. al. [25] and Batzel and Swanson [26]. Watson et. al. focus on vibration analysis and Batzel and Swanson focus on the rotor electrical degradation.

Upon reviewing current published work on aircraft PHM the author could find no work which focusses upon PHM systems for generator thermal management during flight. The following sections will review the components that make the PHM system. First generator thermal modelling techniques are reviewed, then methods of using these models to create condition predictions and finally methods for reconfiguration in flight are discussed.

2.3.1 Prediction

The literature available that is relevant to model based prediction is broadly found under one of two headings; the first is condition monitoring, the second is Remaining Useful Life (RUL). In the review by Nandi et. al. [27] condition monitoring is considered. Of note is that non-predictive fault detection scheme can also come under the heading of condition monitoring. RUL is defined by Xiao-Sheng et. al. [28] as the length from the current time to the end of the useful life. While RUL could be considered a form of condition monitoring the methods described all involve predicting when failure will occur in the future.

Saha et. al. [29] describe PHM as predicting the health condition of a system using knowledge of past usage, its current state and future usage conditions. This prediction of future state is in the form of a model of the usage conditions, for this research this relates to the effect of losses in the winding of the generator for example upon its temperature.

There are two types of model that can be used; statistical models and physics based models. Both are reviewed in the following sections.

2.3.2 Physics-Based Thermal Modelling

The methods currently used for thermal analysis of an electrical machine can be divided into two main types: analytical lumped parameter and numerical methods [30]. This section first looks at the advantages and disadvantages of each method, presenting evidence to justify the selection of lumped parameter and system identification thermal models for this research. The literature detailing work in this area is reviewed showing how the models created for this research will differ from what has been presented before.

Lumped parameter analysis of an electrical machine involves grouping together components that have a similar temperature and modelling them as single node (e.g. the stator windings). The thermal state of these nodes is defined by analysis of the heat flow between these nodes. The models created by this method have low computational requirements and are easier to understand. The accuracy of the method is strongly dependent upon the parameters within the model, especially heat transfer coefficients. The downside of these models is that a large number of the parameters are not directly known and identifying them can be time consuming and complex.

The two main numerical methods are finite element analysis (FEA) and computational fluid dynamics (CFD). A summary of both these methods can be found in the paper by Boglietti et. al. [30].

FEA some similarities with the lumped parameter analysis, the components are split into many nodes and the heat transfer between them are modelled. This allows for a more accurate analysis of the complex geometries found in electrical machines. However the same difficulties in identifying parameters in lumped parameter analysis apply to FEA, as well as seeing a very large increase in computational requirement.

The CFD method analyses coolant flow around the machine. The method allows flows to be predicted in detail therefore ascertaining how heat moves through the liquid and from solid to liquid. This method produces very accurate results and is especially useful for complex regions of geometry. The disadvantage of this type of method is the high computational requirement combined with the largest expert knowledge requirement both surrounding the theory and software for the model.

The last type of method considered is statistical modelling. The author could find no work relating to black box modelling methods used for thermal analysis. This is most likely due to the most common use of thermal models being in generator design. However in this application during validation both input and output data are available allowing a black box model to be created by matching input to output data. A summary of system identification can be found in the survey paper by Ljung [31]. The advantage to this method is that knowledge of the physical laws governing heat transfer are not required to create the model. The downside is that the models are less flexible and only function well with input data similar to that it was trained on.

In this research it was decided to investigate using a lumped parameter thermal model for use as a simulation model during testing. This was because the lumped parameter model will be able to provide predictions accurate enough to predict overheat faults and the added detail of the FEA or CFD model is unneeded and does not justify the increased computation requirement for this application. For the design models the most important factor was the computation speed. This led to the decision to test both a lumped parameter analysis again but in a more simple form and a statistical model and compare the two.

2.3.3 Lumped Parameter Thermal Networks

As mentioned earlier lumped parameter thermal networks are constructed by lumping components of the electrical machine into nodes and modelling the heat transfer between them. The heat transfer is modelled using simple thermodynamic theory that can be found in many texts e.g. Nellis and Klein [32, 33, 34]. The full theory of the model will be explained in chapter 4. This section first analyses the use of lumped parameter thermal models for electrical machines in the literature. The different specifications that these authors had and how this effected the models are then reviewed, including how this effects the models to be presented in this thesis.

Current Application of Lumped Parameter Thermal Models

The vast majority of thermal models for electrical machines in current literature are created to help design electrical machines. This can be seen in the summary paper by Boglietti et. al. [30] and the references therein. This is also the case for more recently published work e.g. Chowduury et. al. [35] and Rostami et. al. [36]. The author could find no work where lumped parameter thermal models were used for an application other than electrical machine design.

Of the research published on lumped parameter thermal models a second trend can be seen; that the majority of the published work focusses on motors. Of the work published on generators the papers by Wu et. al. [37], Aglen and Andersson [38] and Gerlando et. al. [39] focus on permanent magnet generators. The only paper found that presents a model of a synchronous generator, the type available in the experimental set-up for this research, is by Maloberti et. al. [40]. This paper looks at a claw pole type synchronous generator which has a different shaped rotor to the generator available for this research. The other authors that have published research into the thermal analysis of a synchronous generator have both used a FEA method [41, 42].

Review of Models Created by Other Authors

In this section the lumped parameter thermal models designed by other authors are reviewed. The four major areas of interest are the choice of how many nodes are in the model, how certain complex areas were modelled (e.g. stator winding), how internal coolant flow through a machine is modelled and electrical loss modelling.

The first part of designing a thermal network model is to decide how complex the model will be, which is done through node selection. The designer can choose what lumped sections are to be modelled and each one is assigned a node to represent its average temperature. From the literature it can be seen that different authors have used differing numbers of nodes, some having many nodes for a single section (high node) like the stator back iron [38]. Some authors have used a much smaller number of nodes, lumping larger areas together (low node) e.g. Mezani et. al. [43]. The thesis published by Kylander [44] explores mainly high node models, but also investigates low node configurations and how simulation accuracy changes. Kylander showed that while the more detailed model were more accurate, the difference between the high node and low node models was only $1 - 2°C$ which is not significant. This shows that good accuracy can be achieved with a small number of nodes, the main advantage of a high node model is that a temperature gradient can be mapped across a component. Other authors e.g. [36, 45, 46] also obtained good accuracies using low numbers of nodes and since the temperature gradient provided by a high node configuration is not required for detecting overheat faults the models created will use a low number of nodes to model the system.

The next area of interest is to decide how each node is modelled. The research published creating low node models shows two choices; either simulation of heat flow in a single direction (radially), or simulation of heat flow in two directions (radial, axial). The model created by Okoro [46] simulates heat flow in just the radial direction. The results show that the model provides good steady state performance, however transient operation is not as good as models that simulate heat flow in two directions e.g. Mellor et. al. [47]. Considering that the model created by Mellor et. al. has only 8 nodes whereas Okoro's model has 11, this shows that simulating heat flow in two direction is the optimal choice.

Modelling Challenges

The model created by Mellor et. al. [47] is widely cited by many authors in research published. Many models are based on this method which defines heat transfer in two directions: radial and axial. The model created has excellent accuracy and has a low number of nodes and will be used as a basis for the physics based models in this research. The difference between the work of Mellor et. al. [47] and this is that it focusses on induction motors which means certain areas create modelling challenges that need to be addressed. These are the copper windings and modelling an internal air flow.

Modelling of the winding is a choice that has to be made for all electrical machines. The winding itself is a series of copper strands with air and varnish in between, wrapped in some form of insulation. For any lumped parameter model some approximation must be made in how the node is modelled and different authors have made different choices. Mellor et. al. [47] modelled the whole winding as a copper rod using the thermal conductance of copper for heat transfer in the axial direction and a much reduced value accounting for any air, varnish or lining in a single value. This method was also chosen by authors such as Rostami et. al. [36] and Demetriades et. al. [48]. Boglietti et. al. [49] have modelled the winding in more detail. The winding is modelled as a series of areas radiating from the centre of the winding with a series of resistances modelling the heat flow and heat injected at various points. The paper states that this gives an accuracy of $\pm 5°C$ which is shown in an earlier paper [50]. This steady state accuracy is obtained using the simpler method mentioned earlier, with no report of the transient accuracy for comparison. The lack of accuracy gain combined with increased complexity for the Boglietti et. al. [49] winding model means the simple winding model by Mellor et. al. [47] will be used.

The majority of lumped parameter thermal models created are designed to model motors, often with an enclosed design. This allows heat flow from the stator to be modelled as crossing to the rotor. The generator that is to be modelled however has a coolant flow from outside the generator, through the air gap vented to ambient air. This requires special modelling consideration. Yangsoo et al. [51] achieve this by creating two interacting networks: one for the solid sections and one for the coolant network. This seems unnecessary as Nerg et. al. [45] and Jokinen and Saari [52] model the coolant network using thermal resistances, integrated with the network for the solid sections. This method creates a simpler model than using multiple networks and doesn't require the creation of an algorithm to link the two networks.

2.3.4 System Identification

When searching the literature available detailing the creation of thermal models for generators all the work found considers physics based models of the system. This is due to research focussing on the design process for electrical machines, so authors are creating models which can be build without recorded input and output data. For this research the application is a PHM system and hence there will be input and output data available to build a thermal model from.

There are many statistical modelling methods that have been proposed over time, a summary of these can be found in the review paper by Ljung [31]. Ljung describes many different communities that build "black box" models for systems with many different names, e.g. Machine Learning, Artificial Neural Networks and System Identification.

From these many areas the author could find no other research where a black box model for thermal behaviour of an electrical machine is described.

To select a suitable modelling method from the many available it is necessary to look at the expected characteristics of the system. From looking at the lumped parameter analytical models it can be seen that the system is time-invariant and that the equations of the model are largely linear, only the calculation of winding losses has a non-linear component. It can also be seen that there are multiple inputs available although they do not necessarily need to be used and there are multiple outputs that need to be modelled.

The first step in choosing a method of system identification is the choice between a linear and non-linear model. As stated by Nelles [53] a linear model should always be considered before a non-linear one, with a non-linear model only being used when a satisfactory linear model can not be found. The added complexity and addition knowledge requirement does not justify using a non-linear model when a simpler alternative exists. Looking at the previous paragraph the characteristics suggest that a suitable linear model should be available in this case, so this is what will be considered for the work in this thesis.

Analysing the literature there are numerous methods available for linear system identification and these are summarised in survey papers by Young [54], Isermann [55] and Åström and Eykhoff [56].

Maximum likelihood methods were used by Åström and Bohlin [57] to estimate the parameters of single input single output systems. Clarke [58] used the least squares parameter estimation methods. Wong and Polak [59] utilised instrumental variables within their work. Also of note is the work by Levin [60] creating the Levin principle and the work by Peterka and Halouskov [61] using the Tally principle.

For the system identification model in this thesis it was decided that a least squares estimation method would be used as the system is mainly linear and has low signal to noise ratio which as noted by Isermann [55] should allow an acceptable description of the system dynamics to be obtained using this method.

2.3.5 Simulation Method

The models are used to make predictions of the thermal state of the generator in the future. To do this for each period a prediction needs to be made starting from the current state of the system. The final element of the prediction prediction system is to define a method for determining the initial conditions for the model for prediction each period.

The review by Xiao-Sheng et. al. [28] describes different methods for estimating remaining useful life. In the paper Xiao-Sheng et. al. [28] mention that a large amount of traditional RUL is based on a directly observed state process, but that in reality failure data can be rare and this is also true in this present case where a number of state variables are unmeasured.

The second method which is considered in detail here is through use of an indirectly observed state process. Within this category the systems fall into three main types: filtering models, covariate-based hazard models and Hidden Markov Models (HMM).

Of the three methods filtering type models were chosen. The HMM method was eliminated because, as stated by Xiao-Sheng et. al., the process can be computationally intensive which is incompatible with online simulations on-board an aircraft. The covariate-based hazard models were deemed unsuitable because as stated by Zhao et. al. [62] this method is designed for systems with a non-static environment, whereas for this application the model parameters can be assumed static.

Tang et. al. [63] state that the performance of any filtering method is dependent on the accurate portrayal of the target dynamics. For this application the models have been discussed earlier and will provide the required representation of the system dynamics, the remainder of this section will discuss the choice of filter used to update the model states.

Tang et. al. [63] use particle filters applied to crack growth prognosis in a planetary gear transmission. The results look interesting however there is no data provided to compare the system's prediction output with actual fault progression. This technique is primarily designed for non-linear systems and would be unnecessarily computationally expensive when applied to linear models when simpler methods exist.

Benes [64] proposed a type of filter used by Zhang et. al. [65] for RUL estimation. This is used to create good RUL estimates, however the Benes filter is designed for non-linear system so again is unsuitable.

Looking specifically at filters that are optimal for linear systems the extension of the Kalman Filter [66] for use in prediction is shown by Brown and Hwang [67]. Normally a Kalman Filter predicts a single step ahead however it can also be used to predict n-steps ahead. Sarma et. al. [68] used this method in 1978. In this paper the use of Kalman Filter based prediction was used to monitor the condition of aeroengines.

Christer et. al. [69] applied this to furnace maintenance. Importantly showing the method's ability to update observed and non-observed states, this is useful for the present application where using the minimum number of measurements is ideal.

Of the previous work applying Kalman Filter prediction to generators only a single paper was found. This was by Batzel and Swanson [26] which investigates RUL estimation for rotor field circuit degradation in generators. The research presented in this thesis differs as it will apply this method to predicting the thermal dynamics of a generator.

2.4 Reconfiguration

In the previous section the work described looked at estimating RUL for adaptive maintenance programs. In this research the objective is to be able to manage the loads on the generator to prevent overheating. This means that the prediction algorithm is providing prognostic support for a system to adjust load profiles in flight, which is different to a large amount of the work previously referenced. This section analyses the literature focusing on reconfiguration of systems to prevent predicted faults.

Black et. al. [70] discuss reconfigurable control for aircraft fuel systems. While in this case the system is designed for fault detection and isolation, Black et. al. also discuss assessing the capability of a faulty system, something undertaken in this research. The main difference with this system is that the faults are diagnosed then prediction is used to assess the effect of the fault on the system, whereas this research looks to predict faults before they occur. Lin and Lee [71] take a similar approach of using prognostics to assess remaining useful life after a fault as well as control reconfiguration.

Other authors use this method of reconfiguration after faults which differs from the method proposed in this research. Strangas et. al. [72] apply this method to AC motors. Of note is that they show that a number of faults can cause temperature rises in a generator for which the response can be to lower loads.

Closest to this research is the work published in two papers by Tang et. al. [73, 74] looking at automated contingency management with prognostics (ACM+P). Tang et. al. describe a framework to allow a system to adapt to faults currently and in the future. The system is hierarchical looking at component, system and mission level reconfiguration. The framework describes a method for achieving in-flight reconfiguration, the example used in the paper being for an actuator. The work presented in this thesis focusses on the thermal dynamics of an aircraft generator, this can be described as component/system level reconfiguration under Tang et. al.'s methodology.

Within the literature the author could find no work which specifically describes prognostic reconfiguration of generators to prevent overheat faults in-flight.

2.5 Conclusions

This literature review has analysed research in the field of prognostics and health management (PHM) within aircraft load management.

From the literature it can be shown that no current aircraft could be found which use a predictive element in their load management systems. The most advanced algorithms are able to shed and reconnect in real time, but do not predict future capability. This is also shown in the literature where no research has been proposed where predictive load management is used.

Analysing the research into PHM in aircraft there are two main motivators: maintenance and reconfiguration. This research is based around reconfiguration and of the research described no work looks at thermal reconfiguration of generators. Most PHM research focussing on generators addresses bearings or windings. The author could find no published PHM research on generator thermal monitoring either for maintenance or reconfiguration.

The review has shown that the best physics-based modelling method for this research is a lumped parameter thermal model and also showing that this type of model has not been used in a condition monitoring application before. The review also showed that the lumped parameter thermal models in the literature use a non-linear representation of the winding losses, in this research the effect of linearising the losses and how this changes the simulation results will be analysed. The review into modelling techniques also showed that no research could be found which creates a system identification model for the thermal dynamics of a generator, one of the model types to be assessed in this research.

The final sections showed that using a Kalman Filter as part of the prediction system was ideal as well as showing that it had never been applied for prediction of the thermal dynamics for a generator. It was also shown that the general framework for automated contingency management with prognostics (ACM+P) by Tang et. al. [73] describes the work undertaken in this as component/system level reconfiguration, but that this framework had not been applied to aircraft generators.

Chapter 3

Experimental Set-Up

3.1 Introduction

To create the load management system described in chapter 1 two generator models are needed: the simulation model and the design model. For this research a generator rig was commissioned in the lab to allow collection of data to be used to validate these models.

This chapter describes the experimental rig used in this research and how it was adapted, comparing it to the power generators on-board unmanned air vehicle (UAV). This rig will provide the data against which the models described in chapters 4 and 5 will be validated. It will also be used in chapter 7 to test the effectiveness of the proposed load management algorithms.

The chapter begins with a summary of the evolution of power systems on aircraft over time. These generation schemes will be compared to the generator within the experimental set-up. The rig will then be described in detail, including how the generator is driven, what sensors are used and how data is collected and stored.

3.2 Aircraft Generators

The power system on-board modern aircraft is designed to supply electricity to a wide array of consumers. This includes providing both alternating current (AC) and direct current (DC) power dependent upon the system.

Early aircraft designed in the 1940s - 50s started out using 28VDC systems exclusively [1]. From that modest beginning the power requirements upon aircraft have grown drastically with the introduction of 115VAC systems, then 230VAC. Some of the newest military jets have now started to include 270VDC systems with solid state power controllers becoming small enough [2]. Figure 3.1 shows a chart plotting the use of different power generation types as they came into service.

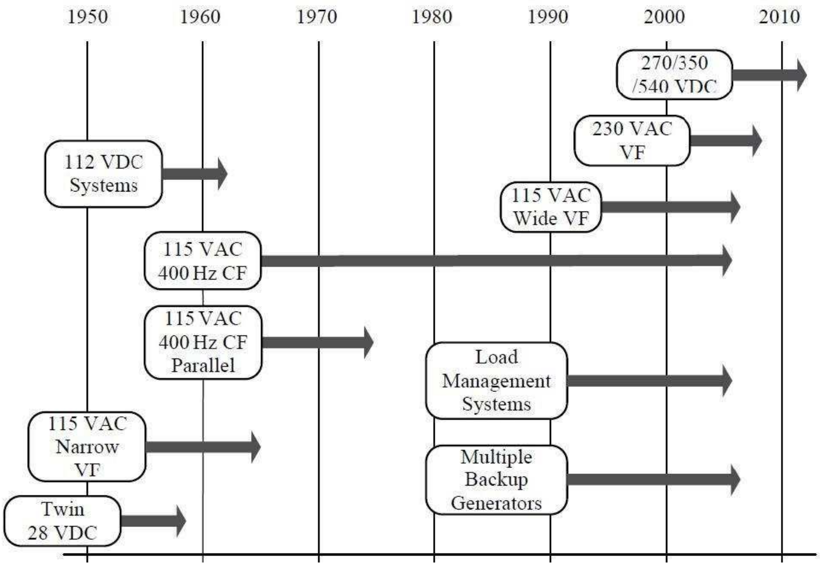

Figure 3.1: Electrical System Evolution [1].

There are four main types of power generation scheme present within aircraft which will be reviewed here. These are:

- Integrated Drive Generators (IDG)
- Variable Speed Constant Frequency (VSCF)
- Variable Frequency (VF)

- 270VDC

Table 3.1 shows some examples of aircraft which use each of these power generation schemes.

Table 3.1: Common Types of Power Generation [2].

<table>
<tr><th>Generation Type</th><th colspan="2">Civil Application</th><th colspan="2">Military Application</th></tr>
<tr><td rowspan="7">IDG/CF
(115VAC/400Hz)</td><td>B777</td><td>2x120kVA</td><td colspan="2" rowspan="7">Eurofighter Typhoon</td></tr>
<tr><td>A340</td><td>4x90kVA</td></tr>
<tr><td>B737NG</td><td>2x90kVA</td></tr>
<tr><td>MD-12</td><td>4x120kVA</td></tr>
<tr><td>B747-X</td><td>4x120kVA</td></tr>
<tr><td>B717</td><td>2x40kVA</td></tr>
<tr><td>B767-400</td><td>2x120kVA</td></tr>
<tr><td>VSCF
(Cycloconverter)
(115VAC/400Hz)</td><td colspan="2"></td><td>F-18C/D

F-18E/F</td><td>2x40/
45kVA
2x60/
65kVA</td></tr>
<tr><td rowspan="2">VSCF (DC Link)
(115VAC/400Hz)</td><td>B777(Backup)</td><td>2x20kVA</td><td colspan="2" rowspan="2"></td></tr>
<tr><td>MD-90</td><td>2x75kVA</td></tr>
<tr><td rowspan="3">VF
(115VAC/380
-760Hz Typical)</td><td>Global Ex</td><td>4x50kVA</td><td rowspan="3">Boeing
JSF (X-32
A/B/C)</td><td rowspan="3">2x50kVA</td></tr>
<tr><td>Horizon</td><td>2x20/25kVA</td></tr>
<tr><td>A380</td><td>4x150kVA</td></tr>
<tr><td>VF
230VAC</td><td>B787</td><td>4x250kVA</td><td colspan="2"></td></tr>
<tr><td rowspan="2">270VDC</td><td colspan="2" rowspan="2"></td><td>F-22
Raptor</td><td>2x70kW</td></tr>
<tr><td colspan="2">Lockheed-Martin F-35 -
Under Review</td></tr>
</table>

3.2.1 Integrated Drive Generator (IDG)

Of the four methods described here IDGs are the oldest, an example is shown in the patent by Reynolds [75]. In this scheme the variable shaft speed of the engine is converted to a constant speed through the use of a hydraulic constant speed drive (CSD). This technology is very mature however the biggest down side is the CSD which has a lower reliability than the rest of the engine or generator. This led to high maintenance costs related to extracting the CSD from the engine and repairing/replacing.

3.2.2 Variable Speed Constant Frequency (VSCF)

The VSCF power generation method represents a step forward from the IDG to reduce the complexity of the mechanism but also make maintenance easier. In a VSCF scheme the CSD is removed and the generator attached to the engine is a variable frequency generator. Then through the use of power electronics, either a cycloconverter or a DC link, the supply is converted to 115VAC 400Hz constant frequency. The power electronics have a higher reliability and not integrated into the engine making maintenance easier.

3.2.3 Variable Frequency (VF)

VF is the natural extrapolation of VSCF. In this scheme the variable frequency generator is kept, but instead of converting to a constant frequency the power supplied to the consumers on-board is left as a varying frequency. This reduces cost and weight of power electronics as a large amount of energy consumers can be supplied with frequency wild current, or a frequency wild alternative exists. However there are some power consumers that still require constant frequency supply so some local power conversion is necessary. Overall though the weight of power conversion equipment is reduced substantially, reducing complexity in the power system and therefore costs.

3.2.4 270VDC

With solid state power controllers becoming small enough some new military aircraft have been fitted with a 270VDC power system. This includes the F-22 Raptor and the Joint Strike Fighter (JSF). The aim of this scheme is to exploit the lower gauge of wire required to transmit DC current, as well as reduced transmission losses. In this scheme AC current from the engine generators is converted to 270VDC for transmission through the airframe.

3.2.5 Typical Generator Specification

While four different power generation architectures have been described, the generators used in these systems bear some notable similarities. Typically the main generators are 3-phase synchronous generators, also referred to as alternators. There is an internal coolant flow, usually oil as part of a two stage process.

The main aspects upon which the generators vary are the output voltage and frequency. The voltage depends upon scheme with modern aircraft in production using generators up to 230VAC or 270VDC, shown in table 3.1. The IDG schemes use 400Hz frequency generators, while the other schemes use variable frequency generators.

3.2.6 Generator Load Profiles

The research undertaken focusses on military UAV applications, as such when describing the loads applied to the generator this is done using military specifications. Load profiles are described according to military specification MIL-E-7016F [76] which describes the load on a generator in terms of the average total load over the period of operation. Each mission stage an aircraft can operate has a defined load requirement; this is the start-up power requirement and the continuous power.

Each flight phase, numbered from one to seven, can be used to build load profiles by putting a series of these blocks together one after another.

Table 3.2: Load conditions

	1	**2**	**3**	**4**	**5**	**6**	**7**
5 mins	40.0%	83.3%	100.0%	83.3%	83.3%	86.7%	100.0%
Continuous	27.3%	66.7%	83.3%	76.7%	70.0%	73.3%	76.7%

Each number represents a specific action as follows:

1 - Loading and Preparation

2 - Start and Warm-Up

3 - Taxi

4 - Take-Off and Climb

5 - Cruise

6 - Cruise/Combat

7 - Landing

Table 3.2 shows the required current for each flight phase as a percentage of the generator maximum and has two values: the first 5 minute value represents the first 5 minutes of the action and is the start up power, while the continuous value is the load for the rest of the duration of the action. Each load condition has a minimum execution time of 15 minutes and no upper limit on duration.

Figure 3.2 shows an example load profile covering all the preparation stages the take-off, follow by a cruise to target. The aircraft then takes a combat action before flying home and landing.

The values in table 3.2 represent load requirements analogous to that of a UAV with dual generators. These values were agreed with the industrial sponsors of the work. In this case due to the sensitive nature of the data the power requirements

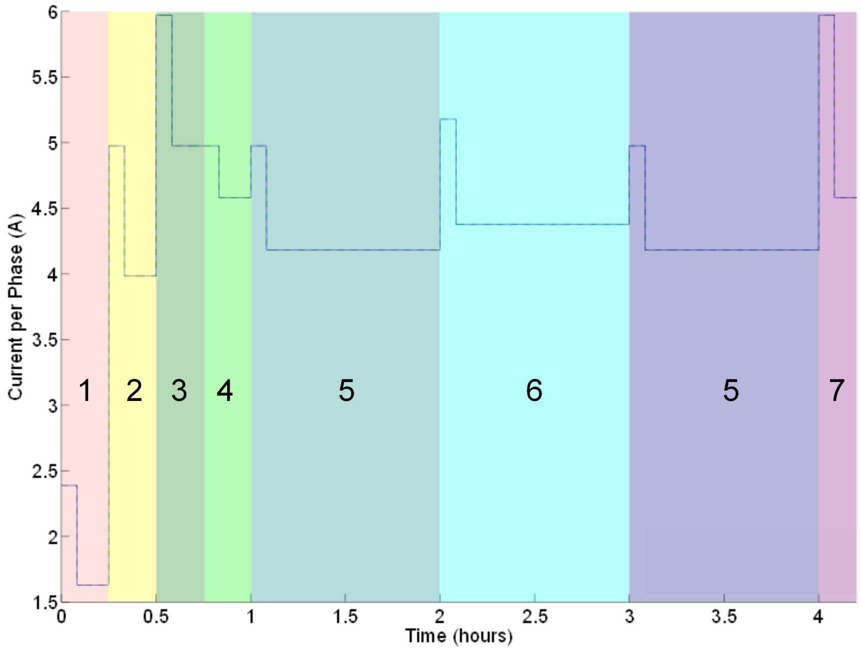

Figure 3.2: Example Load Profile.

have been changed by ± small amounts so that it is different to that of any real aircraft.

3.3 Test Rig

The generator used within the test rig is not an aircraft generator. The generator is a commercial synchronous generator with an internal airflow provided by a fan. While there are a number of differences from an aircraft generator a validated thermal model of this generator could be used to show the research concept functioning.

The generator does share some similarities including that it is synchronous. While the coolant used is air, transitioning to a model using oil as a coolant would only require re-definition of the material properties. The constant shaft speed of the generator is similar to the set-up for an IDG, to simulate a variable frequency generator would require re-definition of the losses in the model. Overall the structure of a thermal model for an aircraft generator would be similar to the model structure for this generator with different parameters.

3.3.1 Plant Description

Figure 3.3 below shows the test rig consisting of a motor driving the shaft of a generator, which rotates the generator shaft at a constant 1500rpm required to produce rated voltage. Loads are applied to the generator through use of a load bank shown in fig. 3.4.

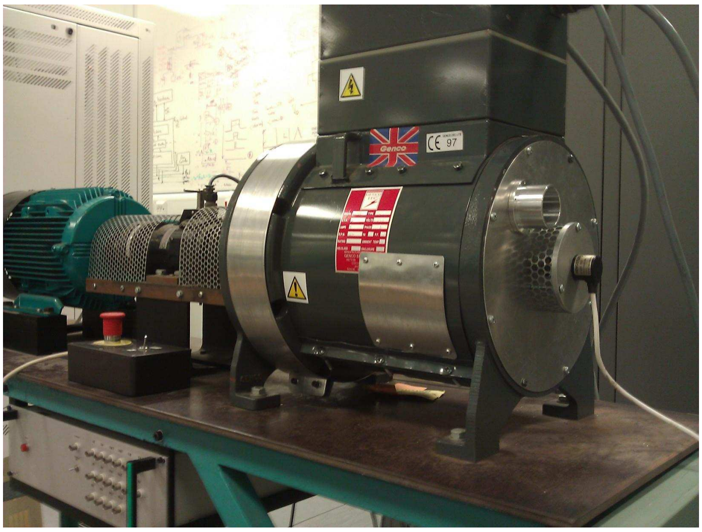

Figure 3.3: Test equipment, showing generator (right), driven by motor (left).

As part of the process of commissioning the rig numerous updates/alterations were made to the equipment. First the electronics in the control cabinet were re-wired as well as connecting the generator and load bank to the cabinet. Next alterations were made to make aspects of the generator more closely mimic what would be present in an aircraft, these are detailed below. With these alterations there are enough similarities that aircraft generators could be modelled by small structural changes as well as re-parametrising the model. Additional temperature sensors were also added to give a better thermal view of the machine and finally the data acquisition system had to be specified and implemented; these are detailed below.

Figure 3.4: Load bank.

Generator

The generator used as part of the test set-up is a Genco RF201A synchronous generator, which includes a damper winding. The specification for this is shown in table 3.3.

In order to allow the generator to more closely mimic the likely set-up on-board a UAV some adjustments were made to the outer casing. The large vents originally present were substituted for solid plates with set inlet and outlet ducts at which input and output air temperature could be measured. These plates shown in figure 3.3 create an internal coolant flow and while on an aircraft the coolant would likely be oil in terms of thermal modelling these would be similar model structure with different parameters.

Motor

The generator is driven by a 3 phase induction motor that is controlled by a Eurotherm 620 series drive. When switched on it is set to drive the generator

Table 3.3: Generator Specification

Type	Genco RF201A; synchronous; including damper winding
Serial number	220399
Power	5 [kVA]
Volts	415/240 [V]
Power factor	0.8
Current	7 [A]
Phases	3
Number of poles	4
Frequency	50 [Hz]
Shaft speed	1500 [rpm]
Excitation	Brushless rotating rectifier, with auxiliary winding for exciter power
Rating	00P
Insulation class	H
Enclosure type	22

shaft at the 1500rpm required for the generator to produce rated voltage.

Load Bank

The load can be set to draw a load between 1A and 7A from each generator phase, with the ability to define the power factor and create unbalanced loads if desired.

3.3.2 Sensor Setup

The test equipment initially had 16 sensors installed. An additional 4 temperature sensors were installed (with capability for two more if necessary) to give 20 in total - these are listed in table 3.4. These fall into the main categories of load currents/voltages, excitation currents/voltages, and generator temperatures.

The signals from all sensors on the rig are routed from the generator to a measurement box (fig. 3.5) where the signals are pre-processed before being logged

Table 3.4: Sensor on the Rig

Variable	**Signal Label**	**Transducer Range**
Stator Phase U Current	Ua1	$\pm 230A$
Stator Phase U Current	Ua2	$\pm 15A$
Stator Phase V Current	Va1	$\pm 230A$
Stator Phase V Current	Va2	$\pm 15A$
Stator Phase W Current	Wa1	$\pm 230A$
Stator Phase W Current	Wa2	$\pm 15A$
Stator Phase U - Neutral Voltage	Uv	$\pm 500V$
Stator Phase V - Neutral Voltage	Vv	$\pm 500V$
Stator Phase W - Neutral Voltage	Wv	$\pm 500V$
Exciter Winding Current	Ea	$\pm 5A$
Exciter Winding Voltage	Ev	$\pm 125V$
Auxiliary Winding Current	Xa	$\pm 2.5A$
Auxiliary Winding Voltage	Xv	$\pm 500V$
Stator Phase U Temperature	Ut	-50 to $300°C$
Stator Phase V Temperature	Vt	-50 to $300°C$
Stator Phase W Temperature	Wt	-50 to $300°C$
Stator Iron Temperature	Iront	-50 to $300°C$
Inlet Temperature	Ait	-50 to $300°C$
Outlet Temperature	Aot	-50 to $300°C$
Mid Air Pocket Temperature	Amt	-50 to $300°C$

by the data acquisition system.

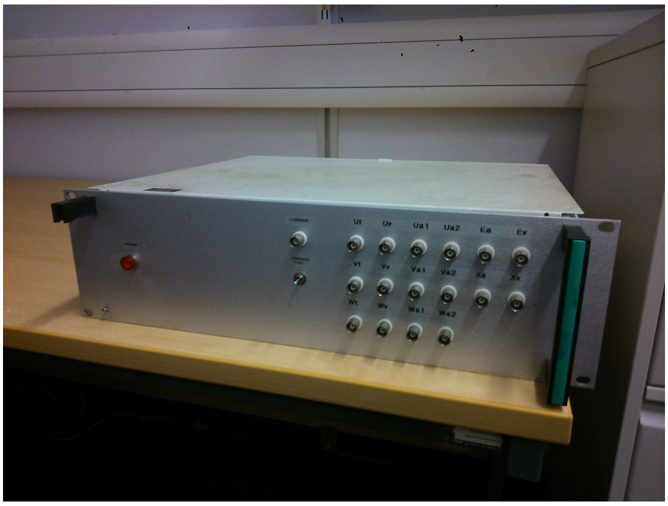

Figure 3.5: Instrumentation box for collecting sensor data from rig.

Voltage and Current Sensors

An overview of the sensor set-up is shown in Fig. 3.6 and 3.7. Voltage transformers (VTs) and current transformers (CTs) are fitted to monitor the voltages and currents in the stator, exciter and auxiliary windings. The transducers are galvanically isolated allowing equipment referenced to ground to be used to analyse the measurements. The transducers are mounted close to the generator terminals with the isolated output signals routed to a box of instrumentation where BNC connectors provide the interface for analysis and recording equipment.

Each CT/VT is connected to the same filtering circuit shown in figure 3.8 which produces the voltage to be read by the DAQ card.

Each of the sensors was calibrated over the current/voltage range; in each case a linear first order transfer characteristic was generated for each sensor. For the current sensors this was in the form:

$$I_A = I_V C_1 + C_2 \tag{3.1}$$

Where I_A is the line current, I_V is output voltage from the measurement box,

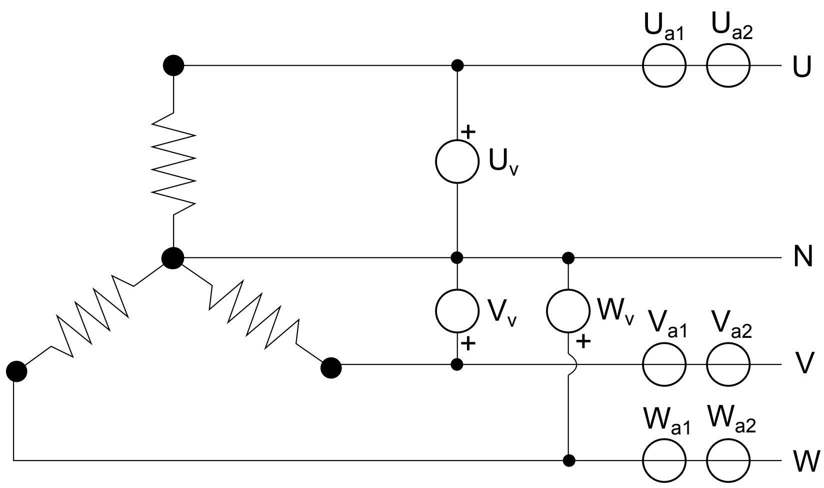

Figure 3.6: Stator Sensor Layout.

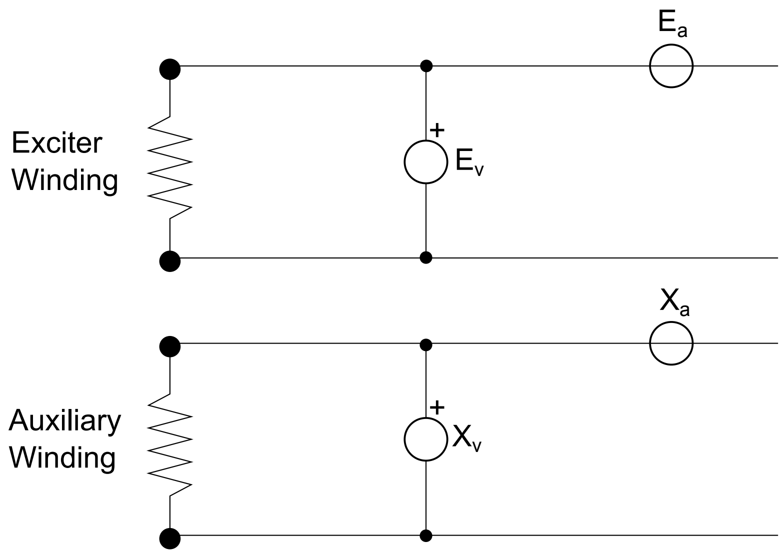

Figure 3.7: Exciter and Auxiliary Winding Sensor Layout.

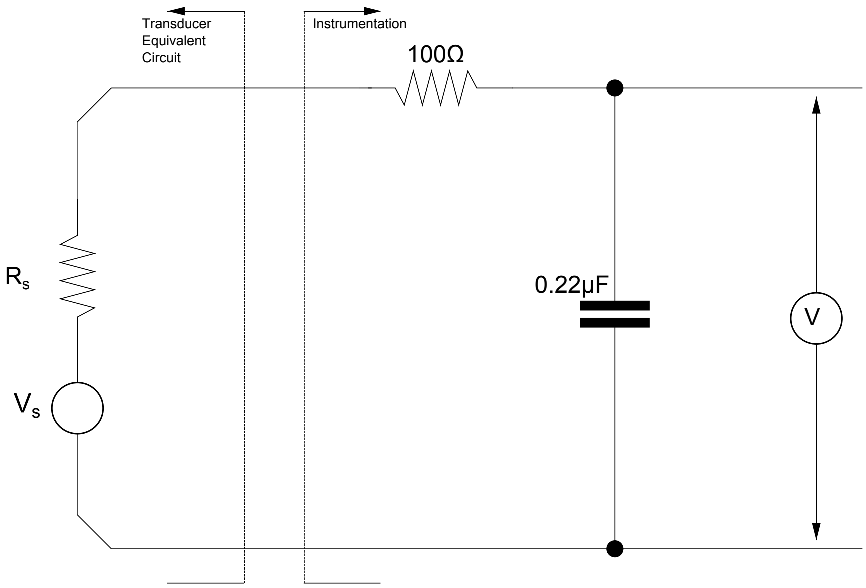

Figure 3.8: Current/Voltage Sensor Circuit Layout.

C_1 is the gradient and C_2 is the offset. For the voltage sensors this was in the form:

$$V_V = V_M C_1 + C_2 \tag{3.2}$$

Where V_V is the line voltage, V_M is output voltage from the measurement box, C_1 is the gradient and C_2 is the offset.

Table 3.5 shows the C_1 and C_2 values for each of the CTs and VTs to an accuracy of 3 significant figures.

Temperature Sensors

Platinum resistance thermometers (PRT) are used to sense the temperature at various points within the generator. In total there are seven different sensors. Three are located in the stator windings, one on the stator itself and three in the air pockets within the generator. The locations are shown in figure 3.9.

All of the temperature sensors are identical; each one is a PT100 type PRT meaning that it has a resistance of 100Ω at $0°C$. The temperature/resistance relationship is defined in the British Standard BS EN 60751:2008 [77]; the tolerance

Table 3.5: CT and VT polynomial gradients and gains

Variable	C_1	C_2
Stator Phase U Current	39.1	0.169
Stator Phase U Current	3.34	-0.0378
Stator Phase V Current	39.1	-0.171
Stator Phase V Current	3.37	-0.113
Stator Phase W Current	39.2	0.191
Stator Phase W Current	3.38	-0.0575
Stator Phase U - Neutral Voltage	66.6	0.491
Stator Phase V - Neutral Voltage	66.9	0.540
Stator Phase W - Neutral Voltage	66.6	0.571
Exciter Winding Current	1.02	0.00224
Exciter Winding Voltage	20.0	0.0697
Auxiliary Winding Current	0.499	0.00484
Auxiliary Winding Voltage	66.6	0.896

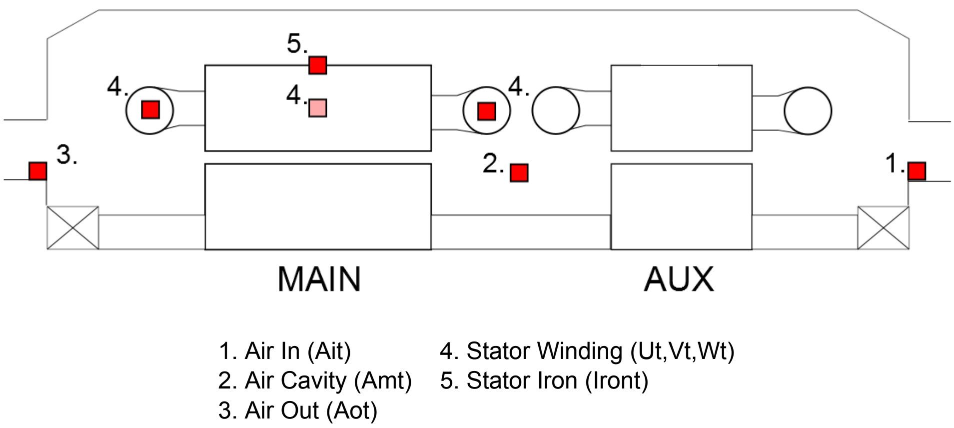

Figure 3.9: Temperature Sensor Locations on a Cross-Section of the Generator Showing Only the Top Half Due to Symmetry.

for each sensor is class B. According to BS EN 60751:2008 the resistance between the temperature range of $0°C$ to $850°C$ can be calculated from a standard equation.

$$R_t = R_0(1 + At + Bt^2) \tag{3.3}$$

Where R_t is the resistance at a temperature t, R_0 is the resistance at $t = 0°C$, and A and B are constants.

$A = 3.9083 \times 10^{-3}°C^{-1}$

$B = -5.775 \times 10^{-7}°C^{-2}$

An overview of one temperature measurement channel is shown fig. 3.10; all the other channels are identical. The PRTs used are the four wire type. A constant current source drives each PRT, the resulting voltage drop being proportional to resistance which in turn is a function of winding resistance. The PRT voltage is routed to a box of instrumentation (which also supplies the constant current) where it is filtered before output via a BNC connector which provides the interface for analysis and recording equipment.

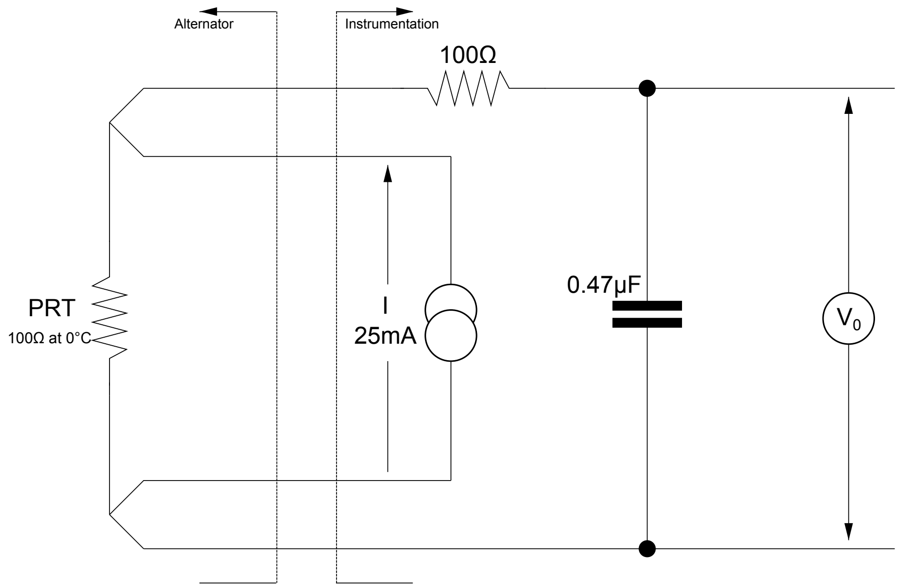

Figure 3.10: Temperature Sensor Circuit Layout.

As each PRT has a set temperature resistance relationship, to calibrate the voltage input to the data acquisition card the PRT was replace with a resistance box. This allowed the voltage to be related to the resistance of the PRT which in turn is related to a temperature using equation 3.3.

3.3.3 Data Acquisition

Each of the sensor streams that are made available from the rig is output from an instrumentation box (figure 3.5) via a BNC connector as a voltage value. To log these signals a data acquisition (DAQ) system needed to be created.

The system created uses a National Instruments (NI) DAQ card to input these signals digitally into a computer system. These signal inputs are then processed and recorded use NI LabVIEW software.

Data Acquisition Card

The DAQ card used within the system is an NI PCI-6229 card with 32 analog inputs, the full specification for this is shown in table 3.6. When using the card all channels have to be sampled at the same rate so a rate of 110Hz was used. This value was chosen as it is twice the generator frequency ($50Hz$) plus 10%. This fulfils the Nyquist sampling rate criterion to allow reconstruction of the voltage/current sinusoid and to prevent aliasing. This is adequate in this application as the currents and voltages are to be converted to root mean square (RMS) values. It should be noted that a sample rate of 110Hz for all 20 analogue channel totals 2200S/s, much lower than the card maximum of 250kS/s.

Data Processing

A LabVIEW VI was developed to collect, process, calibrate and record data from each channel of the DAQ card in use. Each channel has the voltage input transformed into its actual value using calibration curves defined earlier. This can then

Table 3.6: DAQ Card Specification

Type	NI PCI-6229
Analog Inputs	32, 16-Bit, 250kS/s
Analog Outputs	4, 16-Bit, 833kS/s
Digital I/O	48 digital I/O; 32-bit counters; digital triggering
Correlated DIO	32 clocked lines, 1 MHz

be viewed in real time on the data acquisition PC. Simultaneously it is saved to file in a comma separate variable (CSV) format with a time stamp for each data point which can be accessed and applied later.

3.4 Conclusion

In this chapter common power generation schemes used in aircraft have been summarised, including common characteristics of aircraft generators themselves. The generator used in this research as part of a test rig has been compared to common aircraft generator characteristics. While the test rig generator differs in a number of ways, due to the test rig being a synchronous generator and having an internal air flow, a model of the test rig could easily be converted to an aircraft generator with small structural changes and re-parametrisation.

The test rig which has been modified and commissioned as part of this research has been described, including the sensors used to gather electrical and thermal data and the data acquisition system. The generator rig will be used to validate the simulation model described in chapters 4 and the design model in chapter 5.

Chapter 4

Derivation of a Thermal Network Model

4.1 Introduction

In the literature review numerous methods for developing a thermal model of a generator were described. These included computational fluid dynamics (CFD), finite element analysis (FEA) and lumped parameter models. For the purpose of this study a lumped parameter approach was chosen as a good representation of the generator can be achieved with the advantages described in chapter 2.

This chapter covers the development of a non-linear simulation model which provides a good prediction of the thermal states of the generator described in chapter 3, as it undergoes various load profiles. This model will be used for long duration simulation experiments where it is impractical to run multiple tests on the real generator.

The chapter begin by introducing the thermal modelling approach, then showing how the generator can be partitioned into sub-models. The sub-model equations are defined before being combined to give the overall system model. Finally, the method for defining the parameters is presented and the model is validated against data collected from the generator described in chapter 3.

4.2 Model Derivation

The model that has been build is an extension of the work by Perez and Kassakian [78] and Mellor et. al. [47]. The model is formed from the division of the structure of the generator into multiple sections according to its geometry. There is no set requirement for the number of sections. These are chosen to allow the best alignment of the model with the applications requirements.

The main requirement is for the model to provide a good representation of the actual generator. With this in mind it was decided that the generator would be split in broad sections based on the main parts of the generator (e.g. stator, rotor, windings etc.). Work by Kylander [44] shows that a good representation can be achieved even when splitting the generator into as few as 5 sections.

4.2.1 Model Fundamentals

The basis of the thermal network model is the thermal resistance shown in figure 4.1, from this the equation for the change in temperature across the resistance can be defined.

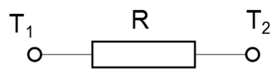

Figure 4.1: Single Thermal Resistance.

$$\Delta T = Q \cdot R \tag{4.1}$$

ΔT is the difference in temperature in $^{\circ}C$ (used here) or Kelvin (K) $T_1 - T_2$, Q the heat input into the system in Watts (W), and R is the thermal resistance in the direction of heat flow in K/W. An example calculation for R for axial heat flow along a rod with circular cross section is given as:

$$R = \frac{L}{\pi r^2 k} \tag{4.2}$$

Where L is the length of the rod in meters (m), r is the rod's radius in m, and k is the thermal conductivity of the material in W/Km. Networks of resistances can be built in the same manner as an electrical circuit, with constant current sources representing heat input, and capacitances representing heat storage.

The cylindrical structure on which the models for all metal sections of the generator are based is shown in figure 4.2. Heat transfer is calculated in two directions; radial (θ_1 to θ_2) and axial (θ_3 to θ_4). This is achieved with two thermal resistance networks. Each thermal network is related to the average temperature of the whole cylinder (θ_m) with an extra thermal resistance (figure 4.3); the two networks can now be connected forming a model for the whole cylinder.

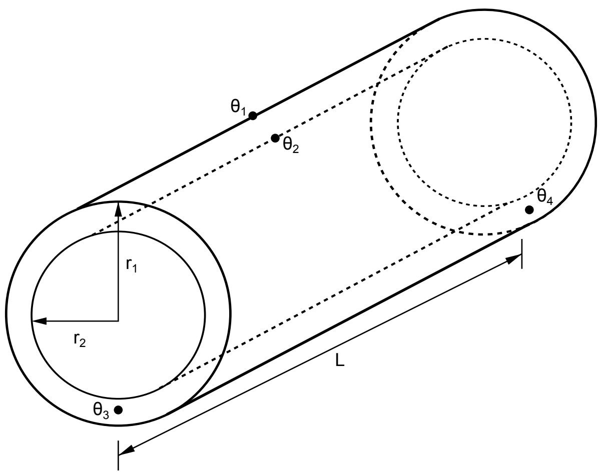

Figure 4.2: Cylindrical component.

It is assumed that the axial temperature across the component is constant, which is shown in figure 4.4 as a single thermal resistance R_a representing the flow of heat from the mean temperature to the ends of the cylinder. The equations for the network can then be defined.

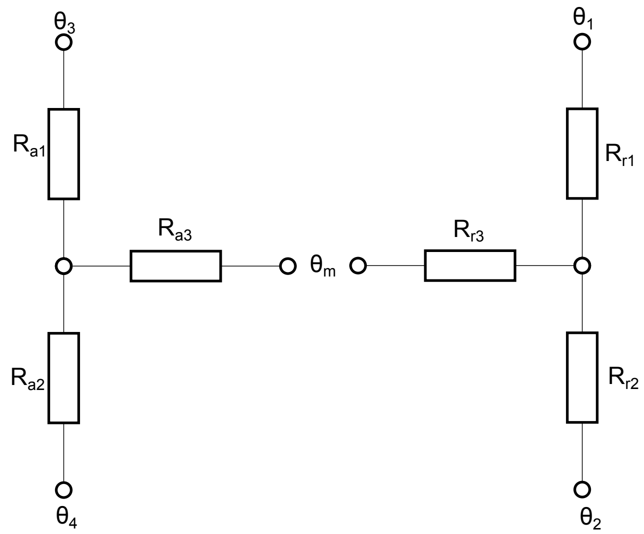

Figure 4.3: Separate thermal networks for axial and radial heat transfer.

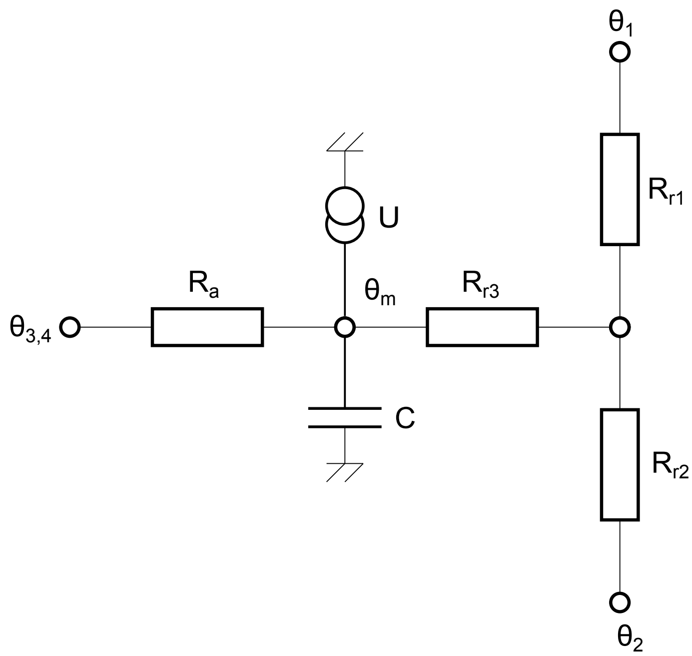

Figure 4.4: Thermal network for cylindrical component.

$$R_a = \frac{L}{12\pi k_a(r_1^2 - r_2^2)} \tag{4.3}$$

$$R_{r1} = \frac{1}{4\pi k_r Ls}\left(1 - \frac{2r_2^2 log(\frac{r_1}{r_2})}{r_1^2 - r_2^2}\right) \tag{4.4}$$

$$R_{r2} = \frac{1}{4\pi k_r Ls}\left(\frac{2r_1^2 log(\frac{r_1}{r_2})}{r_1^2 - r_2^2} - 1\right) \tag{4.5}$$

$$R_{r3} = \frac{1}{8\pi k_r Ls(r_1^2 - r_2^2)}\left(r_1^2 + r_2^2 - \frac{4r_1^2 r_2^2 log(\frac{r_1}{r_2})}{r_1^2 - r_2^2}\right) \tag{4.6}$$

Where $R_{a,r1,r2,r3}$ are the resistance shown in figure 4.4. From figure 4.2, L is the cylinder length, r_1 and $r2$ are the outer and inner radius respectively. Finally k_r and k_a are the axial and radial thermal conductivities, and s is the stacking factor, the ratio of iron to insulation in the laminations where a stacking factor of 0.9 indicated that there is 90% iron.

Figure 4.4 shows the heat storage of the cylinder C represented as a capacitance. The equivalent capacitance of the cylinder is calculated from the cylinder's dimensions and material properties.

$$C = \rho c_p \pi (r_1^2 - r_2^2)L \tag{4.7}$$

Where ρ is the density of the material, c_p is the specific heat capacity, r_1 and $r2$ are the outer and inner radius respectively and L is the cylinder length.

The heat input to the cylinder U is represented in figure 4.4 as a constant current source. This is calculated as a power in Watts from the electrical losses within the cylinder.

Finally some divisions need to be modelled as a rod rather than a cylinder, meaning $r_2 = 0$. This is achieved by removing the resistance R_{r2} then combining R_{r1} and R_{r3}. This gives the final equations as:

$$R_a = \frac{L}{12\pi k_a r_1^2} \tag{4.8}$$

$$R_r = \frac{1}{4\pi k_r L s} \tag{4.9}$$

4.2.2 Model Divisions

In the model the generator was divided into 5 main areas, some of which were further divided. These areas are the frame, stator, rotor, shaft and the air within the generator. The divisions which were modelled are shown in table 4.1 along with the subscript notations used in the equations for each division. For example the thermal resistance R_{r1} for the stator iron would be marked as R_{sir1} and R_{str1} would be the same resistance for the stator teeth. The average temperature for each section θ_m is given the label for the section, i.e. θ_r is the average temperature of the rotor. Subscripts are also added to the surface temperatures $\theta_{1,2,3,4}$, e.g. $\theta_{si1,si2,si3,si4}$ for the stator iron. Figure 4.5 shows an exploded view of the generator with the different divisions except the stator end windings and end air gaps which can be seen in figure 4.6.

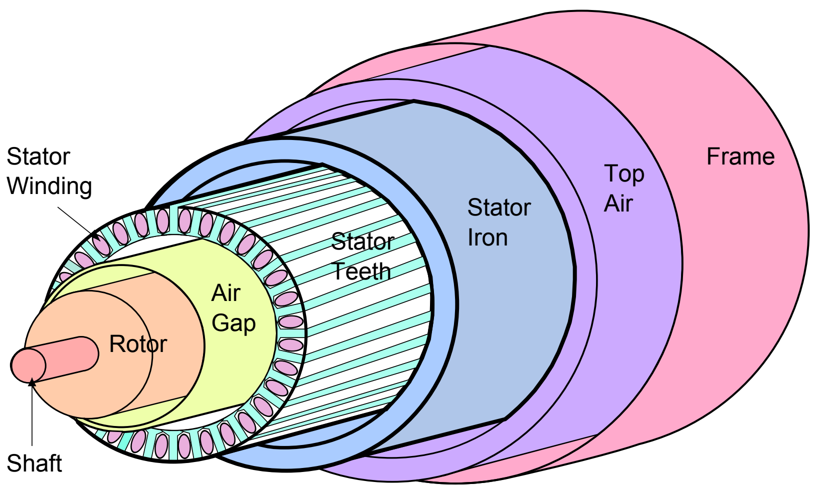

Figure 4.5: Model divisions.

Whilst other authors considered the whole machine in the same amount of

Table 4.1: Model Subdivisions

No.	Generator Part	Label
1	Frame	f
2	Top Air	ta
3	Stator Back iron	si
4	Stator Teeth	st
5	Stator Winding	sw
6	Stator End Winding In	swi
7	Stator End Winding Out	swo
8	End Air In	ai
9	Air Gap	ag
10	End Air Out	ao
11	Rotor	r
12	Shaft	sh

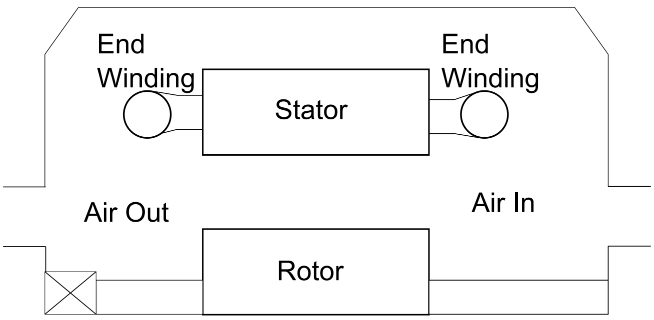

Figure 4.6: Cross section of generator showing end windings and air gaps.

detail [47, 44], whether that be high or low. For this application the most critical heat paths where overheat would occur first were identified and the model was biased to provide the greatest accuracy in these areas. These were the stator, due to the fact that the stator winding will be the hottest part of the motor; and the air flow in the generator, which needs to be modelled carefully in order to reduce error in temperature estimates in the stator iron and windings.

The following sections describe each of the parts of the generator modelled, including the resistance network and how it differs from the cylinder model previously described along with the parameters used.

Frame

The frame is one of the areas that is not derived from the cylinder model shown previously. The important function of this part of the model is to correctly simulate heat flow from the top air gap. Due to this the frame model only simulates heat flow in the radial direction, simulating in the axial direction is unnecessary and causes no significant loss of accuracy.

The resistance network for the frame is shown in figure 4.7. The network consists of five resistances, R_{famb} simulates heat flow to ambient air around the generator. While R_{f1} deals with heat flow to the inner surface of the frame. $R_{fcon1,2,3}$ are the resistances for convective heat transfer to the air sections touched by the frame. Finally C_f is the heat storage of the frame.

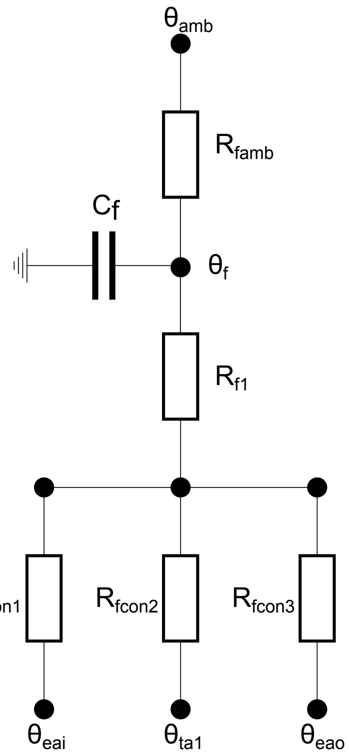

Figure 4.7: Model for generator frame.

$$R_{famb} = \frac{1}{2\pi r_{f2}(L_s + L_{fei} + L_{feo})H_f} \tag{4.10}$$

$$R_{f1} = \frac{1}{2\pi K_{sr} r_{f2} L_s} \tag{4.11}$$

$$R_{fcon1} = \frac{1}{2\pi r_{f2} L_s H_{tar}} \tag{4.12}$$

$$R_{fcon2} = \frac{1}{2\pi r_{f2} L_{fei} H_{tar2}} \tag{4.13}$$

$$R_{fcon3} = \frac{1}{2\pi r_{f2} L_{feo} H_{tar2}} \tag{4.14}$$

$$C_f = \rho_{steel} c_{steel}((\pi L_f((r_f + 0.001)^2 - r_f^2)) + (0.01\pi r_f^2)) \tag{4.15}$$

Where r_{f2} is the inner radius of the frame, L_s is the stator length, $L_{fei,feo}$ are the lengths of the two end air gaps, H_f is the convection co-efficient to ambient air, K_{sr} is the thermal conductivity of steel in the radial direction and $H_{tar,tar2}$ are the convection co-efficents to the inner air gaps. For the heat storage of the material C_f, ρ_{steel} is the density of steel and c_{steel} is the heat capacity of steel.

Stator Back Iron

The stator back iron and stator teeth are modelled separately. The stator back iron is identical to the cylinder model defined in section 4.2.1 with no differences so the model network is identical to that in figure 4.4 with equations (4.3), (4.4), (4.5), (4.6) applying with relevant parameters.

Stator Teeth

The stator teeth model is derived from the cylinder model in section 4.2.1 with the equations adjusted to properly model the teeth which are not a solid piece of steel. An approximation for the ratio of steel to air was defined from the cross section of the stator teeth. The number of individual teeth and air gaps are identical so the ratio of the area of a single tooth to a single air gap is the same as the ratio of steel to air for the whole cross-section. The volume of steel can be found by multiplying the cylinder volume by the ratio of ϕ_{se}/ϕ_{sp} the ratio of tooth angle, to tooth and slot angle. Figure 4.8 shows the final network for the stator teeth.

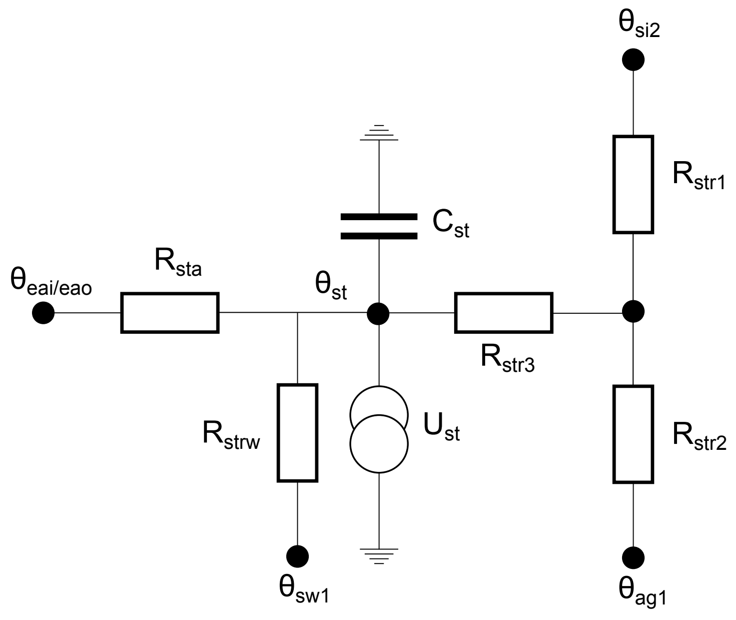

Figure 4.8: Model for stator teeth.

The second change is that in order to model the heat transfer from the stator teeth to the stator winding an extra resistance is required. This is to model the heat transfer to the inside of the slot. The equations for the standard cylinder can then be revised.

$$R_{sta} = \frac{L_s \phi_{sp}}{12\pi k_{sa} \phi_{se}(r_{st1}^2 - r_{st2}^2)} \tag{4.16}$$

$$R_{str1} = \frac{\phi_{sp}}{4\pi k_{sr} L_s \phi_{se} s}\left(1 - \frac{2r_{st2}^2 log(\frac{r_{st1}}{r_{st2}})}{r_{st1}^2 - r_{st2}^2}\right) \tag{4.17}$$

$$R_{str2} = \frac{\phi_{sp}}{4\pi k_{sr} L_s \phi_{se} s}\left(\frac{2r_1^2 log(\frac{r_{st1}}{r_{st2}})}{r_{st1}^2 - r_{st2}^2} - 1\right) \tag{4.18}$$

$$R_{str3} = \frac{\phi_{sp}}{8\pi k_{sr} L_s \phi_{se} s(r_{st1}^2 - r_{st2}^2)}\left(r_{st1}^2 + r_{st2}^2 - \frac{4r_{st1}^2 r_{st2}^2 log(\frac{r_{st1}}{r_{st2}})}{r_{st1}^2 - r_{st2}^2}\right) \tag{4.19}$$

Where $r_{st1,st2}$ are the outer and inner radius of the teeth cross-section and k_{sa} is the axial thermal conductivity of steel including laminations. The equation for the heat path to the inside of the teeth is:

$$R_{strw} = \frac{\pi(r_{st1}^2 - r_{st2}^2)\phi_{se}}{K_{sr} L_s (r_{st1} - r_{st2})^2 n_s^2 \phi_{sp} s} \tag{4.20}$$

Where n_s is the number of slots. With:

$$C_{st} = \rho steel c_{steel} s(\pi L_s(r_{st1}^2 - r_{st2}^2) - (A_{sw} L_s n_s)) \tag{4.21}$$

Where A_{sw} is the cross-sectional area of the stator winding.

Stator Winding

The stator windings are modelled as a series of rods. To achieve this one of the rods is modelled then each resistance is multiplied by n_s, the number of slots. The model differs from the rod model defined earlier as the winding touches both the stator iron and teeth, this requires a resistance modelling heat flow to each division. A final resistance is required to simulate the heat movement from the winding to the air gap. The final network is shown in figure 4.9, and the equations defined.

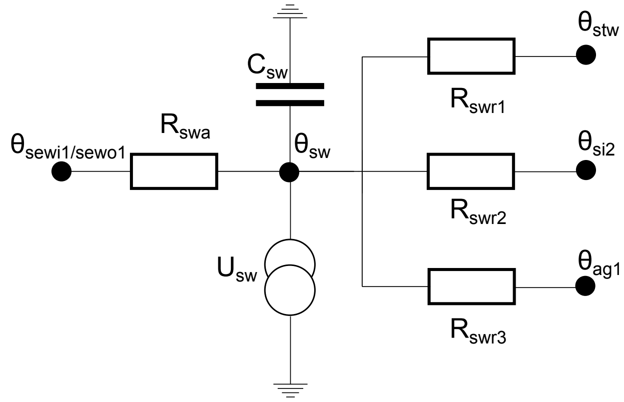

Figure 4.9: Model for stator winding.

$$R_{swa} = \frac{L_s}{12k_{ca}A_{sw}n_s} \tag{4.22}$$

$$R_{swr1} = \frac{4H_i s_c}{\pi k_l L_s r_{sw1} n_s} + \frac{1}{4\pi k_{cr} r_{sw1} L_s n_s} \tag{4.23}$$

$$R_{swr2} = \frac{8H_i s_c}{\pi k_l L_s r_{sw1} n_s} + \frac{1}{2\pi k_{cr} r_{sw1} L_s n_s} \tag{4.24}$$

$$R_{swr3} = \frac{s_c}{2\pi k_{cr} r_{sw1} L_s n_s} \tag{4.25}$$

$$C_{sw} = \rho_{copper} c_{copper} A_{sw} L_s n_s s_c \tag{4.26}$$

Where K_{ca} is the axial thermal conductivity of the copper winding, H_i is the insulation thickness, r_{sw1} is the radius of the winding, K_{cr} is the thermal conductivity of the winding in the radial direction, K_l the thermal conductivity of the insulation and s_c is the copper winding factor. Finally ρ_{copper} and c_{copper} are the density and heat capacity of copper respectively.

Stator End Windings

The stator end windings are more complex than the stator windings and consist of two different parts; one to simulate the section of winding that overhangs the slot and the second to simulate the toroid that links all the winding sections.

The winding overhang is modelled in the same way as the winding, with the exception there is no need to model any insulation around the winding. The toroid is modelled as a single rod that connects at each end then transfers heat to the end air pocket. The final network is shown in Fig 4.10 and the equations are defined.

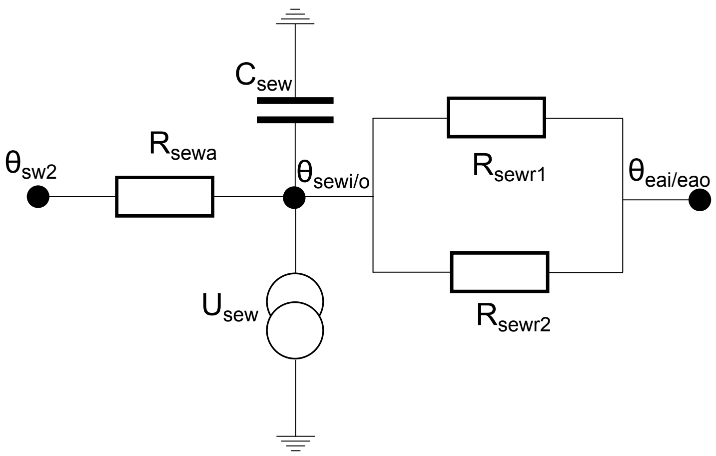

Figure 4.10: Model for stator end windings.

$$R_{sewa} = \frac{L_{sc}}{2k_{ca}A_{sw}n_s} \tag{4.27}$$

$$R_{sewr1} = \frac{0.01^2 s_c}{32\pi r_{sw1}^2 k_{cr} L_{sc} n_s} \tag{4.28}$$

$$R_{sewr2} = \frac{s_c}{16\pi k_{cr} L_t} \tag{4.29}$$

$$C_{sew} = \rho_{copper} c_{copper} s_c (\pi r_{sewt}^2 L_t + A_{sw} L_{sc} n_s) \tag{4.30}$$

Where L_{sc} is the length of the winding slot overhang, L_t is the length of the toroid equal to $2\pi r_{sewa}$. r_{sewa} is the length for the centre of the toroid to the middle of the winding and r_{sewt} is the radius of the toroid.

Rotor

The rotor model serves to simulate heat transfer across the air gap. This means that for the rotor it is only necessary to model it in the radial direction as the axial heat transfer has very little effect on the accuracy of the model where important. The final model for the rotor consists of two resistances and is shown in figure 4.11.

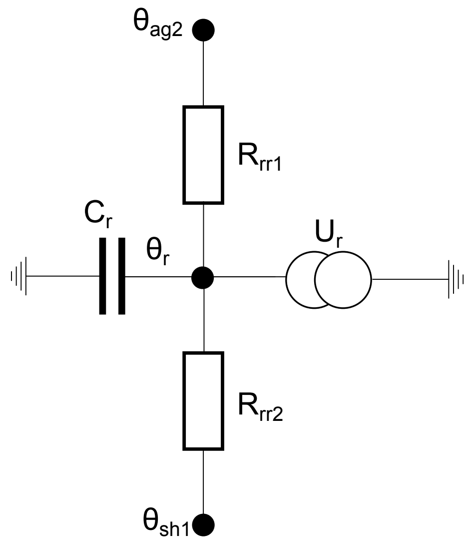

Figure 4.11: Model for rotor.

$$R_{rr1} = \frac{ln(\frac{r_{r1}}{r_{ri}})}{2\pi k_{sr} L_r} \quad (4.31)$$

$$Rrr2 = \frac{ln(\frac{r_{ri}}{r_{r2}})}{2\pi k_{sr} L_r} \quad (4.32)$$

$$C_r = \rho_{steel} c_{steel} \pi L_r s(r_{r1}^2 - r_{r2}^2) \quad (4.33)$$

Where $r_{r1,r2}$ are the outer and inner radius of the rotor, r_{ri} is the midpoint radius of the rotor (i.e $r_{r1} - \frac{r_{r1}-r_{r2}}{2}$) and L_r is the length of the rotor.

Shaft

The shaft is a simple model represented as a rod. In this case a number of different convection resistances are required as it is in contact with most air pockets and the frame. The final network is shown in figure 4.12.

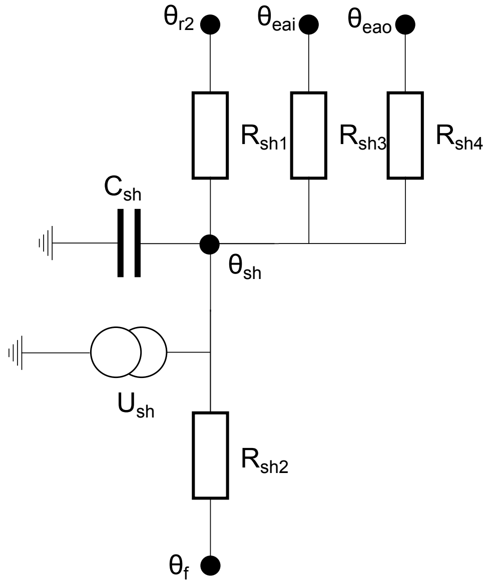

Figure 4.12: Model for shaft.

$$Rsh1 = \frac{1}{8\pi K_{sr} L_r} \tag{4.34}$$
$$Rsh2 = \frac{1}{8\pi K_{sr} L_{shf}} \tag{4.35}$$
$$Rsh3 = \frac{1}{8\pi K_{sr} L_{shai}} \tag{4.36}$$
$$Rsh4 = \frac{1}{8\pi K_{sr} L_{shao}} \tag{4.37}$$

Where L_{shf} is the length of the shaft in contact with the frame and $L_{shai,shao}$ are the lengths of the shaft in contact with the end air in and end air out.

Air Gaps

The generator modelled has an internal air flow generated by a fan on the front of the generator. This is different to models made by Mellor et al. [47] and Perez and Kassakian [78] which look at generators with external cooling and therefore have air excited only by the movement of the rotor. This meant it could be assumed that almost all heat is transferred across the air gap, whereas the forced convection present in the generator modelled means that another component of heat transfer between air gaps was necessary. An overview of the nodes in the air network are shown in figure 4.13. Note that as the generator is symmetrical about the x-x axis only the top half is shown.

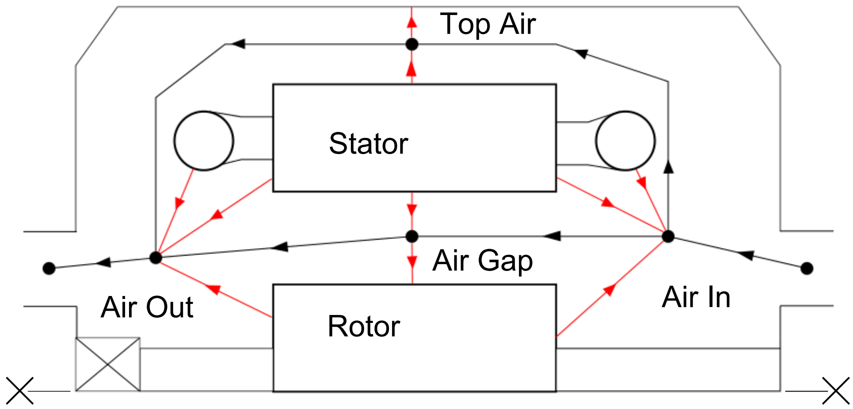

Figure 4.13: Nodes for air flow model.

This leads to the network for each node becoming two resistances to represent the heat transfer through the air pocket due to forced and natural convection, then a series of resistances that represent convective heat transfer from the various parts of the model that touch the air pocket. The network for the air gap is shown in figure 4.14. For the other nodes the model is the same but with a different number of resistances for convection for other model divisions depending on how many are touched by the air gap.

The equations for the resistances for the air pockets take two forms. The first is for the transfer through the generator, the equation for which takes the form:

$$R = \frac{1}{C_{air} M_f} \tag{4.38}$$

Where C_{air} is the specific heat capacity of the fluid, in this case air, and M_f is the mass flow through the air pocket in kg/s. The second type of resistance is for convective heat transfer from the surface of one of the solid section, this equation takes the form:

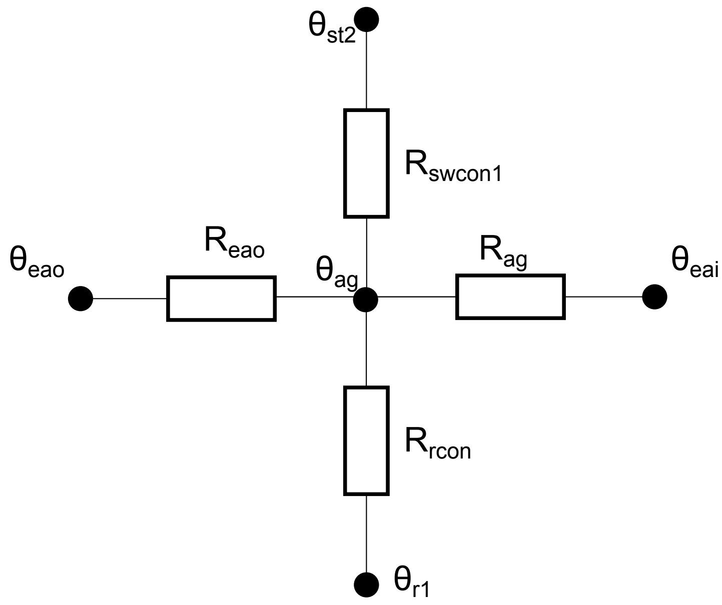

Figure 4.14: Network for air gap.

$$R = \frac{1}{A_c h} \tag{4.39}$$

Where A_c is the contact area between the section and air pocket, and h is the thermal contact transfer coefficient.

4.2.3 Model Parametrisation

Most of the parameters within the thermal network model are based upon physical measurements of the generator. For example, L_s the length of the stator is a measurement taken directly from the generator as are all other dimensions. These dimensions are shown in table 4.2. This section describes how the other properties of the generator were deduced.

Thermal Conductivities

Most of the thermal conductivities were defined from knowledge of the material, the windings are copper, the stator, rotor and frame are made of steel. This also applies to other properties besides thermal conductivity including density (ρ) and

Table 4.2: Model Dimensions

Generator Part	**Label**	$\mathbf{r_1}$ (mm)	$\mathbf{r_2}$ (mm)	**L** (mm)
Frame	f	N/A	159	347
Top Air	ta	159	136	53
Stator Back iron	si	136	111	53
Stator Teeth	st	111	99	53
Stator Winding	sw	6	N/A	53
Stator End Winding In	swi	10 (r_{sewt})	110 (r_{sewa})	347
Stator End Winding Out	swo	10 (r_{sewt})	110 (r_{sewa})	347
End Air In	ai	159	N/A	48
Air Gap	ag	99	98	53
End Air Out	ao	159	N/A	48
Rotor	r	98	23	53
Shaft	sh	23	N/A	239

specific heat ($c_{steel/copper}$), these are all shown in table 4.3. There are two cases where this is not possible, the stator winding radial conductivity and the stator iron and teeth axial conductivity.

Table 4.3: Material Properties

Material	**Thermal Conductivity** $(Wm^{-1}K^{-1})$	**Specific Heat** $(Jkg^{-1}K^{-1})$	**Density** (kgm^{-3})
Steel	20	502	8378
Copper	400.5	383	8933

For the stator winding thermal conductivity, the value in the axial direction can be taken as the thermal conductivity of copper. However because the winding is stranded this means that the thermal conductivity in the radial direction needs to account for any air or varnish between strands.

To simulate this, rather than creating a more complicated model, it is much simpler to define an aggregated thermal conductivity representing the overall conductivity in that direction. From research it was found that the overall conductivity is very low; for example Mellor et. al. [47] used a value of $0.4W/mK$. To find the value an initial value of $0.5W/mK$ was used; this was found to be too large. This parameter is know to effect the size of the temperature increase due to additional loads so to tune this parameter the value was reduced until the correct temperature increase was obtained. The final value for K_{cr} was found to be $0.13W/mK$.

The radial thermal conductivity value for stator iron and teeth can be considered to be that of the steel its made of. Due to laminations in the stator material the axial thermal conductivity (K_{sa}) is considerably reduced. To find this value a starting value of $0.5W/mK$ was used and again found to be too large. This parameter is known to effect the size of the temperature decrease due to the load being lowered, so to tune this parameter the value was reduced until the correct temperature decrease was obtained. The final value for K_{sa} was found to have a value of $0.1W/mK$.

Contact Heat Transfer Coefficients

The process for finding the contact coefficient first requires an estimate to be made based on the geometry. It was then found that while these estimates were of the correct order of magnitude they were not accurate due to the fact that complex shapes were modelled as simple ones. For example it was assumed that the inside of the stator is a perfect cylinder minus the slot gaps, when the real shape is much more complex.

The estimates calculated were used to obtain the correct order of magnitude for the value. This was then adjusted through experimentation against validation data to give a more accurate representation to be used in the model. These parameters are known to effect the average error of the model during all operating conditions. These parameters were tuned last once the parameters effecting the transient operation were tuned to raise or lower the temperature of the entire model output by a set amount.

Stacking and Winding Factors

As shown in the previous sub-sections it was necessary to adjust certain parameters to properly define the stator and winding parameters; neither of which are solid steel/copper. It is also necessary to account for this when defining the thermal resistances and heat storages for these sections. To find these parameters a coefficient of 1 was the starting point and the values were reduced until a suitable output was obtained. The main effect of these values on the model output was the rise time after a load increase for the stator winding factor (s_c) and the time period for the temperature change to occur when a load is reduced for the rotor stacking factor (s).

For the stator and rotor a factor s of 0.97 was found to be required to give the correct adjustment for the heat storage and radial resistances only. This value was In this case it shows that the laminations only have a small effect on these values.

For the stator winding (s_c) the effect is much more pronounced, with a value of 0.5 used. This is because the model assumes that the slot is entirely full which is not the case. The winding is actually an oval passing through a rectangular slot. The final value accounts for air space at the corners of the rectangle as shown in figure 4.15, as well as the effects of any non-copper material in the winding (e.g. slot lining).

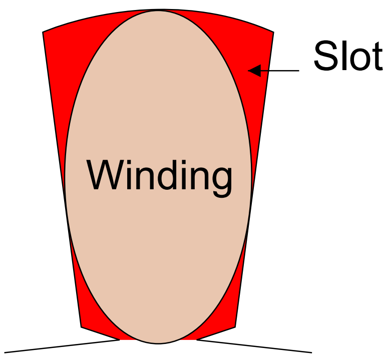

Figure 4.15: Winding slot fill.

Generator losses

There are two types of losses that need to be defined for the model. These are the winding losses and iron losses. The iron losses were defined from the results of various no-load, short circuit and excitation tests. While these values were calculated at a certain temperature/load the variation of these values is small enough that there is no noticeable effect on accuracy.

The representation of the winding losses are the most important due to large variations as the load of the generator changes. These losses are calculated as the power loss in each winding summed together.

$$P_c = I_u^2 R_u + I_v^2 R_v + I_v^2 R_w \tag{4.40}$$

Where P_c is the total copper loss in the windings, $I_{u,v,w}$ are the windings currents and $R_{u,v,w}$ are the winding resistances.

To obtain best accuracy, the change in resistance of the winding as temperature changes was accounted for based upon the resistance of the winding at $0°C$.

$$R_{u,v,w} = (1 + \alpha_{cu}\theta_{u,v,w})R_0 \tag{4.41}$$

Where $\theta_{u,v,w}$ is the current winding temperature, α_{cu} is the temperature coefficient of resistance of copper, in this case 0.0039 and R_0 is the resistance of the winding at $0°C$. By measuring the resistance of the windings directly and noting the room temperature this allowed R_0 to be calculated for each winding by using equation 4.41.

The final stage is to split the total winding resistance between the main winding model and the two end winding models. With no research available to suggest how this might be done it was decided to split the total by the ratio of the masses of the three winding divisions.

4.2.4 Model Solution

With the full network defined a nodal analysis can be undertaken on the full thermal circuit to define the equations that need to be solved to calculate the temperatures over time. Equations 4.42 and 4.43 show the nodal equations that are derived for a cylindrical component, in this case for the stator iron.

$$
\begin{aligned}
C_{si}\frac{d\theta_{sim}}{dt} &= \frac{1}{R_{sia}}(\theta_{sia} - \theta_{sim}) \\
&+\frac{1}{R_{sir3}}(\theta_{sim'} - \theta_{sim}) + U_{si}
\end{aligned}
\tag{4.42}
$$

$$
\begin{aligned}
0 &= \frac{1}{R_{sir1}}(\theta_{sio} - \theta_{sim'}) \\
&+\frac{1}{R_{sir2}}(\theta_{sii} - \theta_{sim'}) + \frac{1}{R_{sir3}}(\theta_{sim} - \theta_{sim'})
\end{aligned}
\tag{4.43}
$$

Where the subscript si denotes that the value is from the stator back iron, with the letters a and r, denoting axial and radial directions respectively, R_{sia} for example is the stator iron axial resistance. C_{si} is the heat storage for the stator back iron, θ_{sim} is the average temperature of the cylinder, U_{si} is the heat input to the stator iron. θ_{sia} and $\theta_{sim'}$ are the temperatures at the adjacent nodes, with R_{sia} and R_{sir3} being the thermal resistance between them.

Each node can be expressed in a similar manner to equation 4.42 and 4.43, these equations can then be expressed in matrix form.

$$
[C]\frac{d[\theta]}{dt} = [G][\theta] + [u] \tag{4.44}
$$

where $[C]$ is a square matrix of thermal heat storage values, $[G]$ is a square matrix of thermal conductance between nodes, $[\theta]$ is the node temperature states, and $[u]$ is a column matrix of heat sources. The above differential equations allow the network to be solved for transient conditions.

Model Reduction

The initial analysis of the thermal network produces a system of 19 equations describing the heat transfer through the generator. Of the nodes representing the solid sections of the generators these can be split into two types:

1. Nodes representing the average temperature of a section.

2. Intermediary nodes.

In the analysis the heat storage of a section was modelled as occurring at the average temperature nodes. This means that all intermediary nodes have zero heat storage as shown in equation 4.43 and as such these equations can be mathematically eliminated. After eliminating equations for these intermediary nodes this leaves 12 equations describing the average temperatures of the solid nodes and the air flow through the system.

Further to this the equations for the air temperatures also have no heat storage i.e. $C = 0$. This allows the temperature states for the air to be mathematically eliminated leaving 8 equations that need to be solved in the final model.

4.3 Validation

To validate the model data was used from the generator rig described in chapter 3, this section describes the various tests that were undertaken to define the accuracy of the model.

4.3.1 Step Input Tests

The first test undertaken was an open loop step input test to identify the performance of the model as the generator temperature reaches steady state. This was achieved by performing a number of tests with different constant current loads ranging from no-load to full load. This allows the model to be tested across the full input range and see if the accuracy is consistent.

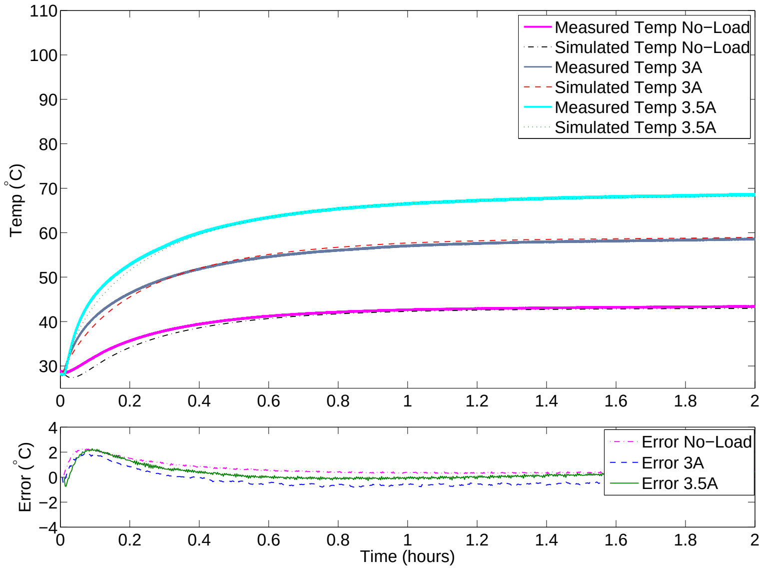

Figure 4.16: Graph showing model performance vs actual generator for a series of step tests for stator winding.

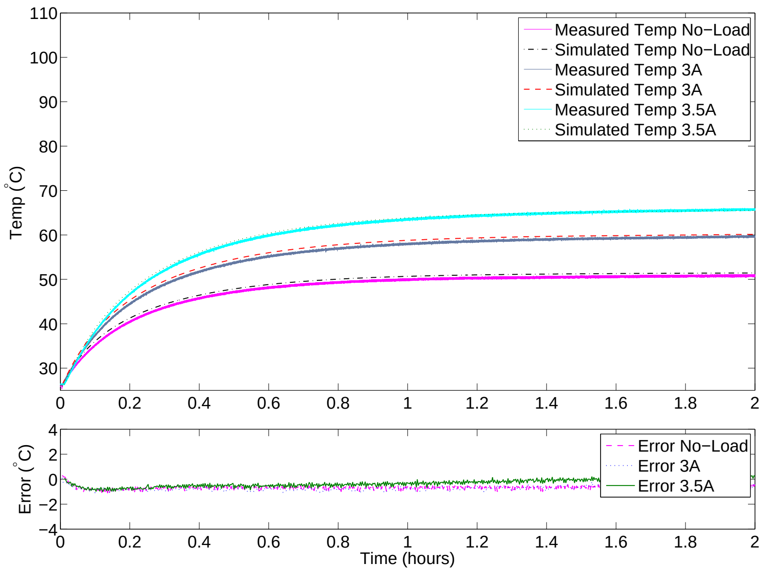

Figure 4.17: Graph showing model performance vs actual generator for a series of step tests for stator iron.

Figures 4.16 and 4.17 show a series of step tests carried out to validate the model. These results show a good agreement throughout, although accuracy is slightly lower at low temperatures. In each case the results settle out to give a steady state error of roughly $\pm 1°C$. What these test show is that the model has reasonable performance during heating with good agreement between the model and real data. This means that the heat storage in the model has been estimated well. The very good match in steady state performance shows that the resistances and air flow modelling has worked.

4.3.2 Varying Load Tests

This test was designed to assess the performance of the model as the load varies from a low loading to full load, with the aim to define how well the model follows large changes in load. Secondly this test is used to determine how long this level of accuracy is maintained for and if the accuracy starts to degrade over time. This will allow a maximum period of accurate prediction to be defined.

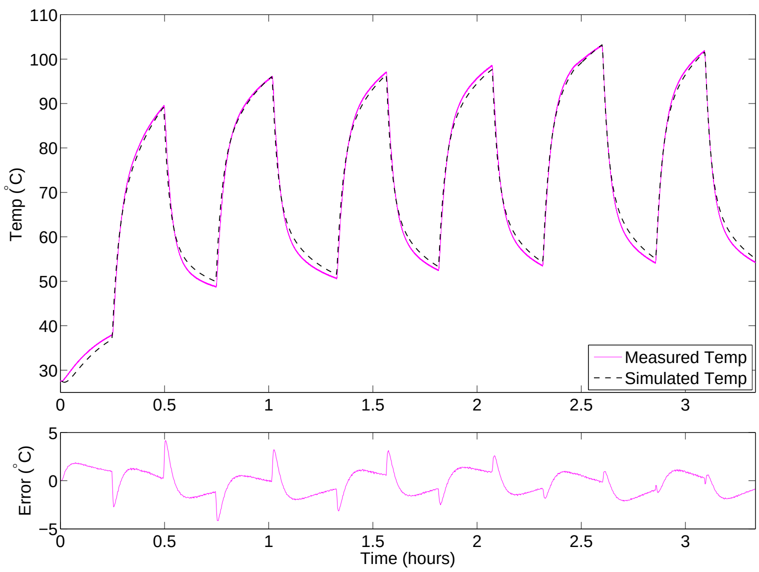

Figure 4.18: Graph showing model performance vs actual generator for a varying load test for stator winding.

Figures 4.18 and 4.19 show the results from the varying load test for the stator

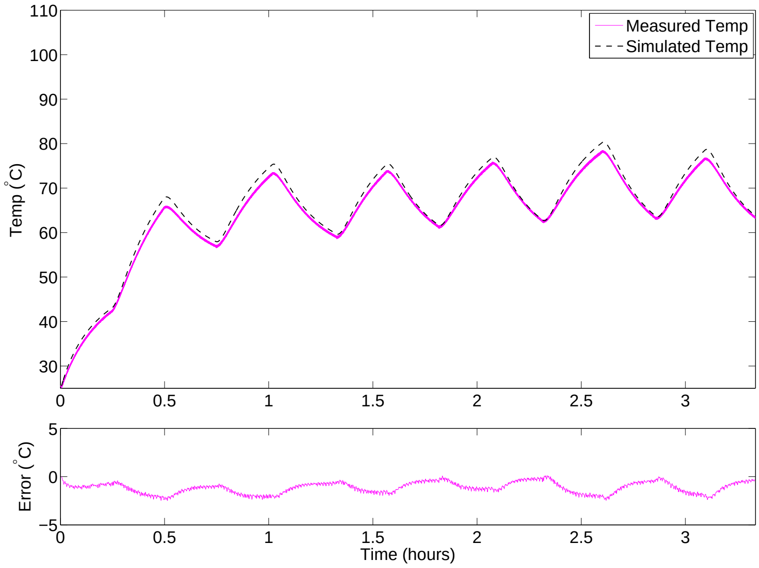

Figure 4.19: Graph showing model performance vs actual generator for a varying load test for stator iron.

iron and stator winding. Figure 4.18 shows that the model winding temperature follows the real temperature very well, with errors generally within $\pm 2°C$. The only time errors go beyond this is shortly after the step change where error can temporarily peak at up to $\pm 5°C$, however the model error quickly drops down again and the model keeps a consistent accuracy.

Figure 4.19 shows an even better agreement for the stator iron with the error consistently being between -1 and $-2°C$. This is probably due to the changing load causing much smaller temperature variations than for the stator winding.

What is seen from both graphs that is unexpected is that neither shows any sign of divergence between the model and the real system, in fact Fig. 4.18 shows the errors decreasing over time. This is believed to be due to the model performing better in the higher temperature range.

This further re-enforces what was seen during the step test in that the steady state performance is very good while the transient performance is slightly worse but still acceptable.

4.3.3 Aircraft Load Test

The final test is to check the model performance using a load profile similar to that which would occur during an aircraft mission. The method of defining this profile using various mission actions was described in chapter 3 and the profile used for the test is shown in figure 4.20. The aim of this test is to ensure the model performs well under the types of load seen in flight.

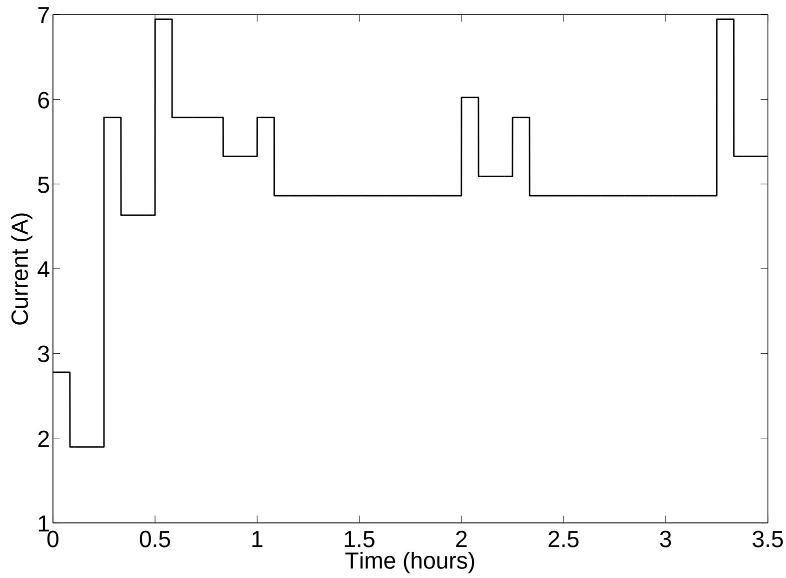

Figure 4.20: Graph showing the load profile per phase for the aircraft load test.

Figures 4.21 and 4.22 show the results for the aircraft load test for the stator windings and stator iron respectively. For the stator winding the graph again shows that the model performs better at higher temperatures, with error of $\pm 3°C$ occurring within the first half an hour but after the larger loads are applied and the generator heats up the agreement between results becomes even better. This is important as the graph shows that the model gives the best performance where it is most needed, in this case when the generator is hottest and the loads are highest.

Figure 4.22 show similar results to Fig. 4.21 but with a better agreement from start to finish. The results show it is suitable for its defined use as the simulation

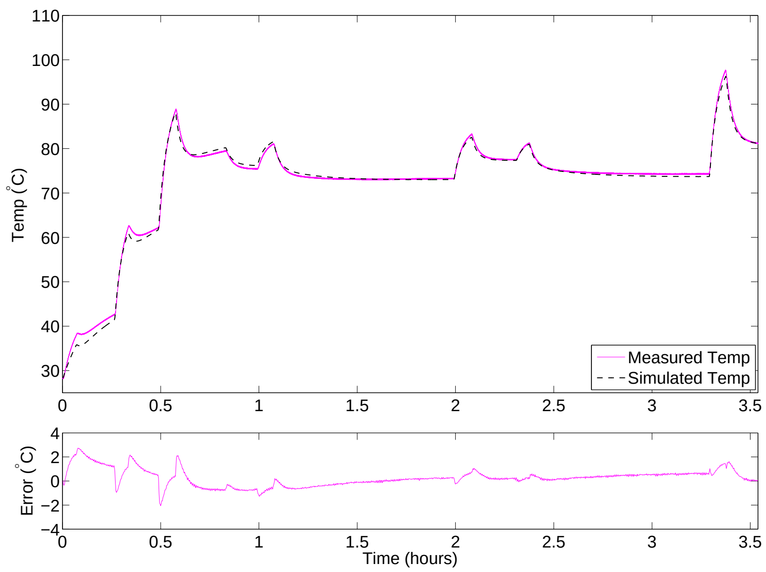

Figure 4.21: Graph showing the plant model performance vs actual generator for an aircraft load test for stator winding.

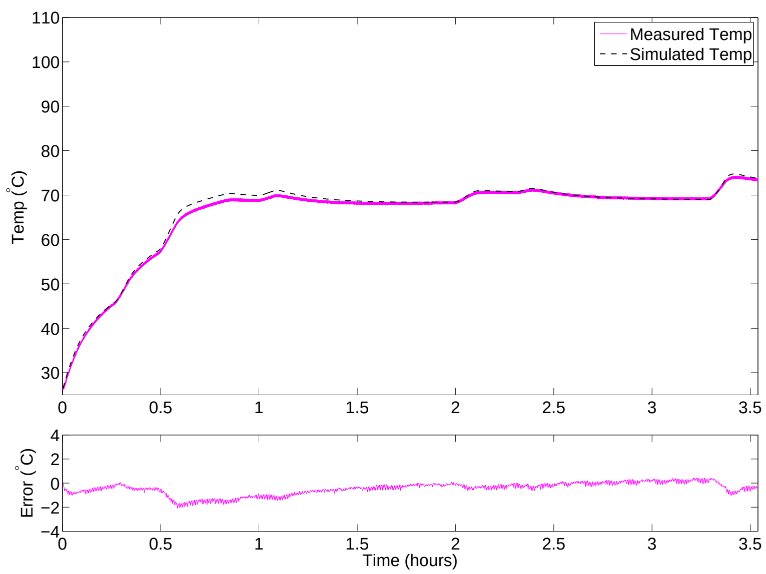

Figure 4.22: Graph showing the plant model performance vs actual generator for an aircraft load test for stator iron.

model.

4.4 Conclusion

This chapter has described the model created to represent the actual generator. Reference has been made to work conducted by previous authors in the creation of thermal network models. The validation was achieved by comparing the model output to that of the actual generator under the same load.

The validation results show the model performing well over a number of tests and in each case errors are low and the shape of the curve is a very close fit. The accuracy of the model is consistent and time invariant even over prolonged tests of several hours. Overall the results show that the model is a good representation of the system and can be used as the simulation model in order to validate the algorithm of the load management system.

Chapter 5

Description and Comparison of Design Models

5.1 Introduction

This chapter discusses the development of a design model to be used as the basis for the design of the Kalman Filter based prediction algorithm. Two modelling approaches are taken and two candidate models are developed and compared. One of these is selected to be the model within the Kalman Filter to provide predictions of future temperature. The first model is a simplified version of the simulation model described in chapter 4; the second is a "black box" model created using system identification method.

Each model is described and validated using data recorded from the experimental rig detailed in chapter 3. The two models are then compared with the positives and negatives of each model described.

5.2 Linear Thermal Network Model

The model described in chapter 4 is formed from a series of linear first order differential equations in the form:

$$[C]\frac{d[\theta]}{dt} = [G][\theta] + [u] \tag{5.1}$$

Where $[C]$ is a square matrix of thermal heat storage values, $[G]$ is a square matrix of thermal conductance between nodes, $[\theta]$ is the node temperature states, and $[u]$ is a column matrix of heat sources.

The input vector $[u]$ is derived from the generator losses and the input temperature. Similar to other methods (e.g. [47, 44]) the winding losses for the model in chapter 4 were derived from the I^2R power losses in the winding. The temperature dependency of the winding resistance R is also modelled, adjusted R depending upon the current winding temperature to improve accuracy.

In order to linearise the model in chapter 4, the I^2R losses were linearised over the current input range and a set value for the winding resistance was used. This model was then validated using the same experimental data that was used for the non-linear physics-based model in chapter 4.

The non-linear model presented in chapter 4 was shown to maintain a consistent accuracy over time; the errors between the measured data and the simulation data did not grow larger over time. Similar results can be observed in the work by Mellor et. al. [47], Kylander [44] and Kral et. al. [79]. While testing the linear model it was found that the accuracy of the open loop results deteriorate over time. Also included is a study looking at how the two major components, (the non-linear loss representation and the winding resistance change with winding temperature) contribute to the accuracy of a thermal network model. While the author could find research exploring how generator losses are distributed [30] or how to model the windings in more detail [45]; this is something which the author could find no other research had attempted to explore.

5.2.1 Linearisation of Winding Losses

The stator winding losses are calculated from the sum of the resistive losses in each winding.

$$P_c = I_u^2 R_u + I_v^2 R_v + I_v^2 R_w \tag{5.2}$$

Where $I_{u,v,w}$ is the current in the winding and $R_{u,v,w}$ is the winding resistance. The steps taken to linearise the winding losses are:

- I^2R losses are linearised.
- Losses are assumed to be three times the loss in a single phase.

The linearisation of the winding losses gives a fully linear design model. The generator for these tests is always running a balanced load the assumption that the losses are three times that in a single phase is accurate.

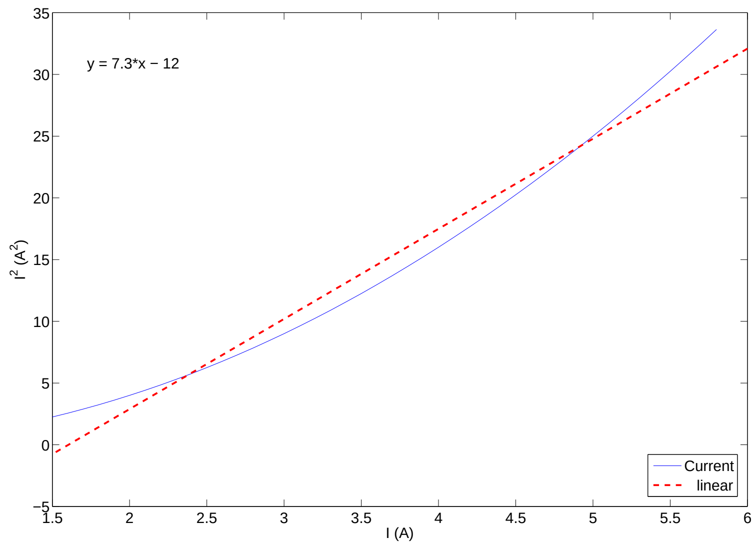

Figure 5.1: Linearisation of $I^2_{u,v,w}$.

Figure 5.1 shows the linearised relationship for $I^2_{u,v,w}$

$$P_c = 3(7.3I_v - 12)R_v \tag{5.3}$$

The coefficient of determination for the linear fit is 0.9764, making this a reasonable representation of the function. For this function the best accuracy will occur at $I = 2.4$ and $I = 4.9$ where the linear fit crosses with I^2 function.

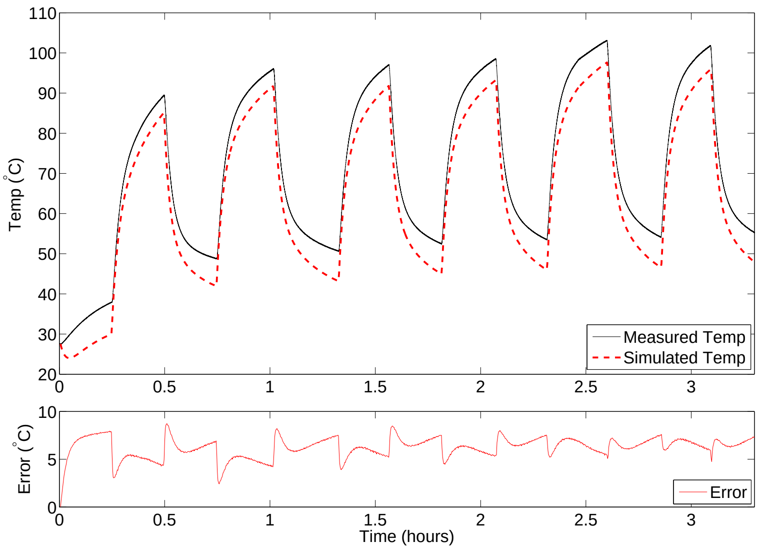

Figure 5.2: Model output for the stator winding with linearised I^2 and constant winding resistance.

Figures 5.2 and 5.3 show the model output against measured data in a test where current was varied between the maximum rating of the generator and the minimum that the load can draw over the length of the test. The model used the linearised I^2 relationship described earlier, with constant winding resistance.

These graphs show that after an initial heat up period the errors between the model and the measured data start to grow although the growth is slower than seen in later results with both a linearised I^2 and constant resistance. This shows that the non-linear I^2 term contributes to the observation in chapter 4 that the errors in the non-linear model remained consistent over time.

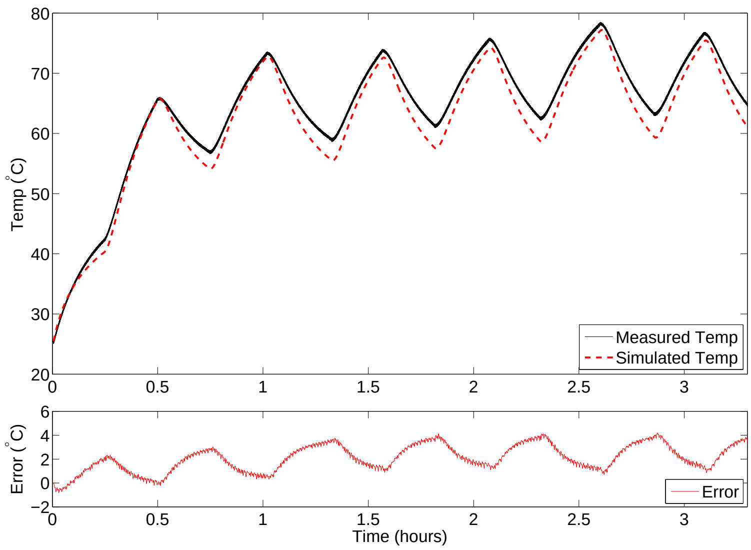

Figure 5.3: Model output for the stator iron with linearised I^2 and constant winding resistance.

5.2.2 Winding Resistance for Linear Model

In chapter 4 the winding resistance was modelled using the function:

$$R_{u,v,w} = (1 + 0.0039\theta_{u,v,w})R_0 \tag{5.4}$$

Where $\theta_{u,v,w}$ is the current winding temperature, and R_0 is the resistance of the winding at $0°C$. By measuring the resistance of the windings directly and noting the room temperature, this allowed R_0 to be calculated for each winding by using equation 5.4.

The second step to simplify the non-linear model was to use a constant winding resistance. Results are also presented showing the effect of updating the winding resistance with temperature.

Figures 5.4 and 5.5 show the model output against measured data in a test where current was varied from maximum to minimum over the length of the test. The model used the non-linear I^2 relationship, with a constant winding resistance.

The results show for both the stator winding and stator iron that using a

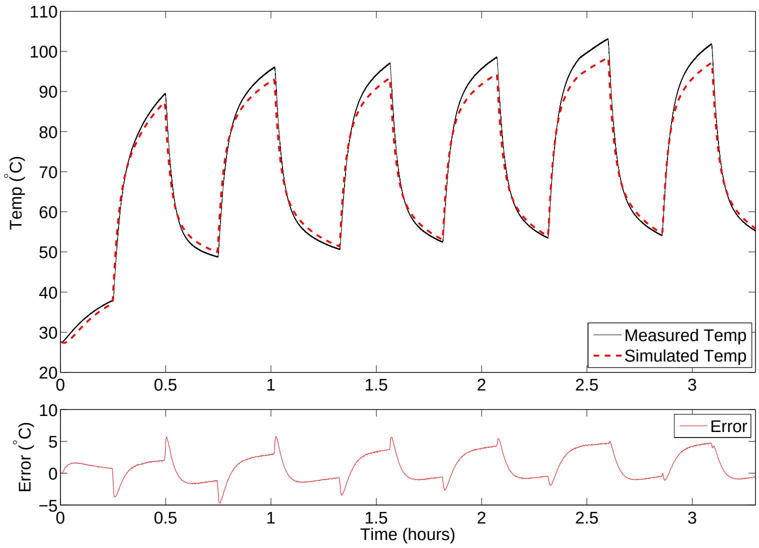

Figure 5.4: Model output for the stator winding with non-linear I^2 and temperature dependent winding resistance.

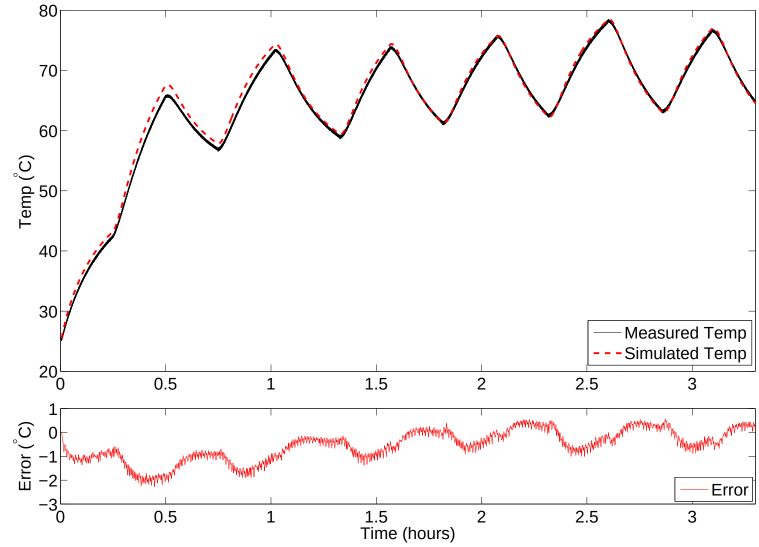

Figure 5.5: Model output for the stator iron with non-linear I^2 and temperature dependent winding resistance.

constant winding resistance results in a loss of overall accuracy, however after about 1.5 hours into the test the errors maintain a consistent cycle and do not seem to grow over time. This suggests that the I^2 relationship is what prevents errors from growing over time, while adjusting the winding resistance according to winding temperature reduces maximum errors seen while simulating transient operation.

5.2.3 Linear Model Validation

The same experimental data that was used to validate the non-linear physics model in chapter 4 is used here. First a simple load step is used as the input to the system. Then the results of a varying load test are presented. Finally results using a simulated load profile analogous to that experienced on-board an aircraft during a mission is presented.

Step Input Test

The first test undertaken was an open loop step input test to identify the performance of the model as the generator temperature reaches steady state. This was achieved by performing a number of tests with different constant current loads ranging from no-load to full load. This allows the model to be tested for consistency across the full input.

Figures 5.6 and 5.7 show the results of the step input tests, the model has varying agreement with the measured data dependent upon the load. The model perform best at higher current loads; this is expected as the model is optimised by choice at linearisation to perform best at or around maximum temperature. At $3.5A$ the model shows an error of roughly $4°C$ for the stator winding and $2.5°C$ for the stator iron, which is sufficiently accurate for the application.

For the no-load case the error is very large; $22°C$ for the stator winding and $11°C$ for the stator iron. The K-conditions from chapter 3 show that the minimum

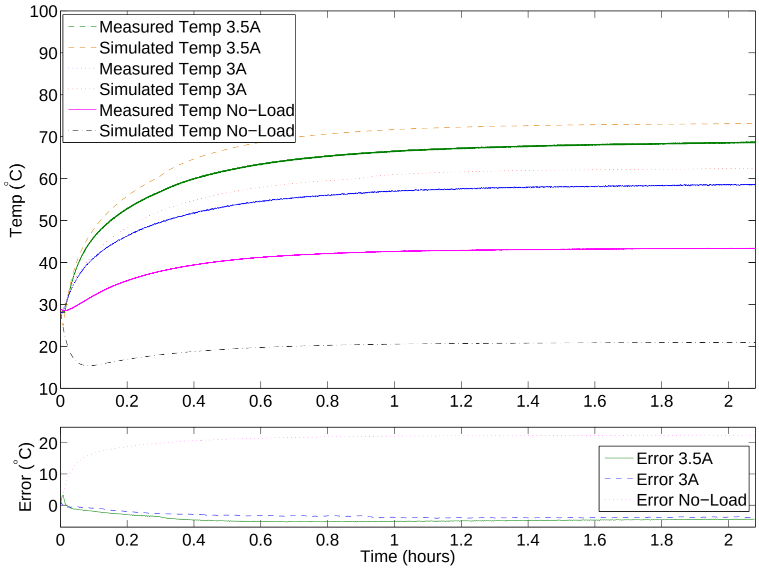

Figure 5.6: Step input test showing stator winding temperature for the linear physics-based model.

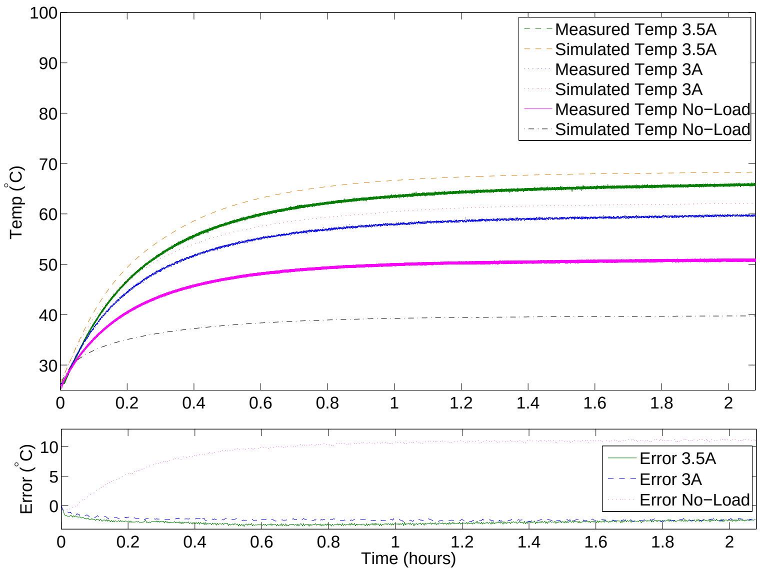

Figure 5.7: Step input test showing stator iron temperature for the linear physics-based model.

expected operation load is 27.3%, which for this generator is about $2A$. The results show that for the higher loads that the error is much lower, the temperatures are also overestimated a design choice to prevent overheat faults being missed.

Varying Load Test

This test was designed to assess the performance of the model as the load varies from a low load to full load, with the aim to define how well the model follows large changes in load.

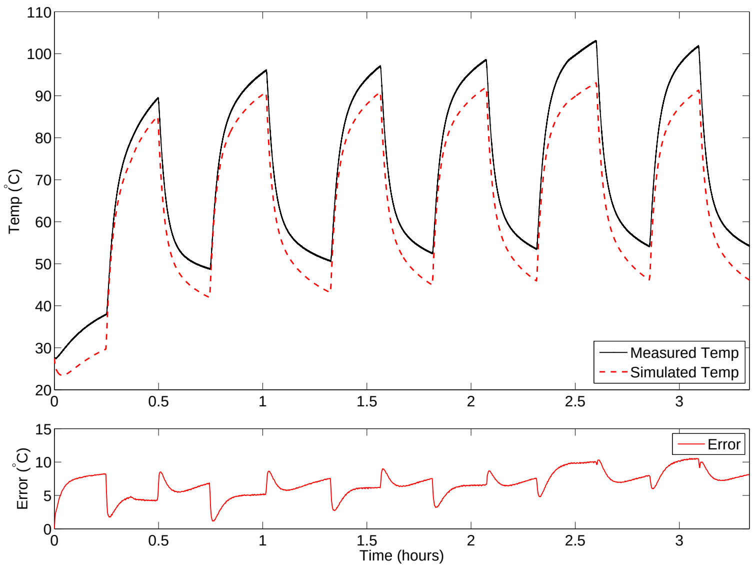

Figure 5.8: Varying load test showing stator winding temperature for the linear physics-based model.

Figures 5.8 and 5.9 show the results of the varying load test. As expected, unlike the non-linear version of the model described in chapter 3 the model and the measured data diverge over time. This was shown to be caused by the linearisation of the winding resistance. With a maximum error of $10°C$ for the stator winding and $4°C$ for the stator iron after 3 hours. The accuracy of the model is still sufficient for the application, as the large variations in current applied in the test do not occur in aircraft mission profiles. This also shows a much worse transient

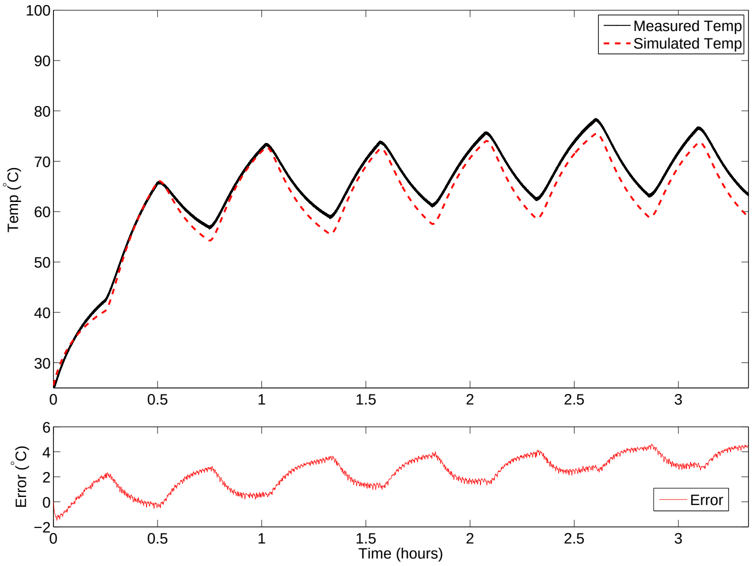

Figure 5.9: Varying load test showing stator iron temperature for the linear physics-based model.

performance than the non-linear model, however good steady state performance is more desirable for load management.

Aircraft Load Test

The final test is to check the model performance using a load profile similar to that of an aircraft mission. The method of defining this profile using K-conditions was described in chapter 3 and the load profile used for the test is shown in figure 5.10.

Figures 5.11 and 5.12 show the results of the analogous load test for the linear physics model. Considering the large inaccuracies observed for the previous tests, this test shows excellent steady state accuracy throughout the test. For both the stator winding and the stator iron the maximum steady state error is around $1°C$. These results also confirm those of the varying load test; that the biggest impact of using a set winding resistance is to transient performance. The agreement between the model and the measured data is good enough for the model to fulfil its purpose as the design model.

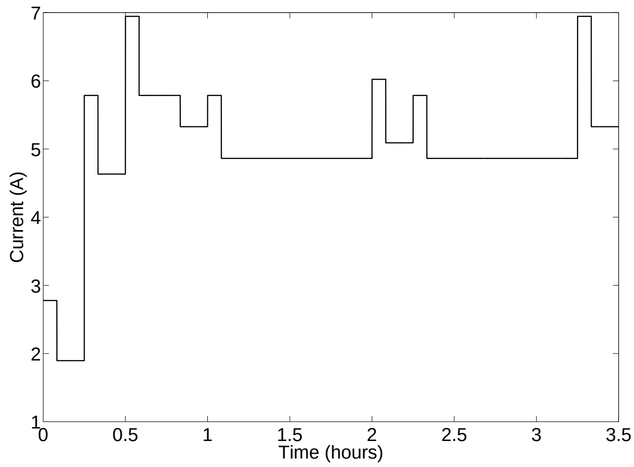

Figure 5.10: Graph showing the load profile per phase for the aircraft load test.

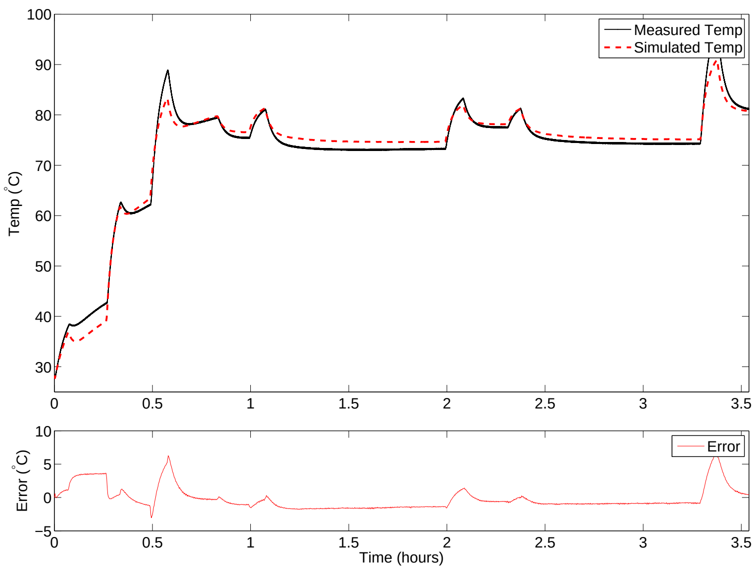

Figure 5.11: Analogous load test showing stator winding temperature for the linear physics-based model.

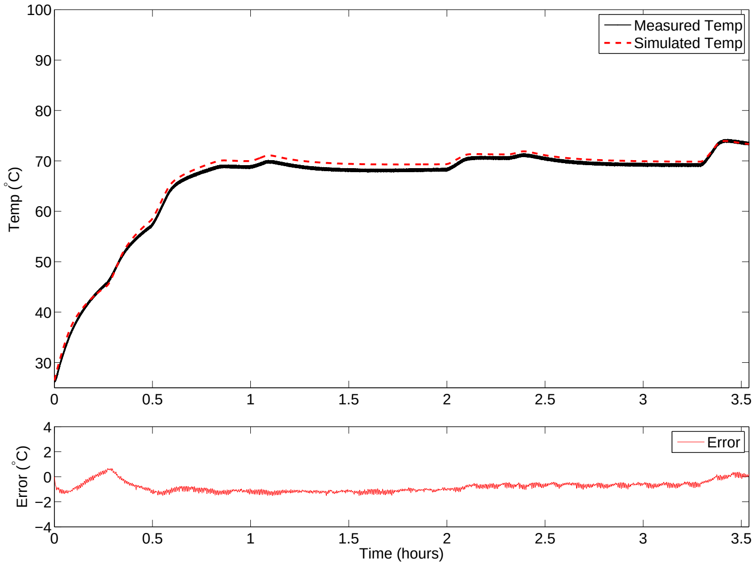

Figure 5.12: Analogous load test showing stator iron temperature for the linear physics-based model.

5.3 System Identification Model

During the literature review no research was found that discussed "black box" methods to create thermal models of generators. These methods could be investigated as a possible linear design model to form part of the prediction system. This section details the method of creating a data driven model using the system identification method, including validating results using similar data to that used for previous models. Throughout this section two aircraft flight profiles are referred to; one is the "training data" and the other is the "validation data". These load profiles both simulate loads over two different flight plans; the "training data" is used to derive the parameters for the model while the "validation data" is used as part of the model testing to define how the model performs under different input loads.

5.3.1 Model Design

The system identification process uses data collected to match the input data recorded to the output. Four different input variables were available to use, which were:

1. Phase-U current.
2. Phase-V current.
3. Phase-W current.
4. Excitation current.

All four of these variables change as the load varies making them viable options to match to the output.

The two outputs that need to be modelled are the stator winding temperature (sw) and the stator iron temperature (si). Each of these were modelled from the inputs individually; the two models were then combined to create the final model.

Each model was defined in the ARX form:

$$y(z) = \frac{B(z)}{A(z)}U(z - n_k) \tag{5.5}$$

where

$$B(z) = b_0 + b_1 z^{-1} + b_2 z^{-2}..... + b_{n_a} z^{-n_a} \tag{5.6}$$

$$A(z) = 1 + a_1 z^{-1} + a_2 z^{-2}..... + a_{n_b} z^{-n_b} \tag{5.7}$$

Where $y(z)$ is the model output (stator winding and iron temperatures), the parameters of the $B(z)$ and $A(z)$ equations were defined using the linear least squares method. $U(z - n_k)$ is the input to the system, with n_k being the number of delays in the system. n_a and n_b are the number of A and B parameters used.

It was found that each output could be mapped to a single input. For both cases all the different input variables were tested to see which gave the best correlation between the recorded data and the model output.

To determine the final model parameters an algorithm was developed that would test how good a fit could be obtained as the number of A and B parameters varied starting with a single A parameter and zero B parameters.

To test quality of the fit obtained the coefficient of determination R^2 was used. This is calculated by dividing the sum of errors between model output and data by the sum of the measured output data minus the output mean squared.

$$R^2 = \frac{\sum e(z)^2}{\sum (y(z) - y_{mean})^2} \tag{5.8}$$

Where $e(z)$ is the error between measured and model data at time z, $y(z)$ is the measured value at time z and y_{mean} is the mean value of the output. This produces a value between 0 and 1 with the value tending towards 1 as the fit improves.

The second measure considered is Akaike's information criterion (AIC) [80]; this is a test showing the trade-off between the 'goodness of the fit' compared to model complexity. The preferred model is the one that has an AIC value closest to 0. AIC rewards not only a good fit but applies a penalty as the number of estimated parameters increases; this is to discourage over-fitting. These two parameters considered together were used to determine the most appropriate solution.

5.3.2 Model Optimisation

When the algorithm was first run to estimate the parameters the results produced a reasonable fit. However it was found that if an integrator in the form:

$$\frac{1}{1 - z^{-1}} \tag{5.9}$$

was applied to the input data a much better fit was obtained. In practice this meant that after the algorithm was run, to reconstruct the actual model the result needed to be be multiplied by equation 5.9.

The data used to train the system identification models is the analogous load profile used to validate the physics-based models. The input load profile is shown in figure 5.13 and the outputs are shown in figure 5.14.

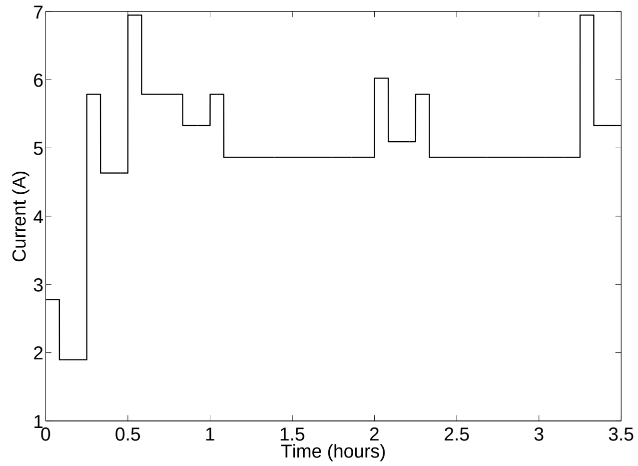

Figure 5.13: Graph showing the input load profile for the system identification algorithm.

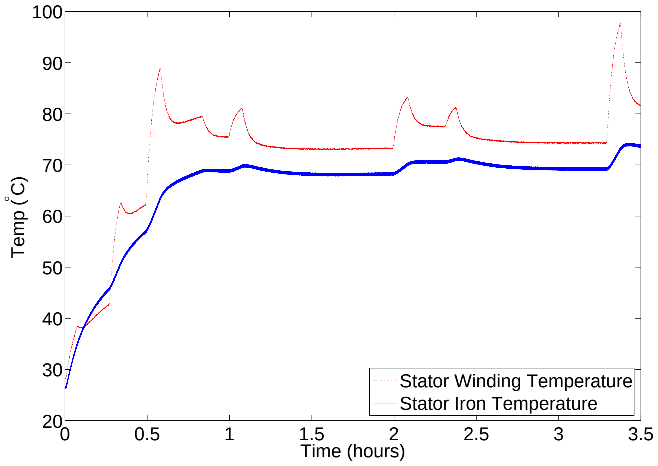

Figure 5.14: Graph showing the output variables for the system identification algorithm.

Stator Iron Model

The algorithm was run to match the input data to the stator winding temperature as described earlier. It was found that using the excitation current gave the best fit between model and recorded data. Table 5.1 shows the top ten best model candidates from those tested.

Table 5.1: 10 best candidate models for the stator iron

No. Params Eqn 5.7	**No. Params Eqn 5.6**	**No. Delays (n_k)**	R^2	**AIC**
1	2	1	0.9845	-3.1527
1	2	2	0.9844	-3.1551
1	3	1	0.9843	-3.1536
1	2	0	0.9843	-3.1496
1	3	0	0.9842	-3.1513
1	3	2	0.9840	-3.1550
1	3	3	0.9837	-3.1552
1	2	3	0.9837	-3.1564
1	2	4	0.9829	-3.1558
2	2	2	0.9824	-3.4101

The results in table 5.1 are sorted by R^2 value. The algorithm showed that the model with the best R^2 value has one A parameter and two B parameters, with one pure time delay. The model was chosen over the more complex model with one A parameter, two B parameters and no time delays. Even though the more complex model achieved better results, the improvement is not enough to justofy more complexity. The coefficient of determination for this configuration is 0.9843 and an AIC value of -3.15, showing the model is a very good fit. The equations for this model are:

$$A(z) = 1 - 0.9886z^{-1} \tag{5.10}$$

$$B(z) = 0.7394 - 0.7393z^{-1} \tag{5.11}$$

Figure 5.16 shows the performance of the model compared to the training data and figure 5.15 shows the distribution of the errors between the model output and measured data.

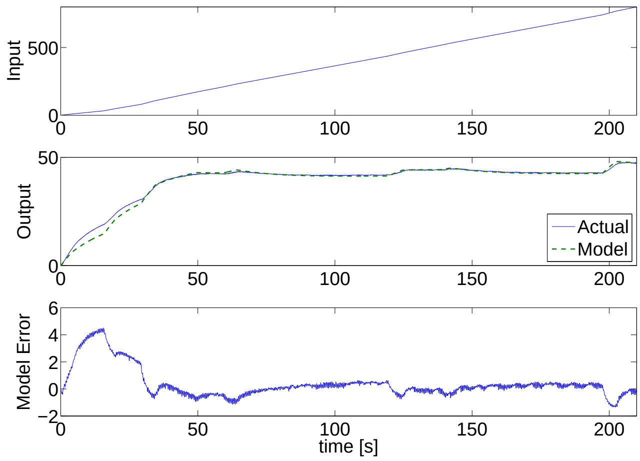

Figure 5.15: Results of the system identification algorithm for the stator iron.

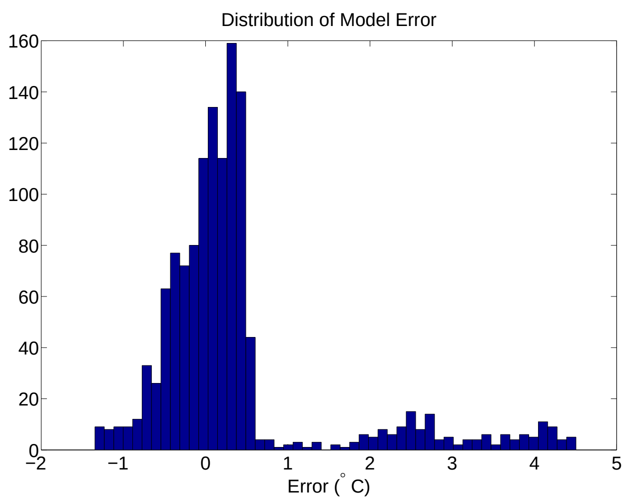

Figure 5.16: Graph showing the distribution of the errors of the stator iron model.

Figure 5.16 showing only small errors between the model and real data, with a maximum error of $4.5°C$. The distribution of errors in figure 5.15 show that most errors fall between $1°C$ and $-1°C$.

Stator Winding Model

The parameters for the stator winding were estimated in a similar fashion to the stator iron. It was again found that the excitation current gave the best fit to the recorded data. The main requirement of the model is that high temperatures are simulated accurately to provide accurate predictions of when overheat faults will occur. To increase the high temperature accuracy, low temperature data (from 0 - 30mins) was discarded from the data set. Table 5.2 shows the top ten best model candidates from those tested.

Table 5.2: 10 best candidate models for the stator winding

No. Params Eqn 5.7	**No. Params Eqn 5.6**	**No. Delays** (n_k)	R^2	**AIC**
1	2	0	0.8658	-3.8429
2	2	0	0.8609	-4.0748
1	3	0	0.8602	-3.9189
1	3	1	0.8509	-3.9128
2	3	1	0.8583	-4.0959
1	2	1	0.8581	-3.9132
2	3	0	0.8572	-4.0881
1	3	2	0.8557	-3.8388
3	2	0	0.8549	-4.1121
3	3	1	0.8545	-4.1459

The results in table 5.1 are sorted by R^2 value. The algorithm showed that the model with the best R^2 value has one A parameter and two B parameters, with no pure time delays. This model was chosen as it not only has the highest R^2 value but is the simplest model in the top ten candidates. The coefficient of determination for this configuration is 0.8658 and an AIC value of -3.84, showing the model is a good fit. The equations for this model are:

$$A(z) = 1 - 0.9584z^{-1} \tag{5.12}$$

$$B(z) = 4.876 - 4.873z^{-1} \tag{5.13}$$

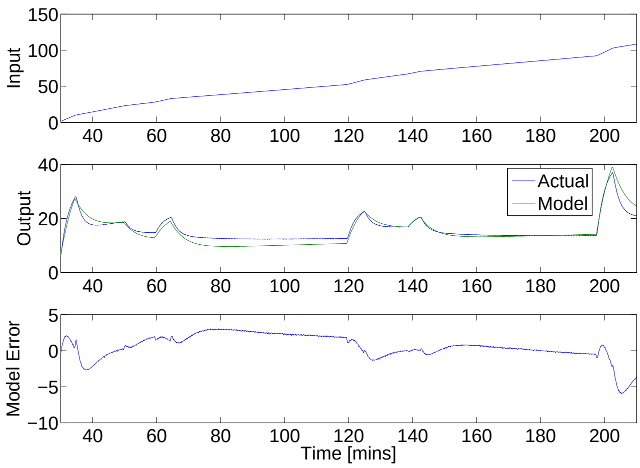

Figure 5.17: Results of the system identification algorithm for the stator winding.

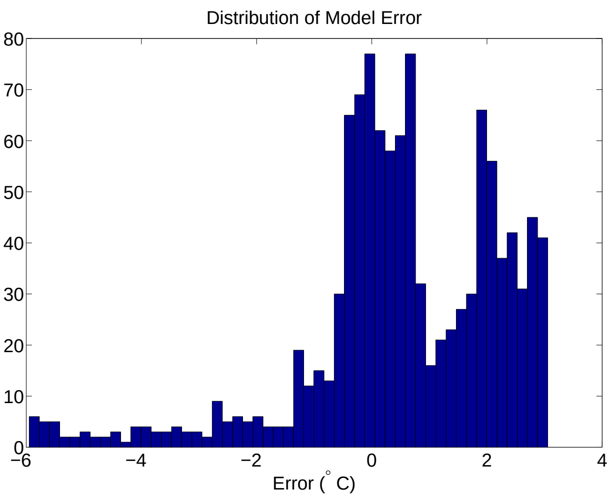

Figure 5.18: Graph showing the distribution of the errors of the stator winding model.

Figure 5.17 shows the results of the fitting algorithm using a subset of the data in the higher temperature range. Figure 5.18 shows that the maximum error is $6°C$ and that most errors fall in the range of $2.5°C$ to $-1.5°C$. While the quality of the fit is not as good as for the stator iron this was expected due to greater transient changes in temperature; the model fit is still good and will suffice for the application it is to be used in.

Final Model

To obtain the final model each of the relationships found for the stator winding and stator iron were multiplied by $1/1 - z^{-1}$ to add the pure integrator back in. This gave the final stator iron equations as:

$$A(z) = 1 - 1.989z^{-1} + 0.9886z^{-2} \tag{5.14}$$

$$B(z) = 0.7394 - 0.7393z^{-1} \tag{5.15}$$

The final stator winding equations are:

$$A(z) = 1 - 1.958z^{-1} + 0.9584z^{-2} \tag{5.16}$$

$$B(z) = 4.876 - 4.873z^{-1} \tag{5.17}$$

These equations are combined then transformed into the state space form:

$$[\dot{\theta}] = [A][\theta] + [B][U] \tag{5.18}$$

$$[y] = [C][\theta] + [D][U] \tag{5.19}$$

Where:

$$[A] = \begin{bmatrix} 1.9885614 & 0.9885614 & 0 & 0 \\ 1 & 0 & 0 & 0 \\ 0 & 0 & 1.9584458 & 0.9584458 \\ 0 & 0 & 1 & 0 \end{bmatrix} \tag{5.20}$$

$$[B] = \begin{bmatrix} 1 & 0 \\ 0 & 0 \\ 0 & 4 \\ 0 & 0 \end{bmatrix} \tag{5.21}$$

$$[C] = \begin{bmatrix} 0.7309406 & -0.7309097 & 0 & 0 \\ 0 & 0 & 1.1690134 & 1.1682635 \end{bmatrix} \tag{5.22}$$

$$[D] = \begin{bmatrix} 0.7393671 & 0 \\ 0 & 4.8756580 \end{bmatrix} \tag{5.23}$$

Finally in each case when the parameter estimation algorithm was run the best results were obtained when the data started at zero, so the initial temperature value was subtracted from all values before running the algorithm. To reconstruct the actual output this offset has to be added back on; $26.5°C$ for the stator iron and $62.7°C$ for the stator winding.

5.3.3 Model Validation

Similar test data to that used in the validation of the non-linear physics model in chapter 4 is also used here. First step input test and varying load test results are presented, then the results on a load profile analogous to that experienced on-board an aircraft during a mission is presented.

Step and Varying Load tests

This section presents the results for both the step tests and varying load tests together. The results are shown in figures 5.19, 5.20, 5.21 and 5.22.

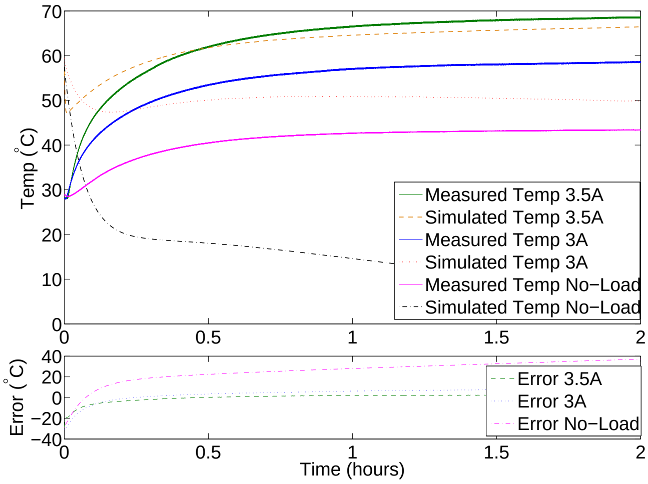

Figure 5.19: Step input test showing stator winding temperature for the system identification model.

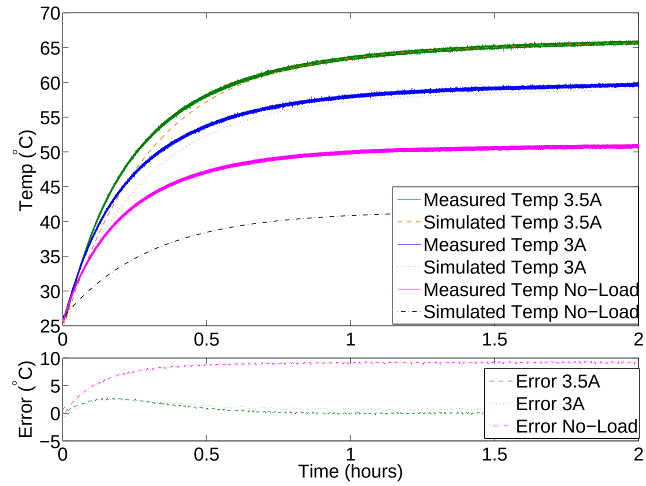

Figure 5.20: Step input test showing stator iron temperature for the system identification model.

The model was trained using a data set that is analogous to that seen in an aircraft, meaning that the model performance is severely reduced when other types of profile are presented. The error shown in this can be very high. Compared to

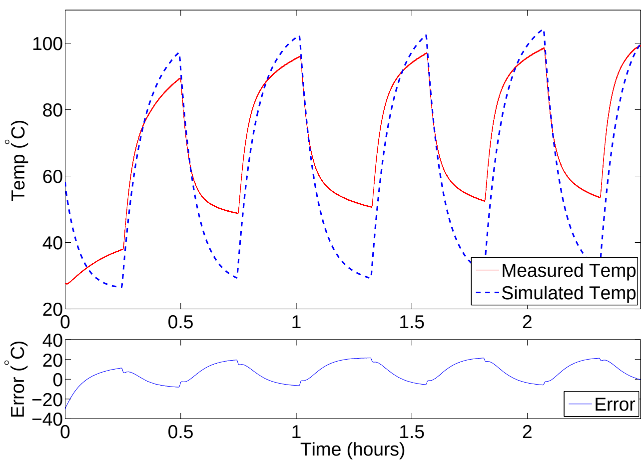

Figure 5.21: Varying load test showing stator winding temperature for the system identification model.

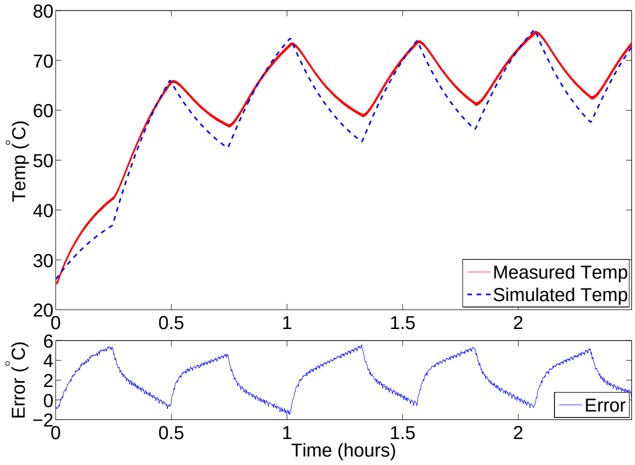

Figure 5.22: Varying load test showing stator iron temperature for the system identification model.

the physics model, the system identification model does not retain accuracy over all possible input profiles.

Aircraft Load Test

The analogous load test was performed using a separate data set to that which was used to train the model, the profile is shown in figure 5.23.

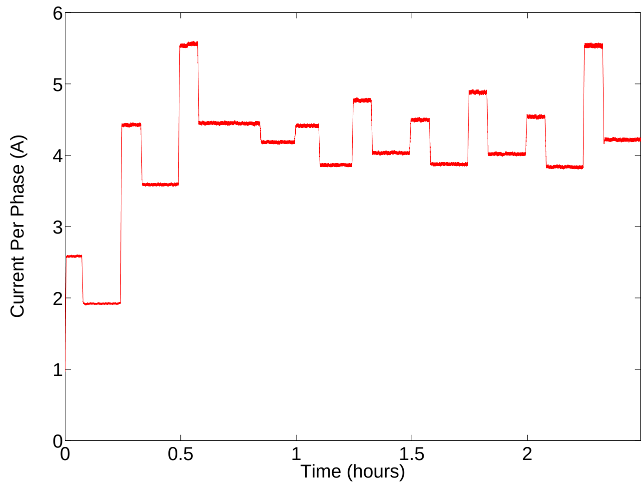

Figure 5.23: Graph showing the load profile per phase for the analogous load test.

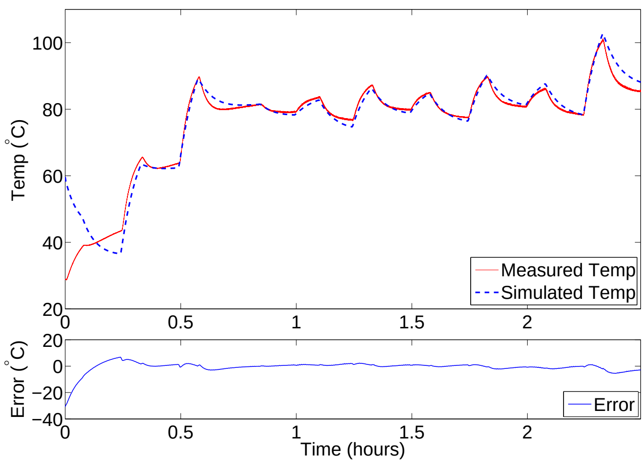

Figure 5.24: Analogous load test showing stator winding temperature for the system identification model.

Figures 5.24 and 5.25 show the model output against the measured output for

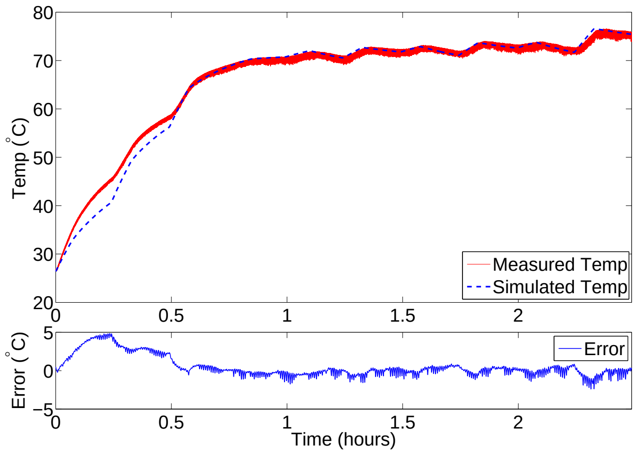

Figure 5.25: Analogous load test showing stator iron temperature for the system identification model.

the input profile shown above. These both show that at high temperatures the model is a good fit for both the stator winding and stator iron. As expected the low temperature performance is worse, especially in the case of the stator winding due to the system identification model only being trained on high temperature data. This is acceptable however, as low temperature performance is not important. The R^2 value for the stator winding is 0.8197 and 0.9760 for the stator iron. These are slightly lower than the results using the training data, however this is expected due to low temperature inaccuracies. Overall these results show that the model is a good fit and will be accurate enough for use within the prediction system.

5.4 Comparison of Possible Design Models

Two possible design models available; the linear physics-based model and the system identification model. The main areas to compare these models are structural complexity and model fit, with ease of construction and implementation taken into account.

Looking first at the complexity of both models, the system identification model is a fourth order model while the linear physics-based model is of eight order. The lower complexity can also be seen in that the system identification model only requires one of the available inputs, while the physics model requires all four and an ambient temperature measurement.

The two models appear to have similar accuracy levels of accuracy. The coefficients of determination for both model show some differences. For the physics-based model the coefficient of determination (R^2) is 0.9786 for the stator winding and 0.9903 for the stator iron. For the system identification model the R^2 value for the stator winding is 0.8197 and 0.9760 for the stator iron. This shows that while both models have very similar values for the stator winding, the physics-based model has a much better R^2 value for the stator winding. Some of this difference can be accounted for due to the performance at low temperatures, however from looking at the R^2 value of 0.8658 obtained from the training data, it can be assumed that the value discounting the low temperature performance will still be lower than the value for the physics model.

While the R^2 values indicate the physics-based model is more accurate, there are other factors which need to be taken into account. In this case it is the system identification model performs slightly better in steady state performance when compared to the physics model which has a steady state error of roughly $1°C$. The steady state error for the system identification model varies between 0 and $1°C$.

A case can be made for the selection of either model for use as the design model. The system identification model is much simpler and has a slightly better steady state performance around its optimisation point of around $70°C$, while the physics based model is more accurate over a greater operating range but much more complex.

Another factor to consider is the ease of conducting the mathematical description of the models. The physics based model requires expert knowledge of the system to construct, while the system identification model requires input and output data to be available to estimate the parameters.

The final point to consider is the ability to model faults upon the generator. In the case of the physics-based model the model can be adjusted to include a faults as long as an equation exists to describe the fault mathematically. This means that some expert knowledge is required, but for a large number of faults these equations exist. For the system identification model fault propagation data is required. Effectively a new model is created using this data for each fault that it is desirable to model. For the generator modelled here this fault propagation data does not exist.

The model that will be used is the physics-based model. While both models have a similar level of accuracy around the normal operating temperature of about $70°C$. For this application model accuracy as the temperature increases towards the maximum of $110°C$ is important and because these results show the linear physics-based model maintaining its accuracy over a greater range it will function better for this application.

5.5 Conclusion

This chapter has described two possible design model for use within the prediction system, showing evidence to define which is the best possible choice.

The linear thermal network model is derived from the more complex non-linear version described in chapter 4. The process of linearising the stator winding losses, showing the effects of both the I^2R term and updating the winding resistance with temperature on the accuracy of the model. The result was a model that has lower transient performance due to not updating the winding resistance with temperature. It was also shown that the non-linear I^2R term is what prevents errors from increasing over time in the non-linear model in chapter 4. The model performance is still sufficient for use in the prediction system.

The system identification process was shown to produce a simpler model, with 4 orders. This model is less accurate than the physics-based model however some of this is due to training the model with only high temperature data, however even when ignoring low temperature data the physics based model is still more accurate. The system identification model is a good fit, with excellent steady state performance around $70°C$.

The model chosen to be used in the prediction system is the physics-based model. The main factor in this choice was the ability to maintain accuracy over a greater range of temperatures.

Chapter 6

Kalman Filter Based Prediction

6.1 Introduction

Figure 6.1 shows an updated version of the flow diagram describing the load management system. This chapter describes the derivation of the prediction method shown in the red box in the diagram. The diagram itself has been updated showing the choice of design model picked in the previous chapter which will be summarised here. The diagram also shows the chosen state update and prediction algorithm which is the Kalman Filter.

In the literature survey the Kalman Filter was chosen over other possible simulation methods. This method would allow both measured and non-measured states to be updated before predictions were made, and due to the fact that the design model is linear would be a computationally light method of achieving this which is a major factor for deployment upon an aircraft.

In this chapter the theory of the Kalman Filter is summarised first. The equations for the Kalman Filter including the physics-based model, the Kalman Gain and n-step prediction method are then described. Finally results validating the state update and prediction of the Kalman Filter are presented.

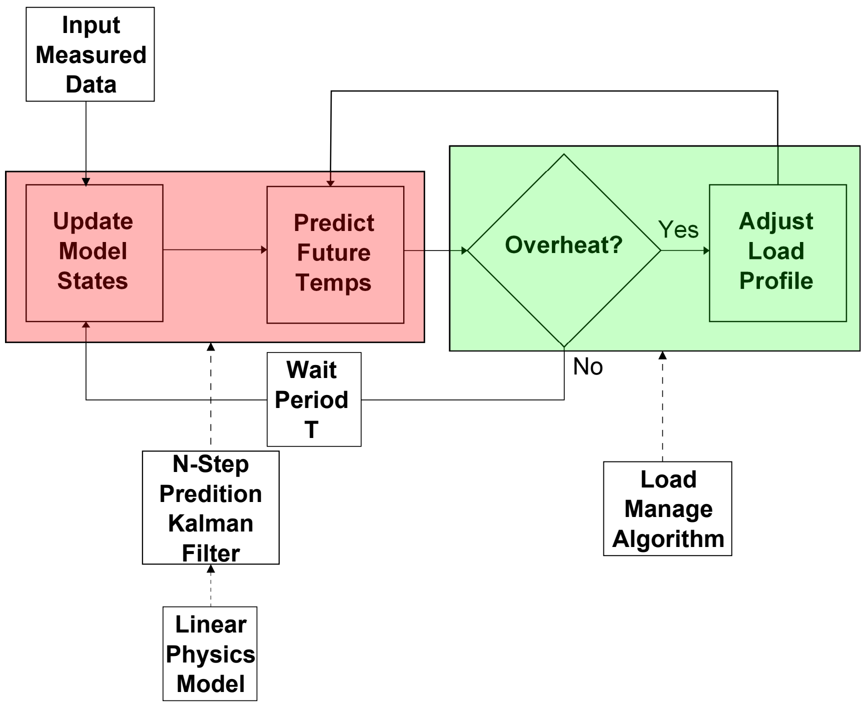

Figure 6.1: Flow Diagram Showing Load Management System.

6.2 Kalman Filter Derivation

In 1960 Kalman first published a paper describing the observer now named the Kalman Filter [66]. The filter is based around the state space representation of a model where at each time interval the model predicts a step ahead, these estimates are then updated using measurements from the real system combined with a Kalman gain. The updated model is then used to predict ahead again, this process can be repeated ad infinitum. Figure 6.2 shows this process loop.

The equations to define the output temperatures $[y]$ are shown in figure 6.2 are:

$$[\dot{\theta}]\ (z+1) = [A][\theta](z) + [B][U](z) + L_k\varepsilon \qquad (6.1)$$

$$[y](z) = [C][\theta](z) + [D][U](z) + noise \qquad (6.2)$$

Where $[A]$, $[B]$, $[C]$ and $[D]$ are the state-space model matrices defined later,

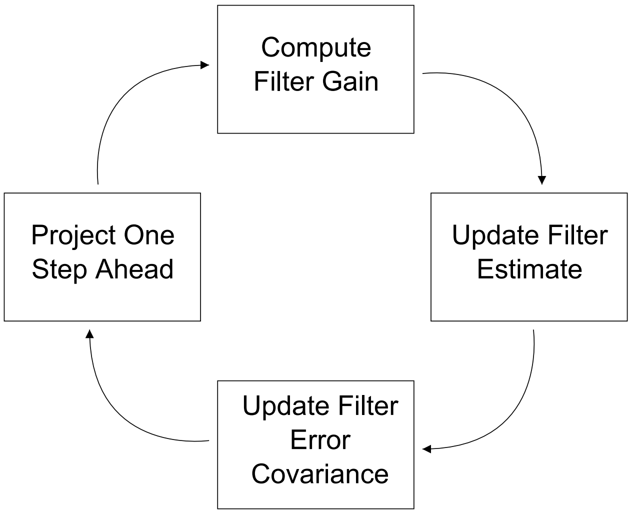

Figure 6.2: Kalman Filter.

$[\theta]$ is the column vector of nodal temperature states, L_k is the Kalman gain, ε is the error between the measured states and model output and $[u]$ is a column matrix of heat sources. To create the Kalman filter a number of elements need to be derived. These are:

- System Model
- Process and Measurement Error Covariance
- Calculation of Kalman Filter

6.2.1 Summary of Physics-Based Design Model

The model described in chapter 5 is in the form:

$$[C]\frac{d[\theta]}{dt} = [G][\theta] + [u] \tag{6.3}$$

Where $[C]$ is a square matrix of thermal heat storage values and $[G]$ is a square matrix of thermal conductance between nodes.

For use within the Kalman Filter this equation is converted into the discrete state-space form:

$$
\begin{aligned}
[\dot{\theta}]\,(z+1) &= [A][\theta](z) + [B][U](z) && (6.4)\\
[y](z) &= [C][\theta](z) + [D][U](z) && (6.5)
\end{aligned}
$$

Where:

$$
\begin{aligned}
[A] &= [C_a]^{-1}[G] && (6.6)\\
[B] &= [C_a]^{-1} && (6.7)\\
[C] &= \begin{bmatrix} 0 & 1 & 0 & 0 & 0 & 0 & 0 & 0 \\ 0 & 0 & 0 & 1 & 0 & 0 & 0 & 0 \end{bmatrix} && (6.8)\\
[D] &= 0 && (6.9)
\end{aligned}
$$

$[C_a]$ and $[G]$ are the capacitance and admittance matrices which were derived in chapter 4.

Finally $[u]$ is derived from linearising the winding losses as shown in chapter 5.

6.2.2 Definition of Process and Measurement Error Covariance Matrices

The final parameters that need to be defined are the process noise error covariance matrix and the measurement noise covariance matrix, Q_k and R_k respectively.

R_k was calculated directly from available data for the stator iron and stator winding. To do this the data was first filtered to give an average value. This average was then subtracted from the signal leaving just the noise. Finally the covariance of the noise was calculated for each input signal. This gives two R_k values which are made into a diagonal matrix with the form:

$$[R_k] = \begin{bmatrix} 0.0082 & 0 \\ 0 & 0.0130 \end{bmatrix} \tag{6.10}$$

With the R_k matrix calculated a Q_k matrix could then be chosen to obtain best results from the filter. A diagonal matrix derived by trial and error was found to be sufficient and is shown below:

$$[Q_k] = \begin{bmatrix} 50 & 0 & 0 & 0 & 0 & 0 & 0 & 0 \\ 0 & 50 & 0 & 0 & 0 & 0 & 0 & 0 \\ 0 & 0 & 50 & 0 & 0 & 0 & 0 & 0 \\ 0 & 0 & 0 & 50 & 0 & 0 & 0 & 0 \\ 0 & 0 & 0 & 0 & 50 & 0 & 0 & 0 \\ 0 & 0 & 0 & 0 & 0 & 50 & 0 & 0 \\ 0 & 0 & 0 & 0 & 0 & 0 & 50 & 0 \\ 0 & 0 & 0 & 0 & 0 & 0 & 0 & 50 \end{bmatrix} \tag{6.11}$$

6.2.3 Kalman Filter Calculations

Figure 6.2 earlier showed the loop that is applied to calculate the output of the Kalman Filter. First equation 6.4 is used to predict a single step ahead. Simultaneously the covariance matrix P_k is calculated from Q and the previous value P_k^-.

$$P_k = AP_k^- A' + BQB' \tag{6.12}$$

The next step is to compute the Kalman gain matrix L_k.

$$L_k = P_{k-1}C(CP_{k-1}C' + R)^{-1} \tag{6.13}$$

The estimated state vector θ is then updated.

$$\theta = \theta^{-} + L_k \varepsilon \tag{6.14}$$

Where ε is the difference between the measured and model output.

The final step is to compute the new error covariance of the updated estimate.

$$P_k^{-} = P_{k-1}(I - L_k C) \tag{6.15}$$

The estimated model output at each time step can be calculated using equation 6.5 after the state vector update step.

During testing of the Kalman Filter it was found that as the loop is repeated the Kalman gain matrix converges to a set value as would be expected for a linear time invariant system. This is shown in figure 6.3.

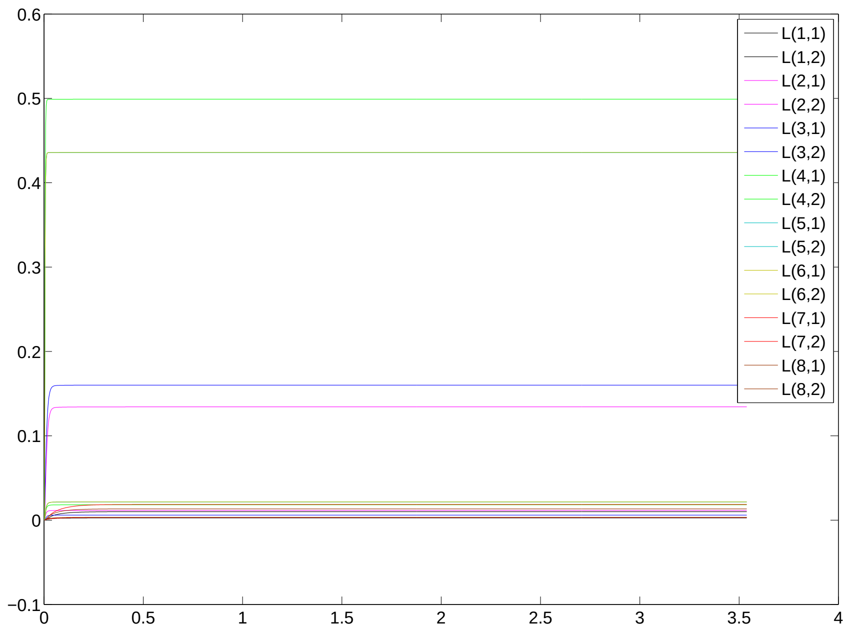

Figure 6.3: Values of Kalman Gain Matrix $[L_k]$ Over 3.5hour Test.

With this being the case instead of calculating a new L_k value each step the converged L_k matrix is substituted in as a constant.

6.2.4 N-Step Ahead Prediction

The classic Kalman filter predicts a single step ahead each cycle before updating the estimates. Brown and Hwang [67] showed that instead of predicting a single step ahead the Kalman Filter can also be used to predict n-steps ahead. This is achieved by allowing the model to predict ahead multiple times after the state vector has been updated and is shown in the updated process loop figure 6.4. Note that in figure 6.4 the computer filter gain stage is missing as a constant value has been substituted in as described earlier.

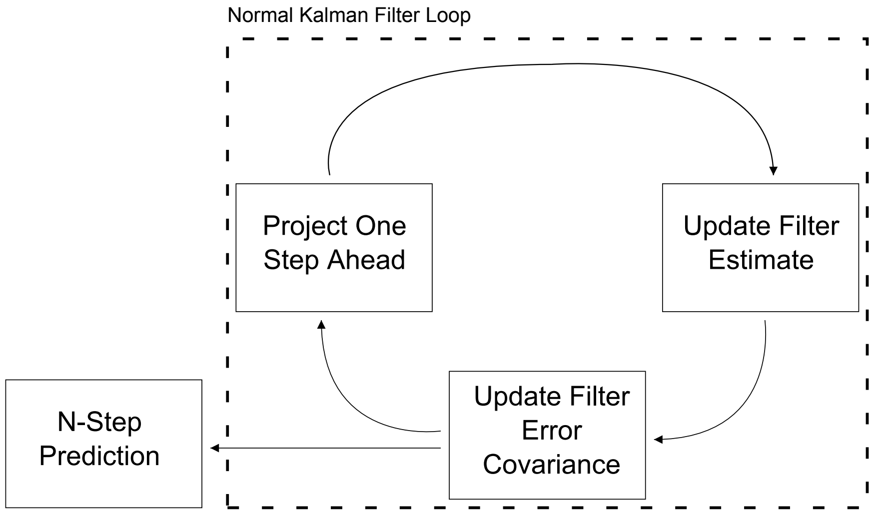

Figure 6.4: Kalman Filter N-Step Prediction.

In real terms this means that to perform a prediction the kalman filter updates the state estimates then the model predicts forward in an open loop mode. The equations for this are:

$$[\dot{\theta}]\ (z+1) = [A][\theta](z) + [B][U](z) + L_k\varepsilon[t \leq T_{pred}] \tag{6.16}$$

$$[y](z) = [C][\theta](z) + [D][U](z) + noise[t \leq T_{pred}] \tag{6.17}$$

Where t is the simulation time and T_{pred} is the time at which prediction starts.

6.3 Validation of the State Update and Prediction System

The next section presents results to validate the prediction system. First results showing that the Kalman filter successfully reduces errors between the model and measured data are shown. Then results which show the prediction performance of the n-step ahead predictor are presented.

For each test the results compare the performance of the Kalman Filter to the two measured states; the stator winding and stator iron. The load profile applied is created using the same K-Conditions described in chapter 3 and is shown in figure 6.5. The discrete step time used by the design model is $T_s = 10s$, which provides a good representation of the output over the long duration test while requiring less computation resources. The aim of the state update tests is for the Kalman Filter to reduce the real-time error to almost zero. In contrast the aim of the prediction validation tests is to define both the accuracy at any point in the future but also to define the amount of time the state update provides increased prediction accuracy when compared to a purely open loop prediction.

6.3.1 Kalman Filter State Update Validation

The first test was to analyse the performance of the Kalman Filter in correcting errors between the model and measured data. The test uses the analogous load profile used to validate models in chapters 4 and 5. The Kalman Filter uses the measured data to update the states in single step prediction mode.

Figures 6.6 and 6.7 show the results of the test. The results show that the Kalman Filter corrects for the errors in the physics-based model with no error greater than $1°C$. This test shows that the state update function of the Kalman Filter works as required.

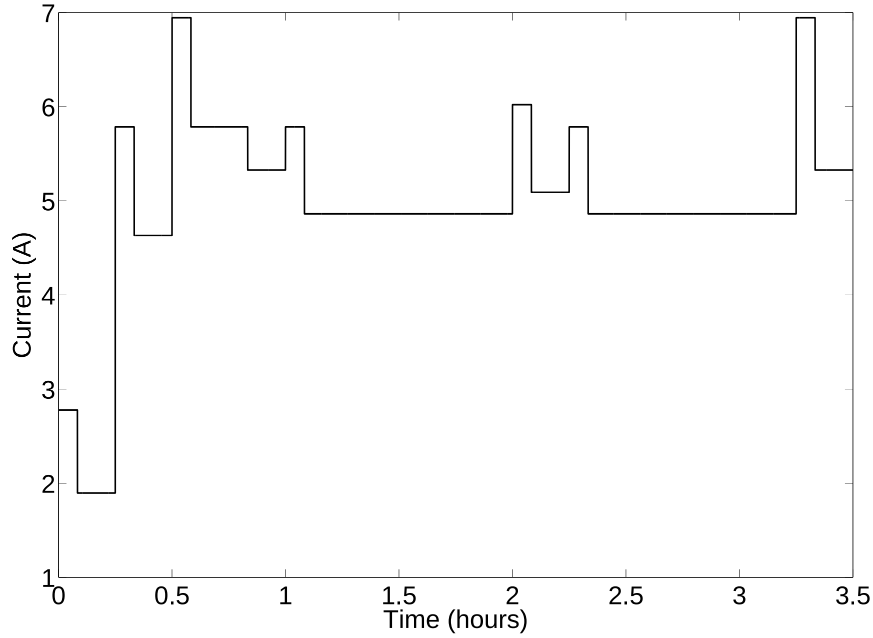

Figure 6.5: Load Profile Per Phase for Prediction System Validation Tests.

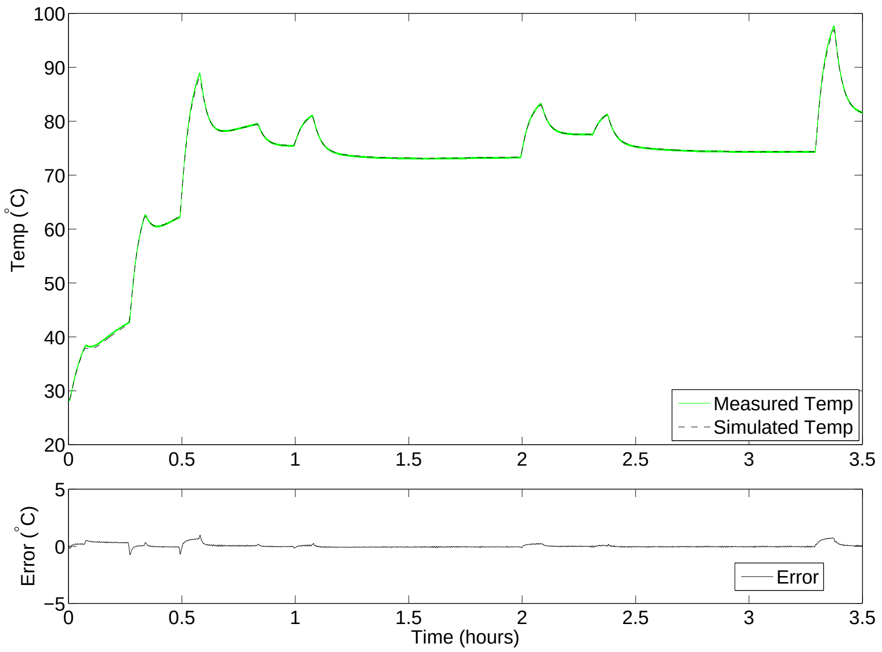

Figure 6.6: Analogous Load Test Showing Kalman Filter Performance for Stator Winding.

6.3.2 N-Step Ahead Prediction Validation

The second test uses the same profile as the first. The aim of this test is to see how accurate predictions starting at a given point in time (e.g. 50, 75, 100 minutes

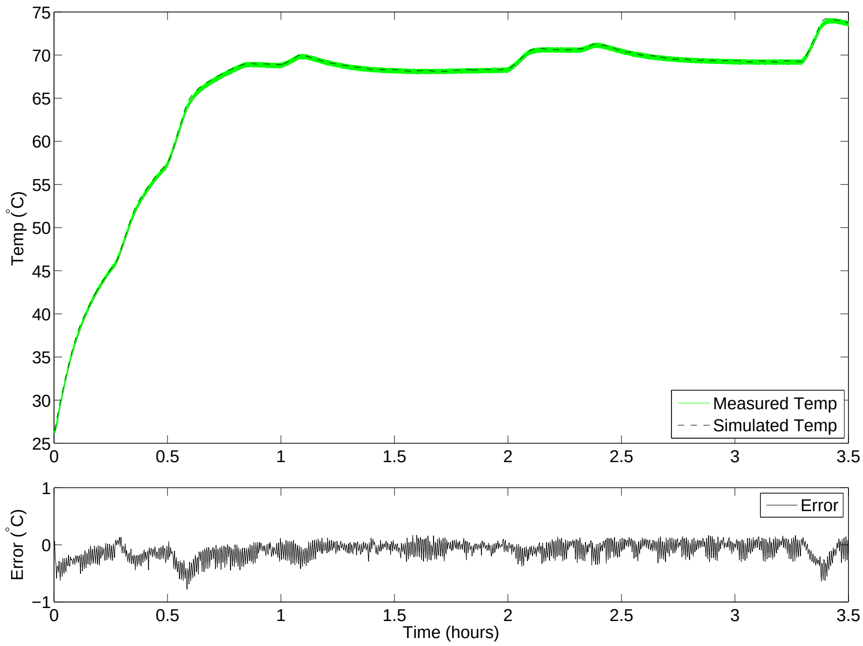

Figure 6.7: Analogous Load Test Showing Kalman Filter Performance for Stator Iron.

etc.) are compared to the open loop performance of the model.

Each test start with the Kalman Filter updating the states of the model as seen in the previous test. Then at the specified time the model is then used to predict ahead without measurement updates from the Kalman Filter. What is seen is that over time the error between the model and the measured data converges toward the error seen when the model is run open loop. The effectiveness of the prediction system is measured in relation to how long the error is lower than what would be seen if the open loop model was used from the start instead of the Kalman Filter. In total the results of six tests starting at different times are used to indicate how effective the Kalman Filter is dependent upon start time.

Figures 6.8 and 6.9 show the results of these tests. For each test it is shown that there is a period of time after the start of the prediction where the error between model and measured data is lower than if the open loop model is used. Figure 6.10 shows how the length of time where the Kalman Filter n-step prediction is more

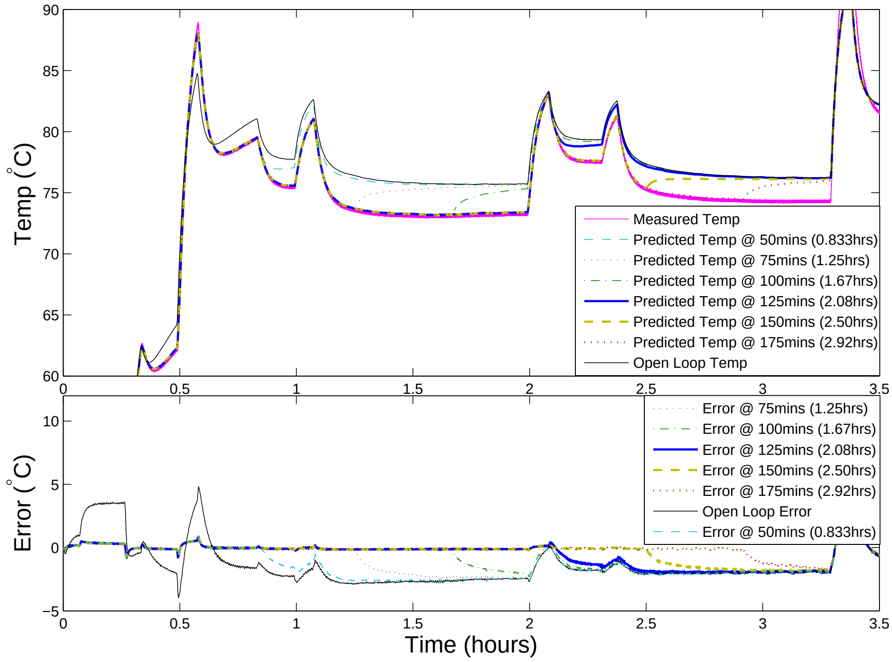

Figure 6.8: Analogous Load Test Showing Prediction Performance for Stator Winding.

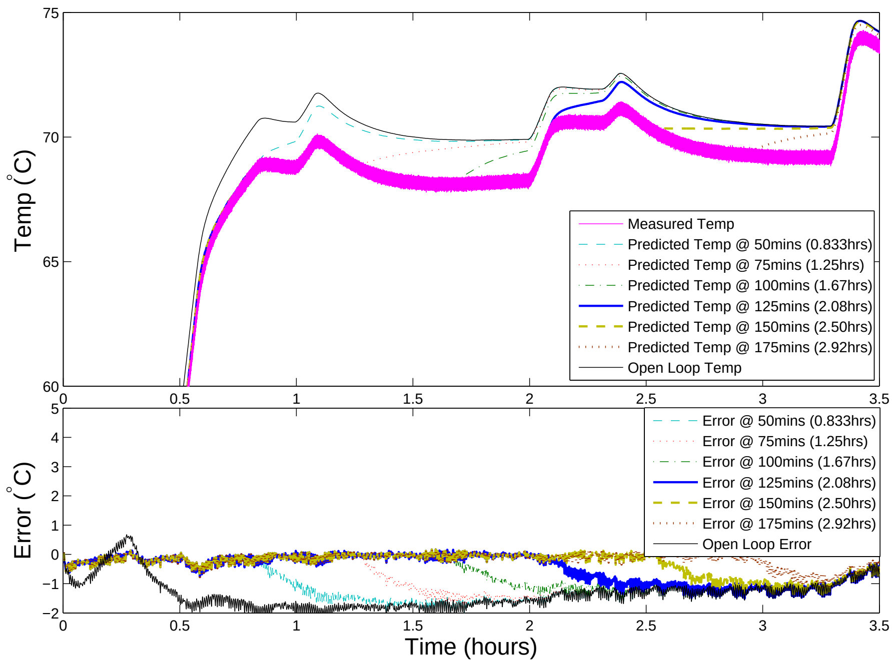

Figure 6.9: Analogous Load Test Showing Prediction Performance for Stator Iron.

accurate than the open loop prediction dependant upon prediction start time.

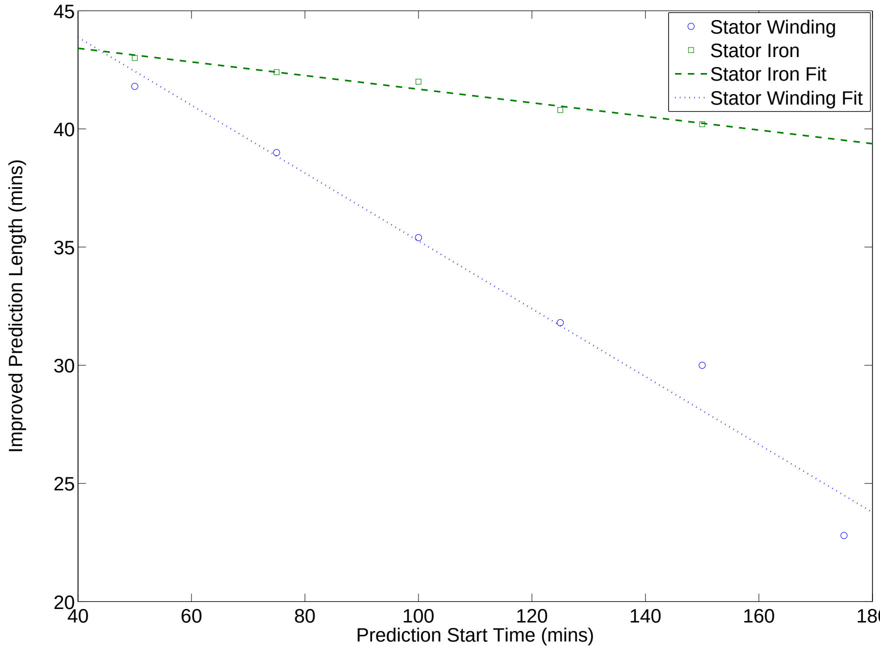

Figure 6.10: Plot showing how the period of increased prediction accuracy varies with prediction start time.

The first thing to note is that the time value for the 175 minute prediction for the stator iron was discarded as the results had not fully converged before the end of the test, producing an anomalous result. Figure 6.10 shows that a trend can be seen for both the stator iron and winding where the later a prediction starts, the smaller the period of increased prediction accuracy. This is probably due to the fact that towards the end of the test the error between the open loop model and measured results is smaller. Also shown is that the minimum period of increased accuracy for the stator iron is 40 minutes if the anomalous result is ignored and 22 minutes for the stator winding. This means that close to the execution of a load on the generator predictions can be made more accurately, acting as a final check upon decisions made.

6.4 Conclusion

In this chapter the implementation of a Kalman Filter to update the states of the generator design model and make prediction has been described.

Using the Kalman Filter it has been shown that the model states can be updated in real time using measured data to give an error of almost zero when compared to the measured output data. It has also been shown that by updating the states in real time the prediction made by the model is significantly more accurate than using the open loop model for at least 20 minutes. This is sufficient to allow the load management system to perform more accurate checks upon decisions made earlier.

Chapter 7

Description of Load Management System

7.1 Introduction

In this chapter the full system for detecting and preventing overheat faults in the aircraft's generators is described. In previous chapters sub-systems to be used within the load management system were developed. In this chapter the prediction algorithm and the design model within it are used as part of the full load management system to allow the optimisation of aircraft load profiles in flight to prevent generator overheating.

Firstly the algorithm for the load management system is described. This includes how previous sub-systems are integrated and a description of the load profile optimisation algorithm. The load management system is then validated first in simulation, then results are obtained by placing a fault on the experimental rig.

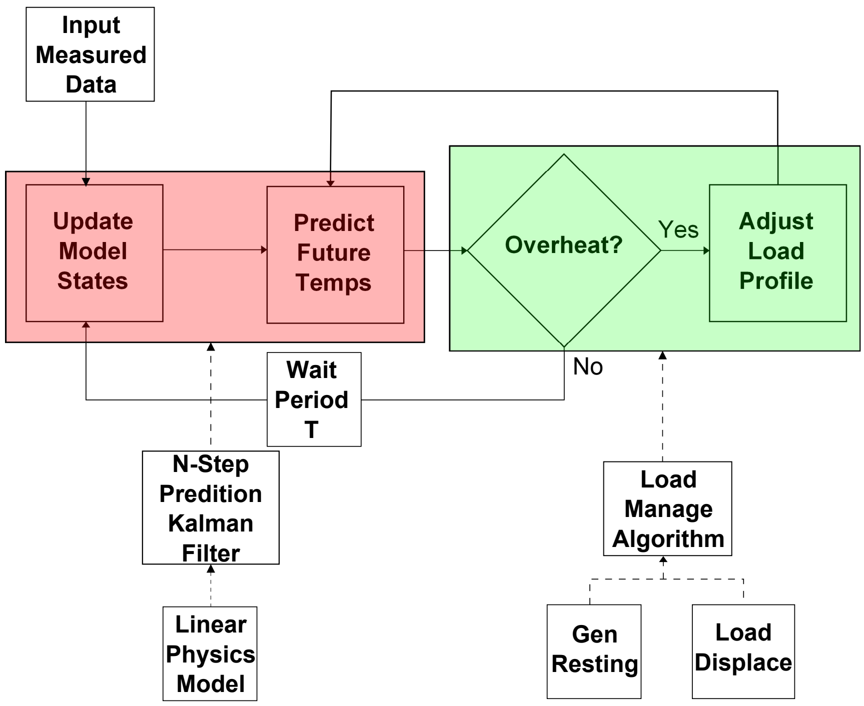

Figure 7.1: Flow Diagram Describing Load Management System

7.2 Load Management System Description

Figure 7.1 shows a flow diagram of how the load management algorithm operates. The cycle shown repeats once for every set time period; five minutes will be used for results presented in this chapter. First the model states are updated using data measured from the generator. Then the model is used to predict ahead for the rest of the flight. Finally the predictions are checked for any overheat faults, with the load management algorithm being run to adjust the load profile if any faults are found.

The state update and prediction have been detailed in previous chapters. The state update is achieved using the Kalman Filter containing the design model. The prediction is done as shown in chapter 6 using the Kalman Filter.

7.2.1 Load Profile Optimisation Problem Formulation

The final part of the load management system that needs to be described is the load profile optimisation system. This is the algorithm used if an overheat fault is detected. It is designed to adjust the load profile so that an overheat doesn't occur. To achieve this the system utilises methods whereby the heat load on a faulty generator can be reduced while still allowing the aircraft to fly.

The rest of the this section describes the two methods of load management; generator resting and load displacement. Then finally describes the full algorithm and how the load management methods are used within it.

Generator Resting

Generator resting is a method by which all non-essential loads are switched off, putting the generator into a minimum power mode which will allow the generator to cool down. If the prediction system predicts that an overheat would occur during a certain action, for example combat, the aim is to cool the generator down before that action is undertaken so that it can be completed without overheat. The method attempts to find the minimum rest time defined in mathematical terms as:

$$\begin{aligned} &Minimise && T_r \\ &Subject\ to && \theta_{si,sw}(t) \leq \theta_{max} \\ & && 0 \leq t \leq (T_r + T_k) \end{aligned} \tag{7.1}$$

Where T_r is the rest time, T_k is the length of the action or K-condition (k) as described in chapter 3, $\theta_{si,sw}(t)$ is the temperature of the stator iron and winding at time t in the mission and θ_{max} being the maximum allowed temperature of the generator.

Load Displacement

Load displacement is applied for aircraft with multiple generators, because in this case the method attempts to move loads from a faulty generator to healthy one if it has spare capacity. This can be defined as:

$$\begin{aligned} &Minimise && I_d(k) && (7.2)\\ &Subject\ to && \theta_{si,sw}(t) \leq \theta_{max} \\ & && 0 \leq t \leq T_k \end{aligned}$$

Where I_d is the amount of load displaced from one generator to another. The current for the faulty and healthy generators, I_{genf} and I_{genh} respectively at each K-condition becomes:

$$I_{genf}(k) = I_{ini}(k) - I_d(k) \tag{7.3}$$

$$I_{genh}(k) = I_{ini}(k) + I_d(k) \tag{7.4}$$

Where I_{ini} is the initial profile current.

Final Algorithm

The final algorithm is aimed at an aircraft with two generators and uses a combination of the two techniques described previously to optimise the loads and prevent overheat. Mathematically this is represented as:

$$\begin{aligned} &\textit{Minimise} && T_m = \sum_{k=1}^{n} T(k) + \sum_{r=1}^{p} T(r) \\ &\textit{Subject to} && \theta_{si,sw}(t) \leq \theta_{max} \\ & && 0 \leq t \leq T_m \end{aligned} \tag{7.5}$$

Where T_m is the total mission length.

The algorithm is minimising the total mission length which is equal to the length of the required actions plus the rest time. This means that the algorithm will attempt to displace loads to a healthy generator before creating rest periods as this adds no extra time to the mission.

Figure 7.2 shows a flow diagram of how equation 7.5 is implemented. When an overheat fault is detected the algorithm first tries to create a solution by only displacing loads to a healthy generator using equation 7.2. If the fault can not be prevented by displacement alone a short rest is added according to equation 7.1. Note both generators are rested which means that more load can be displaced to the healthy generator now so the amount of load to be displaced is checked again. If a solution is still not apparent the rest is extended again, with this process repeating until a solution is found.

7.3 Validation

Presented within this section are two sets of results. First the results of a test undertaken entirely in simulation are presented to show the function of the load management system and test the system before use on the experimental rig to avoid damaging it. Second are the results of a test where the experimental rig is used and the fault placed upon it, showing the system functioning when used on an actual generator.

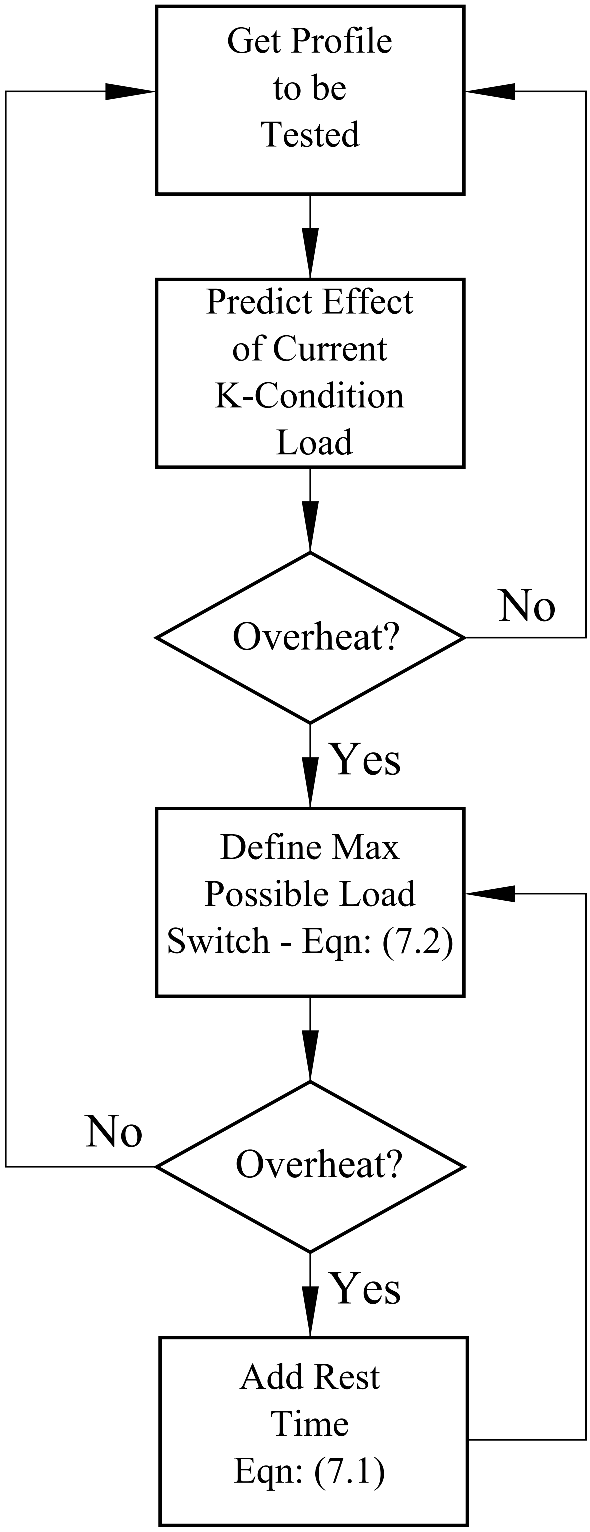

Figure 7.2: Flow Diagram Describing Load Optimisation Algorithm

7.3.1 Blockage Fault Description

For the test results presented here a single type of fault has been applied both in simulation and to the experimental rig to test the ability of the load management system. The simulation of a 'blockage' was chosen as it can be easily implemented upon the experimental rig and its effects are easy to describe. The term 'blockage' is used here to reference a situation where there is a narrowing of either the inlet or outlet for the generator coolant.

To define the effects of the blockage on the system tests were run on the experimental rig using the profile shown in figure 7.3. In these tests a plate with a specified orifice size was placed over the generator coolant outlet, narrowing the size of the exhaust vent.

The generator itself has a defined maximum hotspot temperature of $140°C$. To provide a safety window to avoid actual damage to the generator a maximum temperature for these experiments was set to be $110°C$. The $30°C$ allowance was chosen due to the experimental nature of the algorithm and to provide a more difficult case for the load management algorithm.

From these tests its was seen that the only parameter of the design model that needed to change was the output vent diameter. The other effect seen is an increase in the inlet air temperature, a measured value used as an input to the model, this is shown in figure 7.4.

Figure 7.5 shows both the stator winding and iron temperatures as a blockage that reduces the outlet size from 50mm to 10mm is applied. For this test no action was taken to prevent overheat and it shows that after 111 minutes (1.8 hours) the generator had to be switched off when its temperature had reached $109°C$ before the upper limit of $110°C$ was breached. This shows the need for the load management system in this situation.

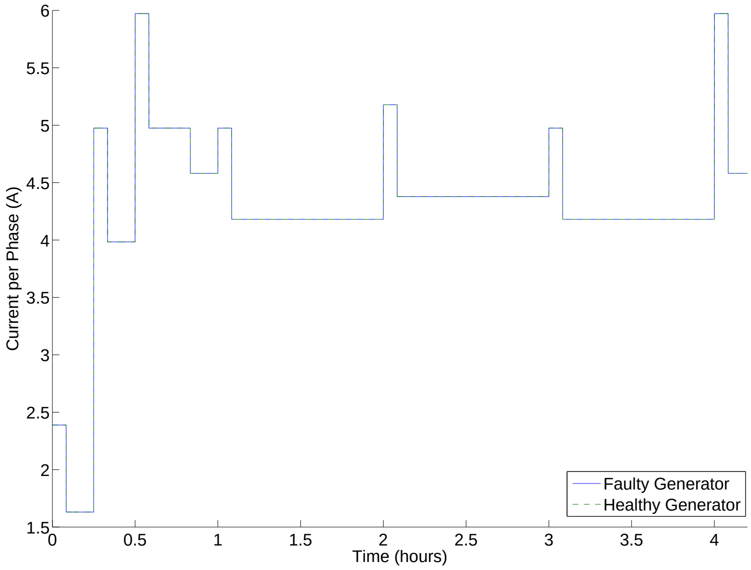

Figure 7.3: Initial Load Profile for Load Management System Validation

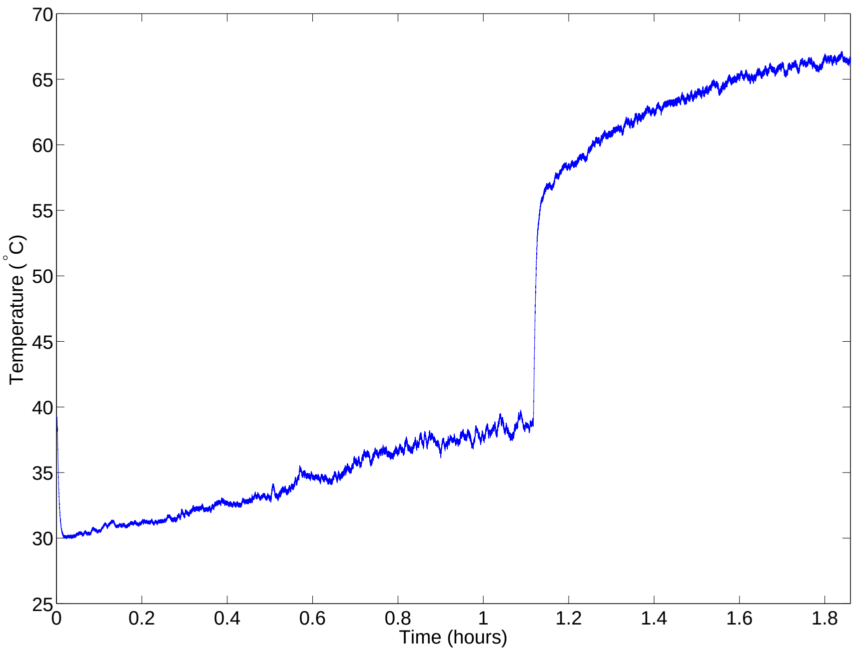

Figure 7.4: Inlet Temperature Rise Occurring After a Blockage Fault is Applied at 67 Minutes (1.1 Hours).

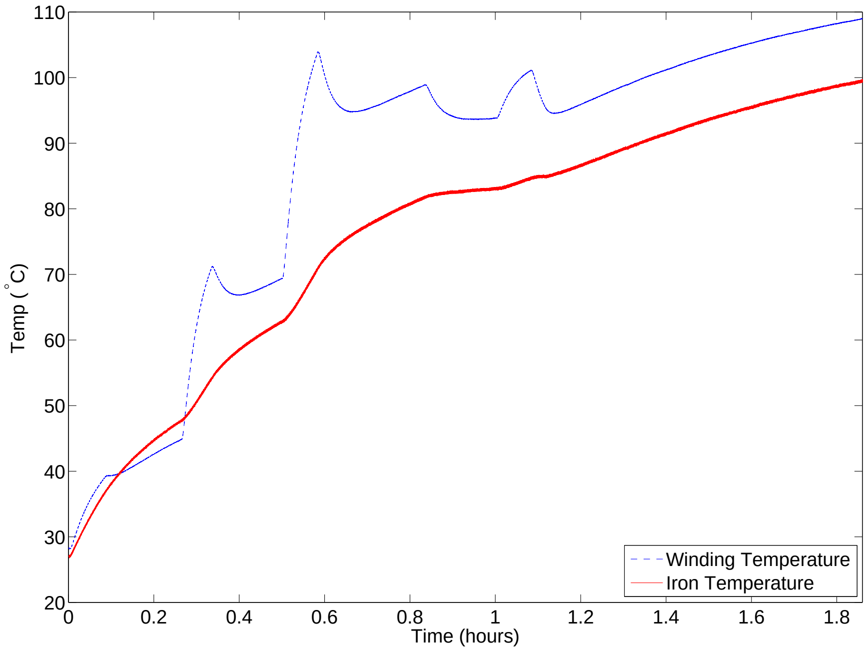

Figure 7.5: Stator Winding and Iron Temperature Rise Occurring After a Blockage Fault is Applied at 67 Minutes (1.1 Hours).

7.3.2 Simulation Set-up

Figure 7.6 shows the simulation set-up to be used within the tests presented here. For this test there will be two copies of the simulation model representing the generators and two Kalman Filters with the design model to make predictions with. The first generator will have the blockage fault injected and will be referred to as the faulty generator. The second will be unaffected for the duration of the test and will be described as the healthy generator.

The profile for the flight will be constructed in the same manner as shown in chapter 3 using the load conditions described there, which are repeated here in table 7.1.

Table 7.1: Flight Conditons

	1	**2**	**3**	**4**	**5**	**6**	**7**
5 mins	40.0%	83.3%	100.0%	83.3%	83.3%	86.7%	100.0%
Continuous	27.3%	66.7%	83.3%	76.7%	70.0%	73.3%	76.7%

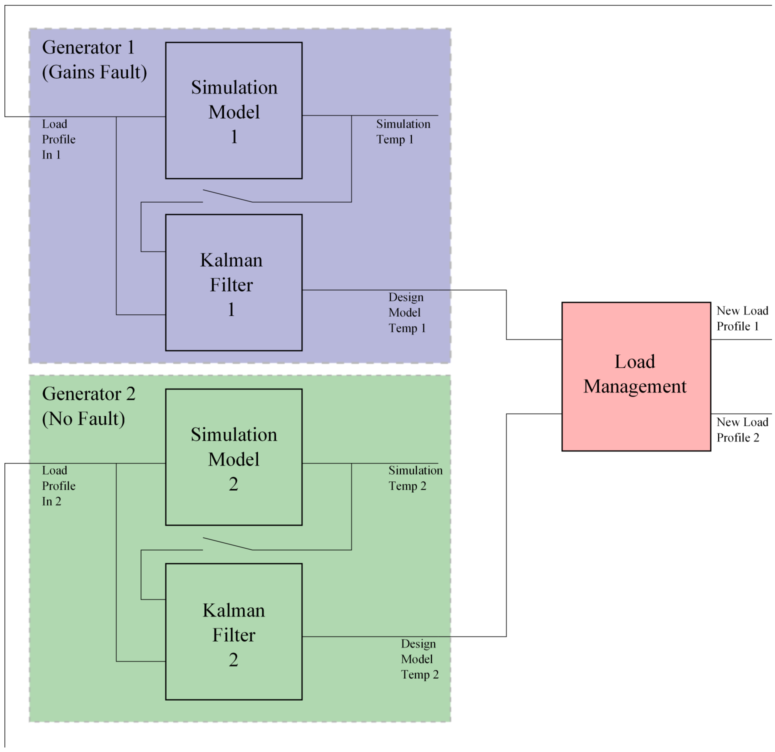

Figure 7.6: Diagram Showing the Simulation Set-up for Validation Tests

Where:

1 - Loading and Preparation

2 - Start and Warm-Up

3 - Taxi

4 - Take-Off and Climb

5 - Cruise

6 - Cruise/Combat

7 - Landing

The profile used for the tests is shown in figure 7.7 and is initially applied to both generators.

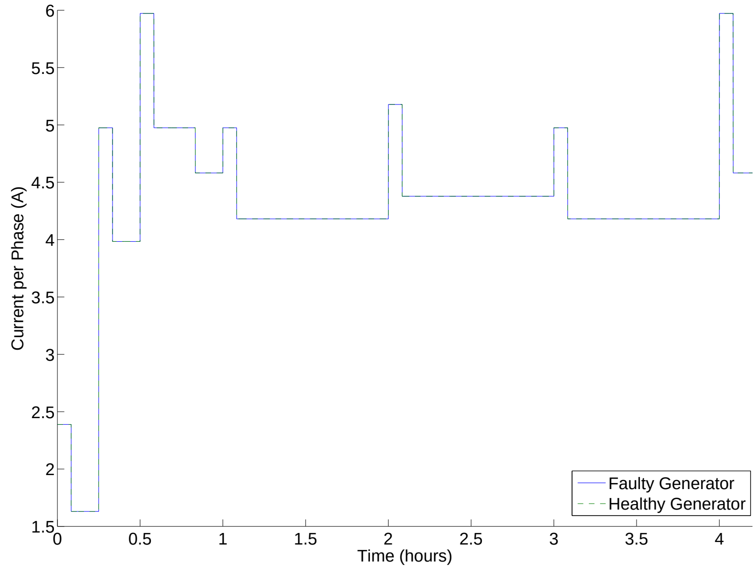

Figure 7.7: Initial Load Profile for Load Management System Validation

Figure 7.8 show the temperature output for the stator winding when the load profile of figure 7.7 is applied, showing that without a fault no overheat faults occur (i.e Temp always less than $110°C$).

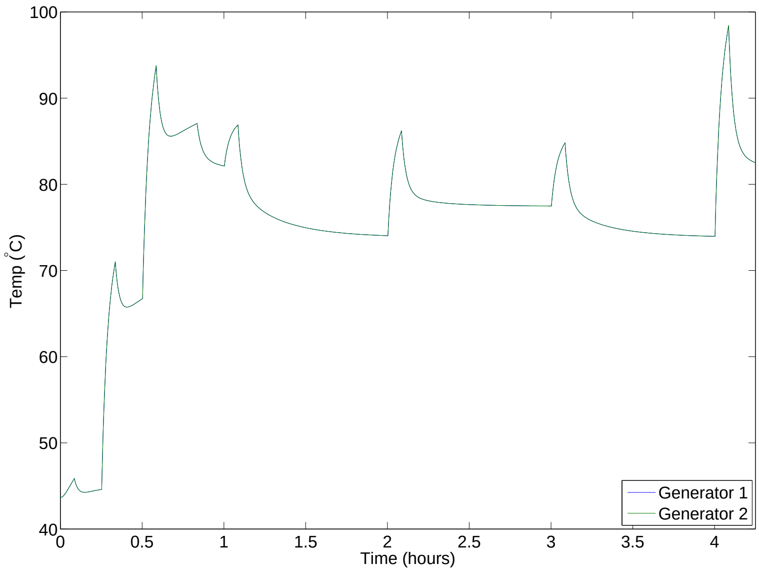

Figure 7.8: Temperature of Generator For Load when No Fault Present

7.3.3 Simulation Results

For the results presented here a number of tests were carried out. First tests to see how large the inlet temperature rise has to be to cause any level of load re-allocation to occur. Second the size of inlet temperature rise required to force the load management system to apply both generator resting and load displacement. Finally testing the system's response to a condition similar to what will be seen in the final tests using the experimental rig.

Minimum Fault Size to Cause Overheat

The first test is to determine the minimum fault level required for the load management system to take action. To determine this the fault is applied 1.1 hours into the flight; this is just after the completion of take-off. This time was chosen as a detected fault before or during take-off would probably lead to an instant mission cancellation.

Figures 7.9 and 7.10 show the load profile and the stator winding temperature for an inlet temperature increase of $4°C$.

Figures 7.9 and 7.10 show that at an increase of $4°C$ requires a short rest and load adjust before landing. At increases of less than $4°C$ the faulty generator is able to cope with the increased heat load. These results show that during landing there is very little spare capacity in either the faulty or healthy generators causing resting to be required to prevent any overheat.

Minimum Fault Size to Adjustments During Cruise

This test is similar to the previous one in that a blockage fault is applied 1.1 hours into the flight. For this test the fault level was increased until the spare capacity in the faulty generator during the cruise and cruise/combat phases was used, forcing action from the load management system.

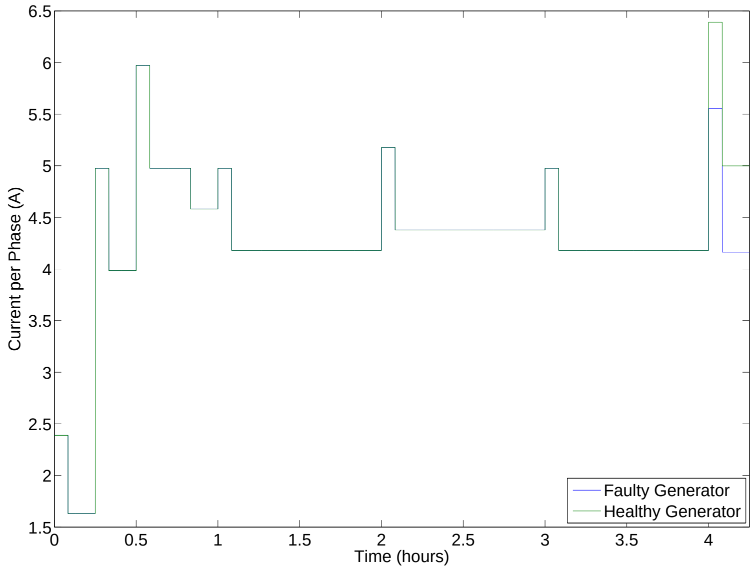

Figure 7.9: Final Load Profile for Minimum Fault Level Requiring Load Management

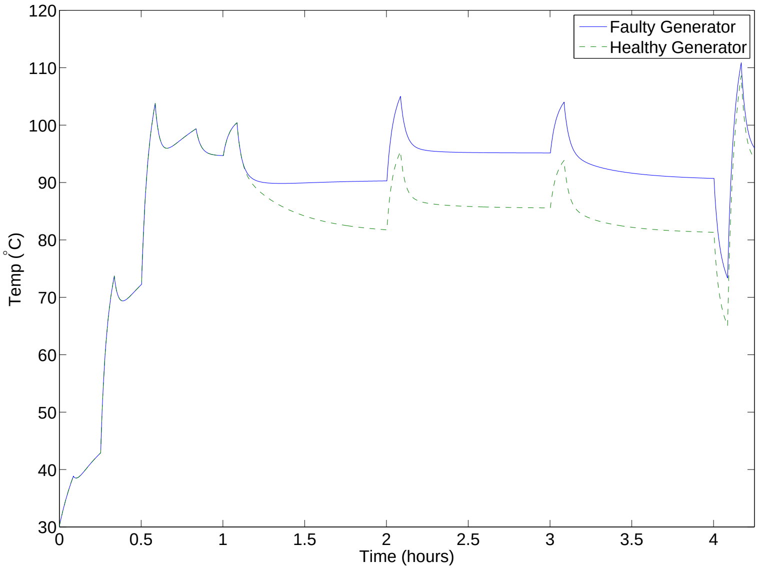

Figure 7.10: Stator Winding Temperature for Minimum Fault Level Requiring Load Management

Figures 7.11 and 7.12 show the load profile and the stator winding temperature for a temperature rise of 16°C.

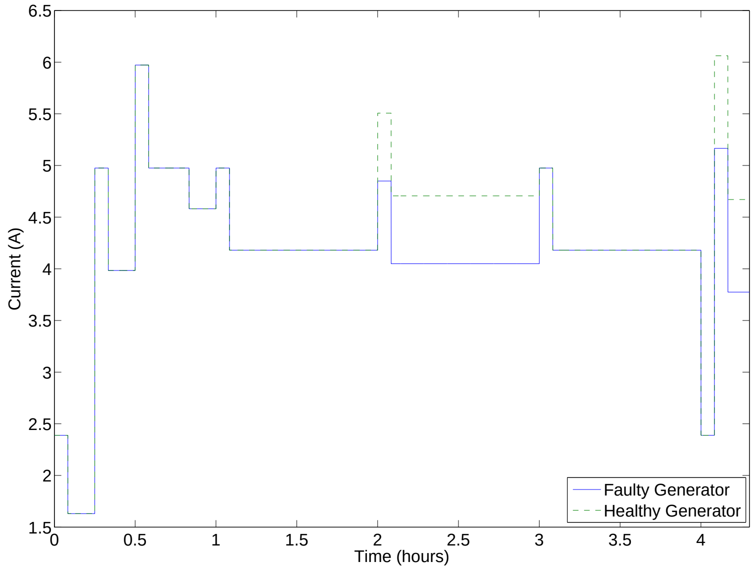

Figure 7.11: Final Load Profile for Minimum Fault Level Requiring Load Management

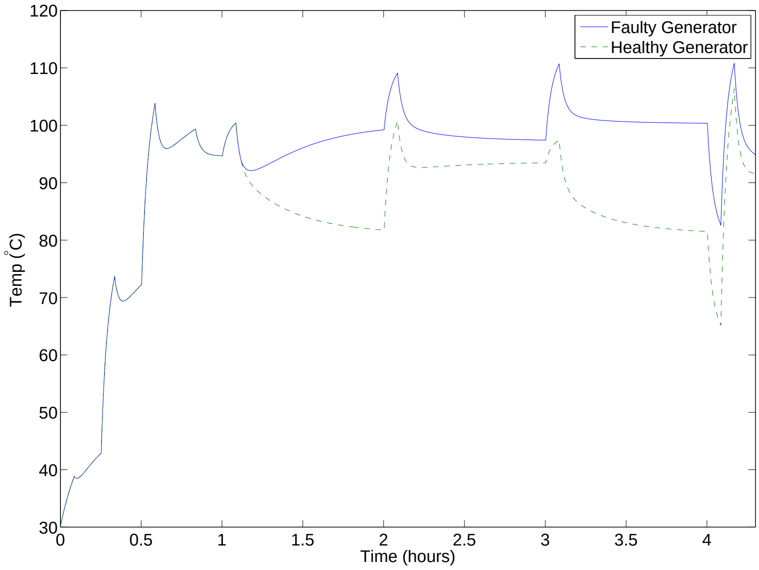

Figure 7.12: Stator Winding Temperature for Minimum Fault Level Requiring Load Management

Figures 7.11 and 7.12 show that from when the fault is applied load displacement is first applied during the cruise/combat phase 2 hours into the test. Before 1.1 hours there is no fault and the generators cope as expected. After 1.1 hours the spare capacity in the faulty generator is able to accommodate the fault without changing the load. Then after 2 hours some load displacement is required during the cruise/combat phase. Then at 3 hours the aircraft goes back to cruise no longer requiring and load displacement. Finally a short rest with some load displacement is required for landing the same as in the previous test.

Large Blockage Fault Test

The final results to be presented are to test the conditions that would be present in tests undertaken using the experimental rig. For this test the outlet port is reduced to 10mm in diameter, 20% of the non-fault state causing the inlet temperature to be around 51°C. While the inlet temperature would naturally vary this is dependent upon both the fault and the load and hence cannot be accurately described , however this will indicate the ability of the load management system to cope with this level of fault.

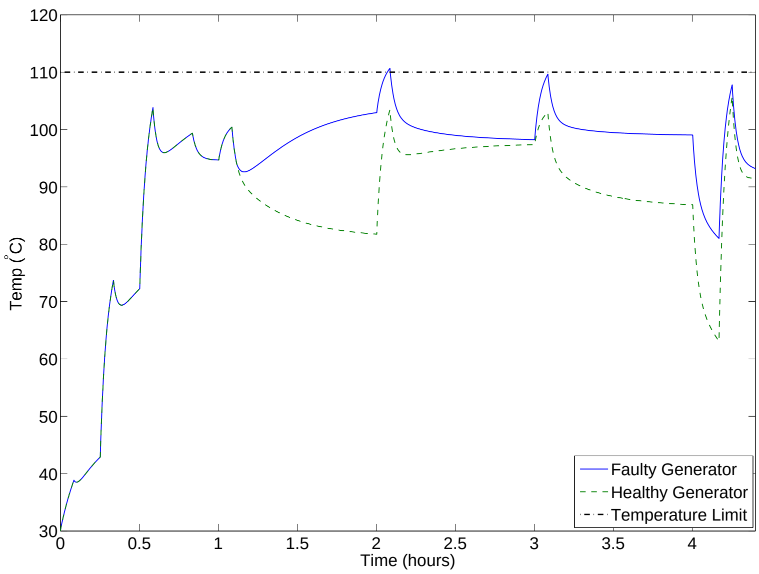

Figure 7.13: Stator Winding Temperature for Load Management System Validation

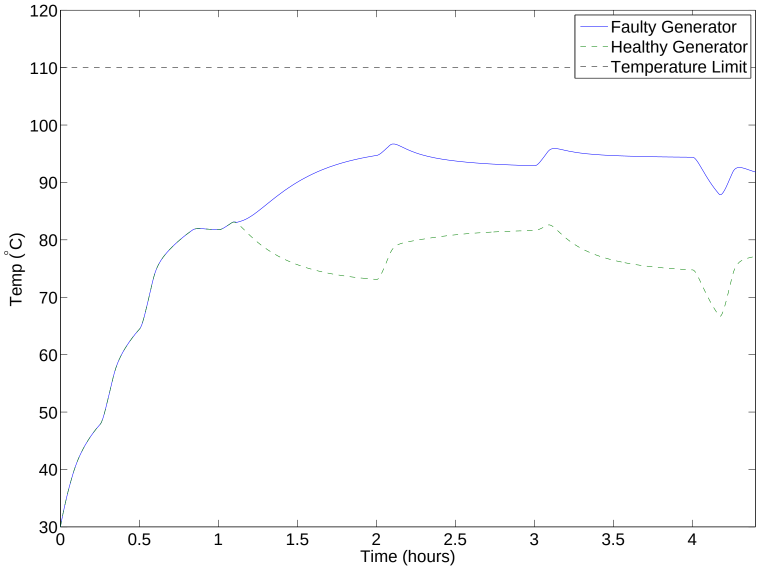

Figure 7.14: Stator Iron Temperature for Load Management System Validation

Figures 7.13 and 7.14 show the temperature of the generator over time during the test. On these graphs it is shown that until 1.1 hours into the test both generators have identical temperatures showing no fault is present. At 1.1 hour the fault occurs; this causes the generators to have different temperatures. It is also shown that throughout the test the generator remains below $110°C$ except for two small breaches of $110.7°C$ at 2 hours and $111°C$ at 3 hours neither of which would cause problems for the generator.

Figure 7.15 shows the load profile that was actually applied to the generator over the test and clearly shows the action of the load management system. Once the fault has occurred at 1.1 hours the next 3 K-conditions are accommodated using only load displacement. After this both generators are placed into rest mode for 10 mins to allow the execution of the final landing K-condition.

7.3.4 Experimental Rig Test

This test is carried out in an identical manner to the simulation test with the exception that the experimental rig will be used to represent the faulty generator

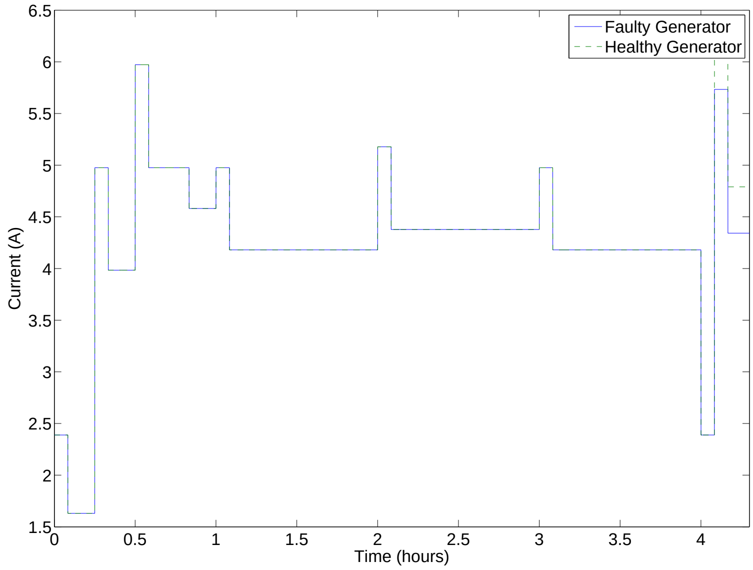

Figure 7.15: Final Load Profile for Load Management System Validation

instead of the design model. This means that the second generator the 'healthy' one will still be represented by the design model and a Kalman Filter containing the simulation model will be used to make predictions for each generator. This is shown in the adjusted set-up diagram in figure 7.16.

7.3.5 Experimental Rig Test Results

Figure 7.17 shows the temperature of the stator winding and stator iron over the length of the final test. The results show that for the length of the test the 110°C temperature limit is not breached. This shows that the load management system is able to function correctly when used on an actual generator.

Figure 7.18 shows the load profiles applied to both the faulty and healthy generator during the test with the experimental rig. This shows that until 1.25 hours into the test the profiles are identical, which is the time of the first update to occur after the fault at 1.1 hours. After this some load displacement is required to complete the next K-condition followed by a 20 minute rest before the next two K-conditions can be completed with some load displacement. Finally another 20

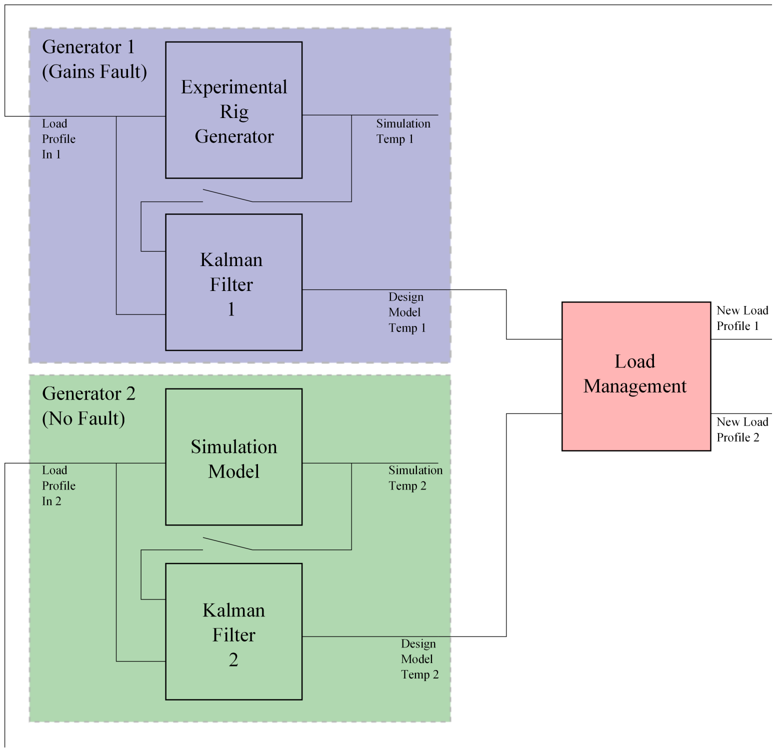

Figure 7.16: Diagram Showing the Simulation Set-up for Validation Tests with Experimental Rig Generator

Figure 7.17: Stator Winding and Iron Temperature for Experimental Rig Test

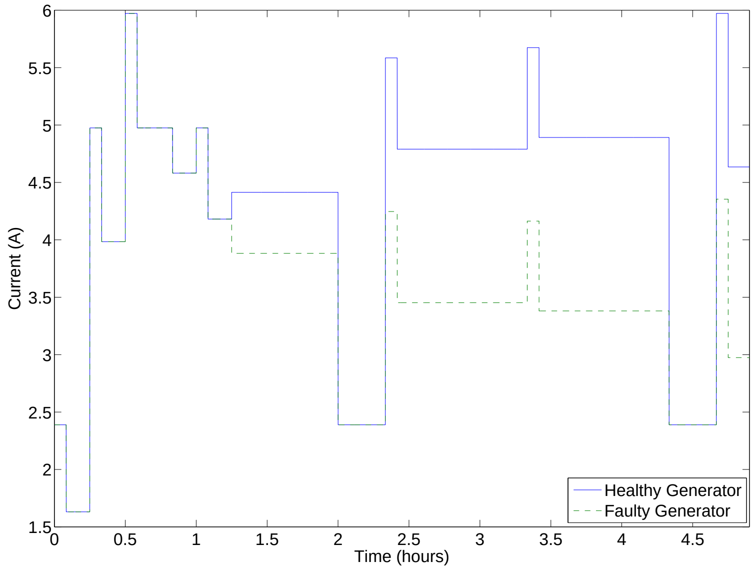

Figure 7.18: Final Load Profile Applied to Generators for Experimental Rig Test

minute rest is required before landing can be undertaken.

7.3.6 Comparison of Experimental Rig Vs Simulation Results

Figure 7.19 compares the output load profile for the faulty generators for a simulation of the generator rig test and the test itself using the generator rig. This graph shows that during the tests with the generator rig a much greater level of action by the load management system was required. This due mostly to the estimation of the coolant inlet temperature during the simulation test. When an accurate measurement of the inlet temperature was available for the beginning of each prediction this showed that an additional rest before a combat action was required, as well as requiring higher levels of load displacement throughout the flight.

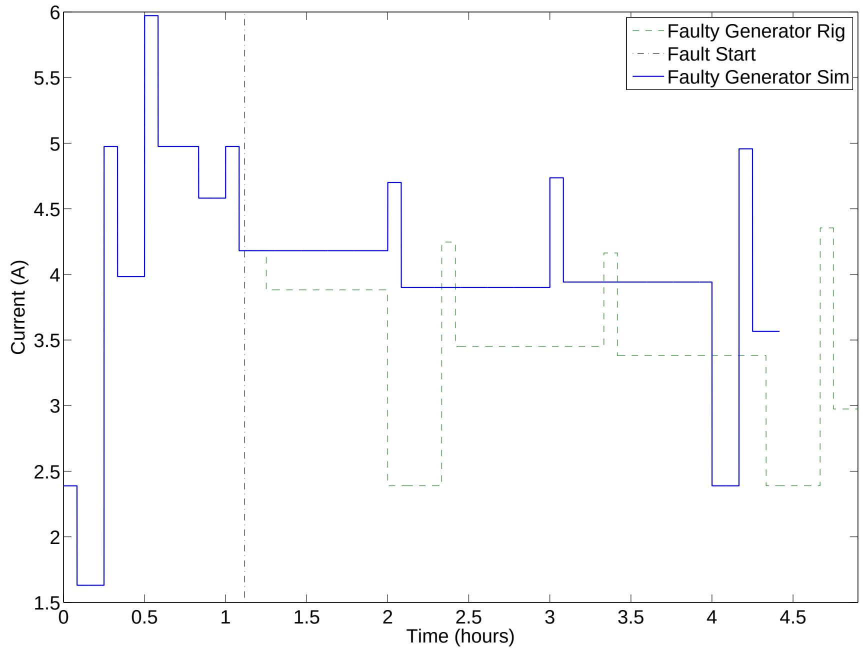

Figure 7.19: Comparison of Final Load Profiles Applied to Generators During Rig and Simulation Tests

7.4 Conclusion

This chapter has described a system for a prognostic approach to load management upon aircraft, presenting results to validate the system created.

A design model is used to predict when an overheat fault will occur and then the load management algorithm changes the load profile to prevent it. The algorithm uses two methods to adjust the load profile; generator resting and load displacement. Using these methods the validation results showed that a generator with a reduced coolant flow could be kept below $110°C$ for the duration of the test both in simulation and using the experimental rig as the faulty generator. This would allow a mission to be completed that would have to have been aborted without the system in place.

Chapter 8

Conclusions and Future Work

8.1 Conclusions

This thesis has presented research relating to the design of a load management system to be used in aircraft generators that uses predictions of the future temperature state to inform load management decision. This allows load profiles to be adjusted in flight to prevent overheats and allow missions to continue. The two inital research questions that were asked during the introduction were:

1. Is it possible to predict when an overheat fault will occur based on the expected power usage defined by mission profiles?

2. Can an overheat fault be prevented while still allowing power to be distributed to necessary loads to allow mission completion?

From the work presented within the thesis it has been shown that it is possible to predict when overheat faults will occur when a coolant blockage occurs. For the second question it was shown that for a non-catastrophic fault mission completion could still be achieved using the load management algorithm presented.

The thesis first presented the background of aircraft load management and prognostics and health management (PHM). Within this review it was concluded that current load management systems on-board aircraft use no prognostic element within the system; load management is undertaken in real time with loads being switched off either manually or by algorithm after an overheat is detected. It was also found that most current PHM research is focussed upon maintenance scheduling rather than on-board reconfiguration and non of the research into on-board reconfiguration looks at overheating in generators. The system presented her offers a method of using predictions of a generator's future temperature state to adjust load profiles in advance, preventing any overheat faults and stopping a generator being shut down entirely.

A survey of thermal modelling techniques showed that of the methods available two were suitable for investigation; lumped parameter thermal networks and system identification. Lumped parameter thermal models were shown to be a well documented technique that has been previously used within the generator design process, however this technique had never being used in a condition monitoring application. No research could be found which created a system identification model of the thermal dynamics of a generator.

The objectives of this thesis were:

1. To commission an experimental generator rig to validate thermal models.
2. To create validated thermal models to represent both the actual generator in simulation and a design model to be used as part of the prediction system
3. To design a system to predict the future temperature state of a generator based on a known mission profile.
4. To develop and test a load management system able to correct overheat faults when detected before they caused catastrophic failure of a generator.

The results which achieve these objectives were presented from chapter 3 onwards. In chapter 3 the commissioning of the generator rig was described including the sensors and data collection method used.

Chapter 4 described the lumped parameter thermal model to be used as the simulation model. The model was fully described and validated against data obtained from the experimental rig.

Chapter 5 described the two potential candidates to be used as a design model. One was a linear version of the lumped parameter thermal model presented in chapter 4 and the other was a system identification model. These models were also validated against data from the experimental rig and were compared. While it was found that the system identification model was slightly more accurate and was of a lower order it was decided that the physics-based model would be used mainly due to the ease with which faults could be modelled.

In chapter 6 it was shown how the chosen design model was to be used within a Kalman Filter both for updating the model states with current data and making prediction into the future. It was shown that using this system predictions could be made with good accuracy far into the future, but also that in the short term the Kalman Filter correction provided additional accuracy for checking results.

Chapter 7 summarises the load management system, showing how the prediction system including the design model from earlier was integrated. The chapter also describes the methods used to balance the load upon the generator to prevent overheat; these were generator resting and load displacement. The results section showed that, through the use of resting the generators and using spare capacity of a healthy generator, the temperature of a faulty generator could be kept below the $110°C$ limit for the duration of a test, even under fault conditions. This includes tests undertaken entirely in simulation and using the experimental rig shown in chapter 3.

8.2 Contributions

The research presented within this thesis has made contributions in two main areas, these are:

8.2.1 Modelling Contributions

First the uses of lumped parameter thermal models for a condition monitoring application is a contribution to knowledge. In chapter 2 it is shown that this type of model has only previously been used as a generator design tool.

Another contribution is the creation and validation of a linear form of this model, described in chapter 5, as well as the analysis of the effect of a non-linear winding loss representation and temperature dependent winding resistance upon long term model performance.

The creation and validation of a system identification model of the thermal dynamics of a generator described in chapter 5 also represents a major contribution to knowledge.

The final modelling contribution is the comparison of the physics-based and system identification methods of modelling the thermal dynamics of a generator.

8.2.2 Generator Health Management Contributions

In this area, the main contribution of this thesis is the creation of a prognostic based load management algorithm for an aircraft generator described in chapter 7. Prior work in this area has used only real-time intervention based on the current state of the generator. By introducing a prediction of the future temperature state of the generator action can be taken in advance allow some generator capacity to be maintained after non-fatal faults.

Within the load management system the use of a Kalman Filter using an n-step ahead prediction described in chapter 6 is novel in relation to aircraft generators.

8.3 Future Work

The research present within this thesis was designed to prove the concept for a prognostic load management system for an aircraft generator. For this reason the scope was kept intentionally narrow focusing on showing that both the prediction of overheat faults and re-allocation of loads in flight could be achieved. Moving forward it will be necessary to expand the scope again and analyse how the load management system would interact with the aircraft it would be on-board, including the operating conditions and what limitations this would place upon it.

The following sections look at the main areas where further research needs to be undertaken to take this research from a proof of concept to a system ready to deploy upon an aircraft.

8.3.1 Interface Research

Further work falling into this category relates to research defining how this system would be deployed on-board an aircraft but also how the limitations of an aircraft will effect the usefulness of this system.

Interface Between Power Generation and Distribution

The first major body of work would involve the interface between power generation and distribution systems. For this work an assumption that loads could be switched between generators at will was made. The discrete nature of loads was not considered either. Further work in this area would analyse what impact the power distribution system would have on the abilities of the algorithm.

In the literature review it was shown that certain power distribution systems have no flexibility there is a left and right bus with half the loads that can be connected in emergency situations. There was also shown work that used more flexible load buses which could switch smaller amounts of loads between generation sources. This means that for any distribution system now or in the near future that load redistribution would either be unavailable or only possible in discrete chunks.

For the system to work under these requirements a further algorithm would need to be created which would take the load redistribution result from the current algorithm (e.g. switch 20% load) and find the minimum actual amount of load that could be transferred and then check if the second generator has this amount of spare capacity. Secondly any system in use would have to create a switching schedule for any loads to avoid causing any in-flight problems caused by temporarily switching them off then back on again.

Deployment of System on Aircraft

For this research a computer was used for data acquisition. Going forward the next step is to move from this set-up where the load has to be manually adjusted to a full hardware in the loop simulation which can implement the load management algorithm automatically.

After this the full operating environment can be studied including measuring the computation requirements of the final algorithm, tests using hardware similar to that on-board an aircraft and researching how this system would interact with other systems on-board and a certification plan.

8.3.2 Further Algorithm Research

This area of further research focuses on how the algorithm itself would be improved moving towards a state where it can be shown what the final system would look like if it were to be deployed.

Additional Failure Modes

This research focussed on one easily reproducible failure mode, however further research needs to analyse the full range of cases which can cause overheat faults. This would include any situation that increased inlet temperature of effected the coolant, an analysis of stator winding short circuits and what level of this is non-catastrophic and what isn't and also research into the effect of using fuel as a cooling medium.

Further work would attempt to model many more of the non-catastrophic failure modes and in some cases fault detection/isolation may be necessary to know when parameters are changing and the effect this has on the system.

Modelling Advances

There are two major steps that are next in regards to the generator modelling the first is to research how to make prediction while using as few sensors as possible and the second is to move from modelling the currently available generator rig to modelling an actual aircraft generator. To achieve this the bulk of the modelling work presented here can be kept the new model would require some small structural changes to represent the different shaped components in the system and then the new parameters would need to be determined.

The second task would be to research the minimum number of sensors required for the system to still function well. The question to answer in this case would be whether a similar level of prediction accuracy could be achieved with only input and output coolant temperature measurements and if not how many additional sensors would have to be installed as a minimum to achieve the required accuracy? The investigation of this would start by reintroducing the output coolant temperature measurement through the C matrix of the state space model equations and testing if the Kalman Filter works well enough using only this measurement to update states. If this is not the case the same test would be repeated adding in the stator winding temp and then if necessary the iron measurement as well.

References

[1] Mike Howse. All-electric aircraft. *Power Engineer*, 17(4):35–37, 2003.

[2] Ian Moir. More-electric aircraft-system considerations. In *Electrical Machines and Systems for the More Electric Aircraft (Ref. No. 1999/180), IEE Colloquium on*, pages 10–1. IET, 1999.

[3] R. Austin. *Unmanned Aircraft Systems: UAVS Design, Development and Deployment*. Aerospace Series. Wiley, 2011.

[4] Daniel Schlabe and Jens Lienig. Energy management of aircraft electrical systems-state of the art and further directions. In *Electrical Systems for Aircraft, Railway and Ship Propulsion (ESARS), 2012*, pages 1–6. IEEE, 2012.

[5] Ian Moir and Allan Seabridge. *Aircraft systems: mechanical, electrical and avionics subsystems integration*, volume 21. John Wiley & Sons, 2008.

[6] Luiz Andrade and Carl Tenning. Design of boeing 777 electric system. *Aerospace and Electronic Systems Magazine, IEEE*, 7(7):4–11, 1992.

[7] David A. Haak and Lawrence W. Messenger. Automatic electric load management centers. 09 1990.

[8] AA AbdElhafez and AJ Forsyth. A review of more-electric aircraft. In *Proceedings of The 13rd international conference on Aerospace Science and Aviation Technology conference*, pages 26–28, 2009.

[9] Timothy F Glennon. Fault tolerant generating and distribution system architecture. In *All Electric Aircraft (Digest No. 1998/260), IEE Colloquium on*, pages 4–1. IET, 1998.

[10] Franz L Worth, VH Forker, and Michael J Cronin. Advanced electrical system (aes). In *Aerospace and Electronics Conference, 1990. NAECON 1990., Proceedings of the IEEE 1990 National*, pages 400–403. IEEE, 1990.

[11] Anthony F Sodoski, Bruce S Hamilton, and Michael P Bradford. Power management under limited power conditions, October 14 2003. US Patent 6,633,802.

[12] Darrell T Hambley, Jeffrey Jouper, Susan Nellis, and Mark A Peabody. Load distribution and management system, April 4 2000. US Patent 6,046,513.

[13] Zhiping Ding, Sanjeev K Srivastava, David A Cartes, and Siddharth Suryanarayanan. Dynamic simulation based analysis of a new load shedding scheme for a notional destroyer class shipboard power system. In *Electric Ship Technologies Symposium, 2007. ESTS'07. IEEE*, pages 95–102. IEEE, 2007.

[14] Michael B McAvoy. Aircraft galley systems and methods for managing electric power for aircraft galley systems, November 27 2012. US Patent 8,321,073.

[15] Kai Huang, D Cartes, and S Srivastava. A novel algorithm for reconfiguration of shipboard ring-structured power system using multi-agent system. In *Reconfiguration and Survivability Symposium*, 2005.

[16] Patrick W Kalgren, Carl S Byington, and Michael J Roemer. Defining phm, a lexical evolution of maintenance and logistics. In *Autotestcon, 2006 IEEE*, pages 353–358. IEEE, 2006.

[17] Abhinav Saxena, Jose Celaya, Edward Balaban, Kai Goebel, Bhaskar Saha, Sankalita Saha, and Mark Schwabacher. Metrics for evaluating performance

of prognostic techniques. In *Prognostics and Health Management, 2008. PHM 2008. International Conference on*, pages 1–17. IEEE, 2008.

[18] Andrew Hess and Leo Fila. The joint strike fighter (jsf) phm concept: potential impact on aging aircraft problems. In *Aerospace Conference Proceedings, 2002. IEEE*, volume 6, pages 6–3021. IEEE, 2002.

[19] Naresh Iyer, Kai Goebel, and P Bonissone. Framework for post-prognostic decision support. In *Aerospace Conference, 2006 IEEE*, pages 10–pp. IEEE, 2006.

[20] Luis Hernandez, Michael Mullins, Charles Morris, and Kirby Keller. A framework for developing an eps health management system. *High Temperature*, 1:1727, 2010.

[21] Andrew Hess, G Calvello, and T Dabney. Phm a key enabler for the jsf autonomic logistics support concept. In *Aerospace Conference, 2004. Proceedings. 2004 IEEE*, volume 6, pages 3543–3550. IEEE, 2004.

[22] JPM Smeulers, R Zeelen, and A Bos. Promis-a generic phm methodology applied to aircraft subsystems. In *Aerospace Conference Proceedings, 2002. IEEE*, volume 6, pages 6–3153. IEEE, 2002.

[23] V. Rouet, K. Moreau, and B. Foucher. Embedded prognostics and health monitoring systems. In *ESTC 2008. 2nd Electronics System-Integration Technology Conference*, 2008.

[24] Liang Tang, M. Roemer, G.J. Kacprzynski, and Jianhua Ge. Dynamic decision support and automated fault accommodation for jet engines. In *IEEE Aerospace Conference*, 2007.

[25] Matthew J Watson, Carl S Byington, and Alireza Behbahani. Very high frequency monitoring system for engine gearbox and generator health management. In *Proceedings of the SAE AeroTech Congress & Exhibition*, 2007.

[26] Todd D Batzel and David C Swanson. Prognostic health management of aircraft power generators. *Aerospace and Electronic Systems, IEEE Transactions on*, 45(2):473–482, 2009.

[27] Subhasis Nandi, Hamid A Toliyat, and Xiaodong Li. Condition monitoring and fault diagnosis of electrical motors-a review. *Energy Conversion, IEEE Transactions on*, 20(4):719–729, 2005.

[28] Xiao-Sheng Si, Wenbin Wang, Chang-Hua Hu, and Dong-Hua Zhou. Remaining useful life estimation–a review on the statistical data driven approaches. *European Journal of Operational Research*, 213(1):1–14, 2011.

[29] Bhaskar Saha, Kai Goebel, Scott Poll, and Jon Christophersen. Prognostics methods for battery health monitoring using a bayesian framework. *Instrumentation and Measurement, IEEE Transactions on*, 58(2):291–296, 2009.

[30] Aldo Boglietti, Andrea Cavagnino, David Staton, Martin Shanel, Markus Mueller, and Carlos Mejuto. Evolution and modern approaches for thermal analysis of electrical machines. *Industrial Electronics, IEEE Transactions on*, 56(3):871–882, 2009.

[31] Lennart Ljung. Perspectives on system identification. *Annual Reviews in Control*, 34(1):1–12, 2010.

[32] G. Nellis and S. Klein. *Heat Transfer*. Cambridge University Press, 2012.

[33] J.H. Lienhard. *A Heat Transfer Textbook*. Dover Books on Engineering. Dover Publications, 2011.

[34] S.P. Sukhatme. *A Textbook on Heat Transfer*. Universities Press, 2005.

[35] S Kar Chowduury, Bikram Dutta, and Diptarshi Bhowmik. Lumped parameter thermal model for induction machine. *Thermal Energy and Power Engineering*, 3(1), 2014.

[36] Naghi Rostami, Mohammad Reza Feyzi, Juha Pyrhonen, Asko Parviainen, and Markku Niemela. Lumped-parameter thermal model for axial flux permanent magnet machines. *Magnetics, IEEE Transactions on*, 49(3):1178–1184, 2013.

[37] W Wu, VS Ramsden, T Crawford, and G Hill. A low speed, high-torque, direct-drive permanent magnet generator for wind turbines. In *Industry Applications Conference, 2000. Conference Record of the 2000 IEEE*, volume 1, pages 147–154. IEEE, 2000.

[38] O Aglen and A Andersson. Thermal analysis of a high-speed generator. In *Industry Applications Conference, 2003. 38th IAS Annual Meeting. Conference Record of the*, volume 1, pages 547–554. IEEE, 2003.

[39] Antonino Di Gerlando, Gianmaria Foglia, and Roberto Perini. Permanent magnet machines for modulated damping of seismic vibrations: Electrical and thermal modeling. *Industrial Electronics, IEEE Transactions on*, 55(10):3602–3610, 2008.

[40] Olivier Maloberti, Anthony Gimeno, Alejandro Ospina, Guy Friedrich, K El-Kadri Benkara, and Loïc Charbonnier. Thermal modeling of a claw-pole electrical generator-steady-state computation and identification of free and forced convection coefficients. 2014.

[41] Stephane Brisset, Darius Vizireanu, and Pascal Brochet. Design and optimization of a nine-phase axial-flux pm synchronous generator with concentrated winding for direct-drive wind turbine. *Industry Applications, IEEE Transactions on*, 44(3):707–715, 2008.

[42] C Mejuto, M Mueller, M Shanel, A Mebarki, and D Staton. Thermal modelling investigation of heat paths due to iron losses in synchronous machines. 2008.

[43] Smail Mezani, N Takorabet, and B Laporte. A combined electromagnetic and thermal analysis of induction motors. *IEEE transactions on magnetics*, 41(5):1572–1575, 2005.

[44] Gunnar Kylander. *Thermal modelling of small cage induction motors*. PhD thesis, School of Electrical and Computer Engineering Chalmers University of Technology, Gteborg, Sweden, 1995.

[45] Janne Nerg, Marko Rilla, and Juha Pyrhonen. Thermal analysis of radial-flux electrical machines with a high power density. *Industrial Electronics, IEEE Transactions on*, 55(10):3543–3554, 2008.

[46] Ogbonnaya I Okoro. Steady and transient states thermal analysis of a 7.5-kw squirrel-cage induction machine at rated-load operation. *Energy Conversion, IEEE Transactions on*, 20(4):730–736, 2005.

[47] PH Mellor, D Roberts, and DR Turner. Lumped parameter thermal model for electrical machines of tefc design. In *IEE Proceedings B (Electric Power Applications)*, volume 138, pages 205–218. IET, 1991.

[48] Georgios D Demetriades, H Zelaya De La Parra, Erik Andersson, and Håkan Olsson. A real-time thermal model of a permanent-magnet synchronous motor. *Power Electronics, IEEE Transactions on*, 25(2):463–474, 2010.

[49] Aldo Boglietti, Andrea Cavagnino, and David Staton. Determination of critical parameters in electrical machine thermal models. *Industry Applications, IEEE Transactions on*, 44(4):1150–1159, 2008.

[50] Aldo Boglietti, Andrea Cavagnino, and DA Staton. Thermal analysis of tefc induction motors. In *Industry Applications Conference, 2003. 38th IAS Annual Meeting. Conference Record of the*, volume 2, pages 849–856. IEEE, 2003.

[51] Yangsoo Lee, Song yop Hahn, and S. Ken Kauh. Thermal analysis of induction motor with forced cooling channels. *IEEE Transactions on Magnetics*, 36(4), July 2000.

[52] T Jokinen and J Saari. Modelling of the coolant flow with heat flow controlled temperature sources in thermal networks. *IEE Proceedings-Electric Power Applications*, 144(5):338–342, 1997.

[53] Oliver Nelles. *Nonlinear system identification: from classical approaches to neural networks and fuzzy models*. Springer, 2001.

[54] Peter Young. Parameter estimation for continuous-time modelsa survey. *Automatica*, 17(1):23–39, 1981.

[55] Rolf Isermann. Process fault detection based on modeling and estimation methodsa survey. *Automatica*, 20(4):387–404, 1984.

[56] Karl Johan Åström and Peter Eykhoff. System identificationa survey. *Automatica*, 7(2):123–162, 1971.

[57] Karl-Johan Åström and Torsten Bohlin. Numerical identification of linear dynamic systems from normal operating records. In *Theory of self-adaptive control systems*, pages 96–111. Springer, 1966.

[58] DW Clarke. Generalized least squares estimation of the parameters of a dynamic model. In *First IFAC Symposium on Identification in Automatic Control Systems, Prague*, 1967.

[59] Kwan Wong and E Polak. Identification of linear discrete time systems using the instrumental variable method. *Automatic Control, IEEE Transactions on*, 12(6):707–718, 1967.

[60] Morris Joseph Levin. *Estimation of the Characteristics of Linear Systems in the Presence of Noise*. PhD thesis, Department of Electrical Engineering, Columbia University, 1959.

[61] V Peterka and A Halousková. Tally estimate of åström model for stochastic systems. In *Proc. 2nd IFAC Symposium on Identification and System Parameter Estimation, Prague, Chechoslovakia*, 1970.

[62] Xuejing Zhao, Mitra Fouladirad, Christophe Bérenguer, and Laurent Bordes. Condition-based inspection/replacement policies for non-monotone deteriorating systems with environmental covariates. *Reliability Engineering & System Safety*, 95(8):921–934, 2010.

[63] Liang Tang, J DeCastro, G Kacprzynski, K Goebel, and G Vachtsevanos. Filtering and prediction techniques for model-based prognosis and uncertainty management. In *Prognostics and Health Management Conference, 2010. PHM'10.*, pages 1–10. IEEE, 2010.

[64] VE Beneš. Exact finite-dimensional filters for certain diffusions with nonlinear drift. *Stochastics: An International Journal of Probability and Stochastic Processes*, 5(1-2):65–92, 1981.

[65] Bin Zhang, Liang Tang, Jonathan DeCastro, and Kai Goebel. A verification methodology for prognostic algorithms. In *AUTOTESTCON, 2010 IEEE*, pages 1–8. IEEE, 2010.

[66] Rudolph Emil Kalman. A new approach to linear filtering and prediction problems. *Journal of Fluids Engineering*, 82(1):35–45, 1960.

[67] R.G. Brown and P.Y.C. Hwang. *Introduction to Random Signals and Applied Kalman Filtering with Matlab Exercises.* CourseSmart Series. Wiley, 2012.

[68] VVS Sarma, KV Kunhikrishnan, and K Ramchand. A decision theory model for health monitoring of aeroengines. *Journal of Aircraft*, 16(3):222–224, 1979.

[69] AH Christer, Wenbin Wang, and JmM Sharp. A state space condition monitoring model for furnace erosion prediction and replacement. *European Journal of Operational Research*, 101(1):1–14, 1997.

[70] Scott E Black, Kirby Keller, Gautam Biswas, and James Davis. Diagnostic/prognostic modeling and reconfigurable control. In *AUTOTESTCON 2004. Proceedings*, pages 344–350. IEEE, 2004.

[71] Paul P Lin and Xiaolong Li. Fault diagnosis, prognosis and self-reconfiguration for nonlinear dynamic systems using soft computing techniques. In *Systems, Man and Cybernetics, 2006. SMC'06. IEEE International Conference on*, volume 3, pages 2234–2239. IEEE, 2006.

[72] Elias G Strangas, Selin Aviyente, John D Neely, and Syed Sajjad H Zaidi. The effect of failure prognosis and mitigation on the reliability of permanent-magnet ac motor drives. *Industrial Electronics, IEEE Transactions on*, 60(8):3519–3528, 2013.

[73] Liang Tang, Gregory J Kacprzynski, Kai Goebel, Abhinav Saxena, Bhaskar Saha, and George Vachtsevanos. Prognostics-enhanced automated contingency management for advanced autonomous systems. In *Prognostics and Health Management, 2008. PHM 2008. International Conference on*, pages 1–9. IEEE, 2008.

[74] Liang Tang, Eric Hettler, Bin Zhang, and Jonathan DeCastro. A testbed for real-time autonomous vehicle phm and contingency management applica-

tions. In *Annual conference of the prognostics and health management society*, pages 1–11, 2011.

[75] R.W. Reynolds. Integrated drive generator system with direct motor drive prime mover starting, July 2 1991. US Patent 5,028,803.

[76] DoD. Electric load and power source capacity, aircraft, analysis of. Military Specification MIL-STD-7016F, United States Department of Defense, London, United Kingdom, 1976.

[77] BSI. Industrial platinum resistance thermometers and platinum temperature sensors. BS EN 60751:2008, British Standards Institution, London, United Kingdom, 2008.

[78] I.J. Perez and J.G. Kassakian. Stationary thermal-model for smooth air-gap rotating electric machines. *Electrical Machines and Electromechanics*, 3(3 - 4), 1979.

[79] C. Kral, A. Haumer, and T. Bauml. Thermal model and behavior of a totally-enclosed-water-cooled squirrel-cage induction machine for traction applications. *Industrial Electronics, IEEE Transactions on*, 55(10):3555–3565, Oct.

[80] Hirotogu Akaike. Information theory and an extension of the maximum likelihood principle. In *Selected Papers of Hirotugu Akaike*, pages 199–213. Springer, 1998.